MODELING STARVATION EFFECTS IN PISTON SKIRT'S ELASTOHYDRODYNAMIC LUBRICATION AT INITIAL ENGINE START UP CONDITIONS

BY

AZHAR MAHMOOD

MS60-09-409

SESSION 2009-2013

ADVISOR

DR. ABDUAL WAHEED BADAR

NATIONAL UNIVERSITY OF SCIENCES AND TECHNOLOGY
COLLEGE OF ELECTRICAL & MECHANICAL ENGINEERING
RAWALPINDI

TABLE OF CONTENTS

ABSTRACT

There always has been a desire of improving the performance and efficiency of an automobile engine in order to reduce energy usage and control the losses. As a result the demand for better performance of important engine components has increased. Friction forces between surfaces of components in relative motion with each other are major source of energy loss in an IC Engine. There are many sources of friction in IC Engines such as Piston Assembly, Connecting Rod, Bearing, Valve train, Oil and Water Pumps and other components. Studies revealed that Power Cylinder (Piston and Ring/Liner) contributes a significant portion of mechanical friction losses. In general Piston Skirt–Liner conjunction is considered as major source of engine rubbing friction and cylinder friction power loss (1). Inadequate Skirt-Liner lubrication due to starvation has dramatic impact over the entire system efficiency. Piston Skirts experience starved elastohydrodynamic lubrication at engine startup and at some points along their stroke in normal operation. It is therefore quiet important to understand lubricant starvation and consider its effect. Starvation, as the name signifies is inadequate lubricant supply conditions. The aim of this research is therefore to mathematically model hydrodynamic and elastohydrodynamic lubrication of piston skirts under starvation conditions at initial engine startup. The mathematical model, thus developed will be used for prediction of lubrication behavior of piston skirt under various degrees of starvation. The results will be compared with those under fully flooded lubrication conditions in order to study the effects of starvation.

ACKNOWLEDGEMENTS

I would like to give special thanks to my ex-advisor Dr.Afzal Ahmed Malik and current advisor Dr. Abdual Waheed Badar who contributed to every aspect of my research work and helped me to achieve what I desired from it. Further I would like to thank my committee members for their guidance and constructive advice. In addition I would like to express my gratitude to Dr. Imran Akhtar who evaluated my research and reviewed my writeup in a very short time despite of his official commitments. Of course I need to give special thanks to Dr.Syed Adnan Qasim who continually guided me throughout my entire research work. Without his valuable guidance and motivation I would never be able to achieve my goals. Thank you sir Adnan for your patience and for providing me such an excellent learning and friendly environment at your home during the long working hours. I am also thankful to my fellow colleagues who kept in touch with me and provided support and encouragement during our graduate studies. Finally my all the family members, specially my wife, parents and children deserve hearties regards for compromising with my busy schedule during the research phase. They were always a source of great motivation and inspiration for me throughout my research work.

CHAPTER 1
INTRODUCTION

RESEARCH MOTIVATION

1.1 The operation of an Internal Combustion (IC) Engine involves relative motion of interacting surfaces of its critical parts. The critical parts and subassemblies of an (IC) engine include Piston and Ring Assembly, Cylinder Bore or Liner Assembly, Crankshaft, Camshaft and Valves Drive Mechanism (2). The relative motion of interacting surfaces of these parts can cause energy dissipation and power loss due to high static and kinetic friction resulting from forces of adhesion. Therefore the interacting surfaces, in relative motion, should be sufficiently, effectively and continuously lubricated throughout the engine operation in order to reduce frictional losses and adhesive wear. For this purpose a liquid lubricant is introduced between the interacting surfaces. This lubricant is forced to flow between the interacting surfaces by an Oil Pump which is normally driven by the engine, itself. An (IC) engine, therefore, has an inherent tendency of suffering from inadequate lubrication at startup. Also, low starting speed under low loads and high radial clearance are the typical operating conditions for an (IC) engine at the startup. These operating conditions make the effective lubrication of the piston skirts, quite a challenging task. Modeling of piston skirt lubrication at the startup would really be helpful in understanding the effects of starvation and finding optimum operating conditions for minimized wear and friction losses.

INTRODUCTION TO AN IC ENGINE SYSTEM

1.2 The Piston

The Piston is the major component of an IC Engine (Fig-1.1), with its main task being the conversion of thermal energy into mechanical work. It transmits the pressure forces generated during combustion to crankshaft through piston pin and connecting-rod, thereby converting the energy of combustion gases to rotational kinetic energy of the crankshaft. Piston performs reciprocatry motion in axial direction of the cylinder bore as the engine operates. One complete

motion of the piston between the two extremes positions in the cylinder bore is called a piston stroke. A complete operating cycle of power cylinder of an IC Engine consists of four piston strokes. In the intake stroke, the piston moves down, thereby creating a vacuum in the cylinder bore to extract the mixture of air and fuel into the cylinder. In the compression stroke it moves up to compress the air-fuel mixture. Combustion of the compressed air-fuel mixture takes place at the beginning of third stroke when the piston is travelling down. The pressure of combustion gases is transmitted to the top of piston, thereby pushing it down with a great force. This is called the working stroke because in this stroke, the energy of combustion gases is transmitted to crankshaft. Finally the piston travels up to exhaust the burnt gases to complete one operating cycle of power cylinder of an IC engine.

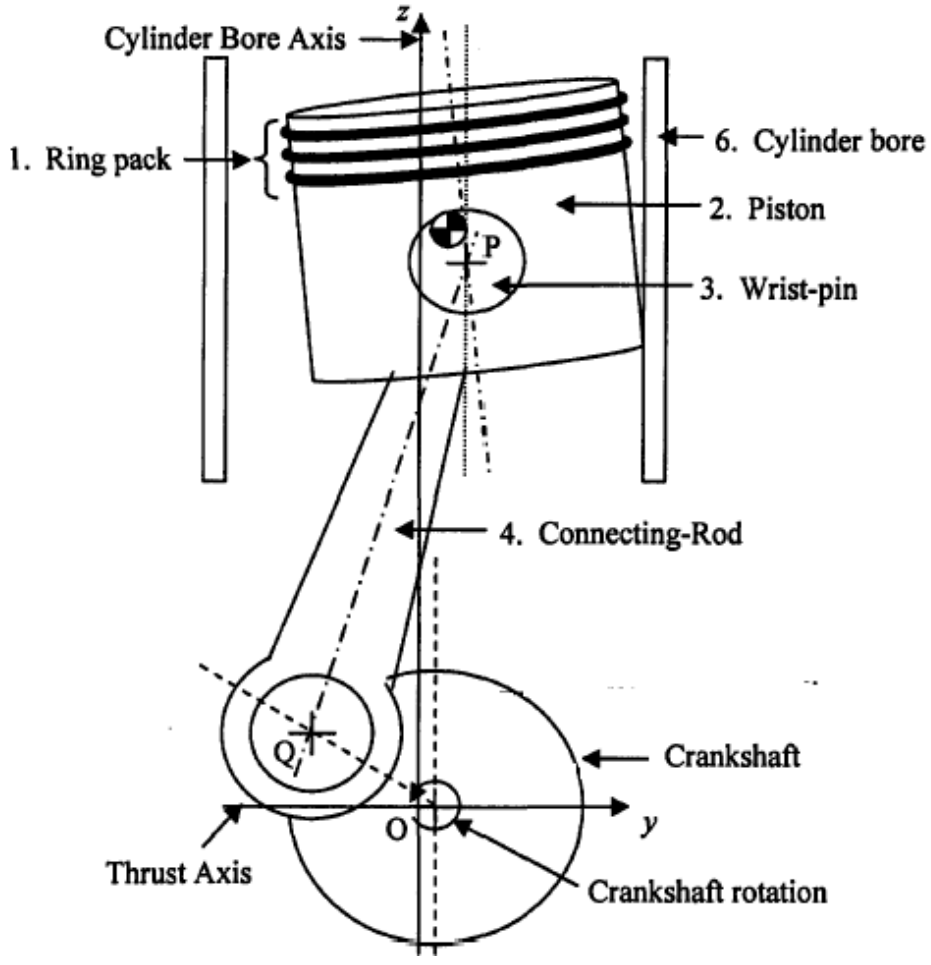

Fig-1.1: Components of the Power Cylinder of an IC Engine (2)

Ideally the piston should travel in axial direction only, to perform its reciprocatry motion. Hence motion of piston in axial direction is called its primary motion. In reality however, the connecting-rod angle results in significant side forces being transmitted through the piston causing lateral motion. The resulting secondary motion is often referred to as piston slap (2). Combustion gas loads due to secondary piston dynamics are born by piston skirt (Fig-1.2).

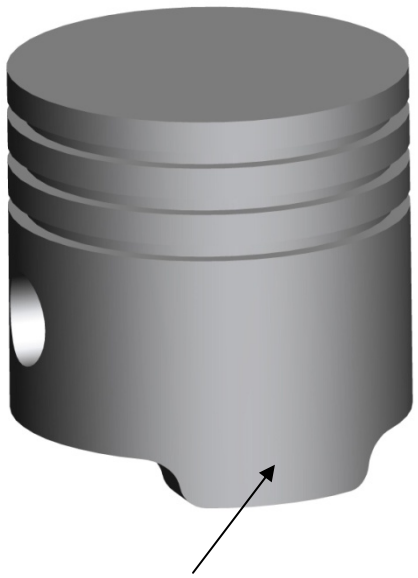

Fig-1.2: Piston Skirt

Piston Skirt is therefore, one of the most essential areas of piston. It acts as a load-carrying surface. It bears a significant portion of the combustion gas force due to piston secondary motion and keeps the piston properly aligned within the cylinder bore. Therefore the lubrication of piston skirt-liner needs proper attention.

1.3 **Piston Rings**

The prime functions of Piston Rings are to provide seal to gases in combustion chamber during compression and combustion strokes and to control and distribute the lubricating oil (3). Normally a set of two or three Rings operate in series in an I.C. Engine. This set of rings is called the Ring Pack. The lubricant is sprayed by oil pump into the crank case from where it is carried

along the piston-liner interface by the Ring Pack. In addition to this, piston rings transfer the combustion heat to the cylinder liner and stabilize the Piston (3).

1.4 Wrist Pin

The Wrist Pin provides a link between Piston and Connecting Rod for transmitting forces between the two. The connection between Piston and Connecting Rod through Wrist Pin allows them to rotate relative to and independent of each other.

1.5 Connecting Rod

The Connecting Rod transfers force from wrist pin to crankshaft. One end of the Connecting Rod is linked with Wrist Pin while other one is connected to Crankshaft. The Loads transmitted by Connecting Rod to Crankshaft are typically of the order of 100 KN (2). The Connecting Rod must be strong enough to transmit these loads without significant deformation.

1.6 Crankshaft

Crankshaft Converts reciprocatry motion of Piston into continuous rotary motion of drive train and engine Fly Wheel. Crankshaft has a rigid structure and large rotational inertia, in order to smooth out the pulses in combustion pressure (2).

1.7 Cylinder Bore

Cylinder Bore houses the piston and Rings Assemblies. It provides the space which acts as combustion chamber and constrains the motion of Piston.

LUBRICATION OF PISTON SKIRT

Piston skirt lubrication is provided by lubricating oil, which generally is picked up from the oil sump and thrown onto the cylinder bore by the motion of crankshaft. The lubrication oil is then transported along the cylinder bore by the motion of piston and piston-rings, and gravity. In normal operating conditions, piston skirt operates with an interference fit in cylinder bore because of thermal deformation. It is elastic flexibility that enables the piston to function efficiently. The field of study that incorporates the effects of elastic deformations in hydrodynamic lubrication is known as elastohydrodynamics or EHD (4). The deformations

induced in the surfaces of piston skirts due to hydrodynamic pressures are of the order of lubricant film thickness. Therefore, the EHD theory is needed in order to understand and mathematically model the lubrication of Piston Skirt (4). In this case the effects of pressure-induced deformation have to be accounted for, in lubricant-film gap equation. Reynolds equation is still applicable for calculation of hydrodynamic pressures. When piston skirt surface deformations are included in the lubricant film gap expression, the equation becomes non linear. Consequently a considerable complication is involved in the solution procedure. The major challenge in EHD study is determination of film thickness between the interacting surfaces. The film thickness depends upon the surface deformations resulting from pressures developed in the fluid film. Since the pressure causing the deformation of surfaces can only be determined if film thickness is known, the solution process is therefore iterative in nature.

1.8 Lubrication in Initial Engine Startup and Under Normal Operating Conditions

Lubrication of piston skirts of an IC Engine at initial startup is quite different than under normal operating conditions. During Normal operation of an IC Engine, an elastohydrodynamic (EHD) lubricating film is completely developed between piston and liner surfaces. Therefore contact and adhesive wear between the surfaces can be avoided (5). The lubricant film established under normal operating conditions continuously absorbs the combustion heat. In addition, the heat resulting from viscous shearing of lubricant is also accumulated with combustion heat. Consequently, the temperature of lubricant is increased substantially. This results in reduction of lubricant viscosity, the thickness of its film and hydrodynamic load carrying capacity. On the other hand sufficient quantity of lubricating oil is not available at initial engine startup. This is due to the fact that a mechanical pump starts sending the lubricant to the piston and rings with the startup of an engine (5). Since engine speeds are very low at the startup, lubricant flow rate is also low at this stage. Due to delay in supply of oil there is a momentary dry sliding of piston in the cylinder bore resulting in metal to metal contact of interacting surfaces. Absence of completely established EHD film due to partially flooded conditions and low hydrodynamic pressures result in ineffective, boundary lubrication at initial startup. In boundary lubrication regime the contact between asperity peaks of the two opposing surfaces cannot be prevented (5). As the engine continues its operation, continuous supply of lubricant strengthens the partially

developed thin layer of lubricant film and its thickness starts increasing. When the lubricant film attains the thickness of a few microns, some of the asperities of opposing piston skirt-liner surfaces are completely separated. The boundary lubrication regime changes to one of partial or mixed lubrication as the opposing surfaces are partially separated from each other. Adhesive wear of the sliding surfaces of piston and liner can be partially avoided in the mixed lubrication regime. When flooding conditions are achieved, the mixed lubrication regime changes into rigid hydrodynamic lubrication. In hydrodynamic lubrication regime, hydrodynamic pressures developed due to wedging action between non-parallel surfaces of piston and liner are sufficient enough to completely separate the opposing surfaces. Another important characteristic of initial engine startup is high secondary transverse piston oscillations. There are many factors which are responsible for generation of these high oscillations. High piston to bore radial clearance, ambient viscosity of the lubricant, absence of complete EHL film due to limited lubricant supply, the forces of adhesion and surface energy at the interface and secondary piston displacements are some of the important factors that contribute towards generation of relatively high oscillations.

1.9 Initial Engine Startup Conditions

There are many phases in initial engine startup operation. Operating conditions vary for each phase. A brief description of operating conditions at each phase is given below:

1.9.1 *Engine Cranking:*

Initially an engine is cranked by a motor at 300-400 rpm for 2 to 3 seconds.

1.9.2 *Very Low Speed Engine Startup*

After cranking, engine starts up at very low speed of 500 to 600 rpm for 5 to 6 seconds.

1.9.3 *Low Speed Engine Startup*

In initial few seconds after very low speed startup, the air-fuel ratio of lean mixture and lubricant flow improves slightly, thereby decreasing the kinetic friction. The engine startup speed increases and achieves a range of 700-1000 rpm. Time duration of this phase is from 5 to 15 seconds.

1.9.4 ***Low Speed Engine Warm-up***

After a few seconds of engine startup operation, the air-fuel ratio is improved further. Consequently, the volumetric efficiency is improved slightly and accumulation of some combustion heat reduces the radial clearance to some extent. As a result, the startup speed increases to attain a new range of 1100 to 1400 rpm. The engine operates in this speed range for 15 to 30 seconds.

1.9.5 ***High Speed Engine Warm-up***

Normally the air intake passage of an IC Engine is closed by automatic choke and speed control in order to bring an engine to its normal operating conditions, relatively quickly. Consequently air-fuel mixture becomes richer with time. The thermal loads on piston and liner surface increase with the engine startup speed due to corresponding increase in volumetric and thermal efficiencies. The effect of increase in thermal loads at low warm-up speed enhances the low warm-up speed further to attain the speeds in high warm-up range of 1500-2000 rpm. The engine operates at this speed range for 15 to 30 seconds.

1.9.6 ***Idling Speed Engine Startup***

After running at high warm-up speed for a few seconds, the engine becomes close to normal operating temperatures. The air intake passage starts opening in order to avoid accumulation of excessive heat and air-fuel ratio changes correspondingly. The mixture become less rich in fuel and after few more seconds the speed is initially reduced to 1200-1300 rpm and then further reduced to around 1000 rpm. At this stage, the engine attains the predefined normal operating temperature and the speed drops to 800-900 rpm. The air-fuel mixture is neither lean nor rich and radial clearance decreases resulting in effective sealing and reduced secondary transverse piston oscillations. This is the idling engine speed range when piston has achieved normal operating conditions at the low loads (5).

During engine startup cycle, lubrication performance parameters, including film thickness, hydrodynamic pressures and load carrying capacity vary at each speed. Such changes affect the viscosity of the lubricant. The viscosity-grade of the lubricant is also significant in initial engine startup. Therefore different lubricants are categorized as very low viscosity, low viscosity, fairly

viscous and high viscosity grade lubricants for parametric studies which are part of this research work.

Initial engine startup conditions at various phases are summarized in table given below (5):

Phases of initial Engine Startup operation	**Time of operation**	**Engine Startup speeds**	**Piston to Bore Radial Clearance**
Engine Cranking	2 to 3 Seconds	300 - 400 rpm	100-90 micron
Very low Speed Engine Startup.	5 to 6 Seconds	500 - 600 rpm	100-90 micron
Low Speed Engine Startup.	5 to 15 Seconds	700 -1000 rpm	90-80 micron
Low Speed Engine Warm-up	15 to 30 Seconds	1100 - 1400 rpm	80-50 micron
High Speed Engine Warm-up.	30 to 90 Seconds	1500-2000 rpm	50-20 micron
Idling Speed Engine Startup		700-800 rpm	20-10 micron

REVIEW OF RELEVANT RESEARCH

In the past an extensive research has been carried out to model the phenomenon of Piston Skirt Lubrication. Rifat Keribar et al presented hydrodynamic lubrication model of Piston Skirts under medium and high speed normal operating conditions (6). The model was based on flooding of the lubricant and it considered effect of different profiles of Piston Skirt and distortion of Liner bore on the lubrication performance. Pawan K. Goenka et al carried out frictional analysis of Piston Skirt Lubrication in mixed and EHL regimes at normal operating speeds. They described various analytical methods for prediction of friction and compared the results of each method with experimental data based on an experimental rig designed for measuring friction of piston assembly under normal operating condition (7). Modeling of Piston Assembly Lubrication under Mixed and EHL Regimes and normal operating speeds was also presented by Xuijie Hu (8) in

his research work. He incorporated secondary piston dynamics and effects of surface roughness in his lubrication model to study the effects of bulk elastic deformations and thermal distortions of piston assembly on lubrication performance. Another very interesting work of Zhu modeled the breakdown of EHL film (9). He concluded that breakdown of film was mainly caused by reduction in speed and viscosity. A mixed lubrication model was presented by Ozgen Akalim et al for determining frictional losses resulting from the contact between piston ring and liner (10). They predicted high cylinder liner wear at top dead centre by generating the asperity contact pressure profile against the crank angle. Chengwei et al used a dimensionless contact parameter to simplify average Reynolds Equation to study partial EHL (11). Dowson and Hamrock gave a detailed discussion of EHL for elliptical contacts (12). They divided EHL regime further in four types and gave dimensionless minimum film thickness parameter equations for each type. Harigaya et al carried out an unsteady thermo hydrodynamic lubrication analysis of piston ring to predict temperature, viscosity and film thickness (13). They concluded that increase in speed resulted in thicker oil film and reduced lubricant viscosity. Experimental work of Hault et al included determining lubricant film thickness on the interface of cylinder wall and piston by using laser fluorescent apparatus (14). They observed that there was not any significant variation in film thickness between compression and exhaust stroke or that between expansion and intake stroke. C.M Taylor carried out an extensive research about frictional and wear losses in an engine (15). He recommended that only by combining the lubrication and wear analysis tribological performance of piston rings assembly could be analyzed.

Some of the researchers have modeled piston lubrication at initial engine startup conditions to investigate the issue of wear of piston, ring and liner surfaces at this phase and understand the factors and dynamics of the system contributing to towards such wear (16) (17). Initial works suggested that improvement in pumpability and lubricant flow rate were the remedy against the startup wear (18) (19) (20) . EHL of Piston Rings with distorted bore was also modeled in order to investigate whether distortion was the major cause of startup wear. This hypothesis was verified experimentally on an engine test bench. A comparison of the results showed that distortion of cylinder bore caused significant reduction in lubricant film thickness (21) (22). Then thermal effects were investigated in the studies at low temperature engine startup

conditions (23) (24). Shear thinning of lubricants considering thermodynamic affects was also considered by some researchers for investigating startup wear (25) (26).

While initial studies (until 1960 and early 1970) of Elastohydrodynamic Lubrication assumed fully flooding conditions at the inlet of lubricated conjunction (27), lubrication under starvation conditions were considered later. Earlier approach adopted to see the influence of partial filling of inlet to an elastohydrodynamic conjunction on pressure and film thickness was based on adopting different starting points for inlet pressure boundary. This approach was first adopted by Orcutt and Cheng (28). Their results showed that film thickness was reduced due to lubricant starvation. A similar approach was adopted by B.J. Hamrock and D. Dowson (29) to investigate the influence of lubricant starvation on minimum film thickness. This study of lubricant starvation was performed by moving the position of inlet meniscus closer to the contact center. They determined an expression for dimensionless inlet distance m□ at the boundary between the fully flooded and starved conditions. For a dimensionless inlet distance, m less than m□, starvation occurs and for m $\geq$ m□, a fully flooded condition exists. . Floberg (30) Wedeven, Evans and Cameron (31) provide experimental evidence supporting the idea that the location of incipient pressure rise is determined by the oil supply. Rajesh Kumar (32) and his co-workers adopted the same approach of shifting the position of inlet meniscus towards the contact zone for analyzing starvation effects in line contacts. Another approach adopted by M.K. Ghosh, B.J. Hamrock and D.E Brew (33) for studying effects of starvation is based on defining the fluid level at the inlet. Starvation is effected by systematically reducing the fluid inlet level. D.E. Brew and B.J. Hamrock (34) have analyzed the effects of lubricant starvation on point contacts. Again the starvation has been effected by varying the fluid inlet level. They determined a film reduction factor as a function of fluid inlet level for varying degrees of starvations. R.J. Bones (35) analyzed the effects of restricted lubricant supply to a roller bearing. He accomplished the theoretical analysis by changing the location of boundary where the pressure begins to build up and noting the effect of hydrodynamic forces. He also verified his findings by experimental method.

Most of the research relevant to lubrication under starvation conditions consider is in conjunction with cavitation phenomenon. This involves defining the boundaries of the cavitated regions and the boundary conditions to be used on them. Hooshang Heshmat (36) has treated starvation in

journal bearing as a free boundary problem analysis and extended it to include temperature effects in starved journal bearings. G. Popovici (37) has followed the approach of Jakobsson and Flodeberg (38), Elord (39), Chevalier (40) and Wijnant (41) to account for starvation in elastohydrodynamically lubricated contacts. The main idea of above works is to define fractional film content (θ) as the ratio between the thickness of the lubricant layer (h_{oil}) and the gap height (h) as follows:

$$\theta(x,y) = \frac{h_{oil}(x,y)}{h(x,y)}$$

This term (θ) is incorporated in Reynolds Equation and boundaries of pressurized region ($\theta = 1$) and cavitated region ($0 \leq \theta \leq 1$) are defined to solve modified Reynolds Equation. E.H. Smith and M-T Ma have developed a flow continuity based algorithm for starved lubrication of a single ring in distorted bore. Brew and Hamrock have suggested a film reduction factor for film thickness of non conforming contacts under starved lubrication (42). Yeau Ren Jeng (43) has derived a set of non linear equations for lubricant supply rate, starved pressure distribution and Dynamic Load for piston rings in order to analyze starved lubrication of ring pack.

RESEARCH OBJECTIVES

From the studies mentioned above, essential insight in the effects of starvation on the performance of elastohydrodynamically lubricated contact is obtained. However information on contacts in real applications like piston skirt-liner conjunction of an IC engine is still needed. The aim of current research was to understand the effect of starvation on piston skirt lubrication at initial engine startup. Mandate of the research includes:

- Understanding the initial engine startup and normal operating conditions.
- Understanding the Starvation Phenomena and factors contributing to it.
- Developing an elastohydrodynamic lubrication model for piston skirt of an IC engine at initial startup under starvation conditions.

In order to have an insight into the effects of starvation on performance of Piston Skirt EHL, Results of starvation model will be compared with those under fully flooded conditions. The

mandate of research work also includes, undertaking a parametric study of important parameters associated with lubrication of piston skirts at initial engine startup, in order to find the optimum conditions for minimizing the effects of starvation.

CHAPTER 2

FUNDAMENTAL CONCEPTS

HYDRODYNAMIC LUBRICATION

Basic principal of Hydrodynamic Lubrication can be explained by considering two fundamental conditions for its occurrence (4):

1. The two surfaces must move relative to each other. The relative velocity of moving surfaces must be sufficient to generate a lubricating film of desired load carrying capacity.
2. The surfaces must be inclined to each other at some angle. If the surfaces are parallel, no pressure will be generated in the lubricating film to support the load.

There are two exceptions to 2nd rule. If the surfaces are parallel to each other, hydrodynamic pressure can still be generated if the surfaces can move towards each other or they are stepped surfaces.

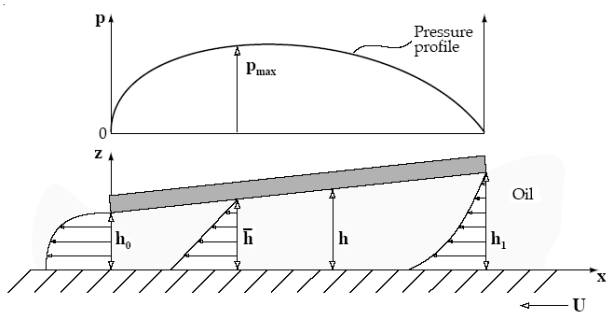

Fig-2.1: Principal of Hydrodynamic pressure generation between non-parallel surfaces. (4)

When these two conditions are met, continuity of lubricant flow between the moving surfaces is disturbed and consequently a pressure is developed inside the lubricant layer to cancel the effect of disturbance. If the relative velocity of moving surfaces is sufficient enough, this pressure can support normal load on these surfaces without allowing the contact between them.

2.1 Reynolds' Equation:

Reynolds Equation is the governing Equation for hydrodynamic pressure generation. It is given by:

$$\frac{\partial}{\partial x}\left(\frac{h^3}{\eta}\frac{\partial p}{\partial x}\right)+\frac{\partial}{\partial y}\left(\frac{h^3}{\eta}\frac{\partial p}{\partial y}\right)=6\left(U\frac{dh}{dx}+V\frac{dh}{dx}\right)+12(w_h-w_o) \qquad (2.1)$$

Where, U and V are relative velocities of lubricated surfaces in axial and transverse directions respectively. 'w_h' and $'w_o'$ are normal velocities of lubricated surfaces and 'h' is film thickness which can be calculated from the geometry of gap between the surfaces.

ELASTOHYDRODYNAMIC LUBRICATION BACKGROUND:

Reynolds' theory was successfully used in design of journal bearings and many other applications. However, there were still many applications which could not be explained by hydrodynamic theory only. For example, life of heavily loaded gears and roller bearing was much longer than expected. The film thickness calculated by hydrodynamic theory was insufficient to carry such huge loads. These observations remained unexplained until the theory of elastohydrodynamic lubrication emerged. According to this theory dramatic increase in load carrying capacity in such applications was due to piezo-viscous effects. Under huge pressures interacting surfaces of the lubricated conjunction deform elastically and viscosity of lubricant entrapped between the surfaces rises exponentially. Therefore elastohydrodynamic involve essentially the incorporation of three effects.

1. Hydrodynamics
2. Elastic deformation of the metal surfaces
3. Increase in the viscosity of oil under extreme pressures

LUBRICATION UNDER STARVATION CONDITIONS:

Starved lubrication is the lubrication under limited supply of lubricant. A lubricated contact is said to suffer from starvation when the lubricant is insufficient to completely fill the contact inlet.

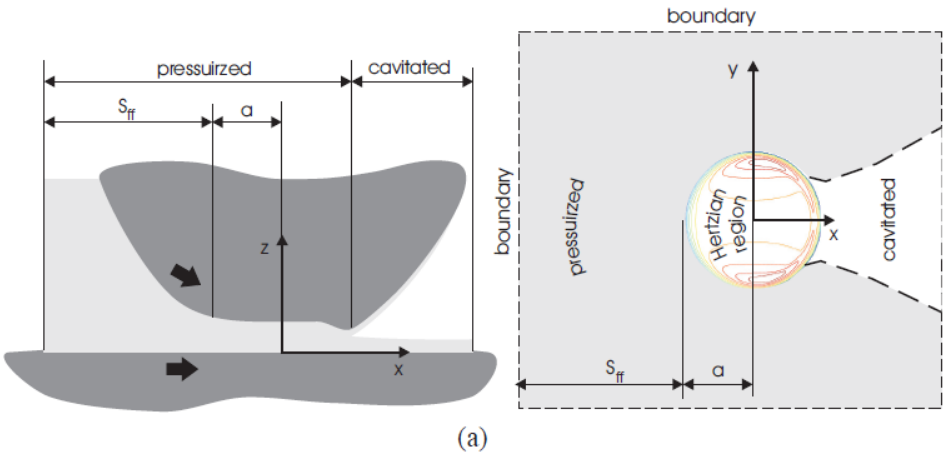

Fig-2.1: A Fully Flooded EHL Contact (37)

An elastohydrodynamically lubricated contact under fully flooded conditions is shown in Fig-2.1. The inlet of contact is completely filled with the lubricant and the entire inlet region is pressurized. In case of starvation conditions the inlet of contact is partially filled with lubricant as shown in Fig-2.2. Inlet region is partially pressurized and partially cavitated.

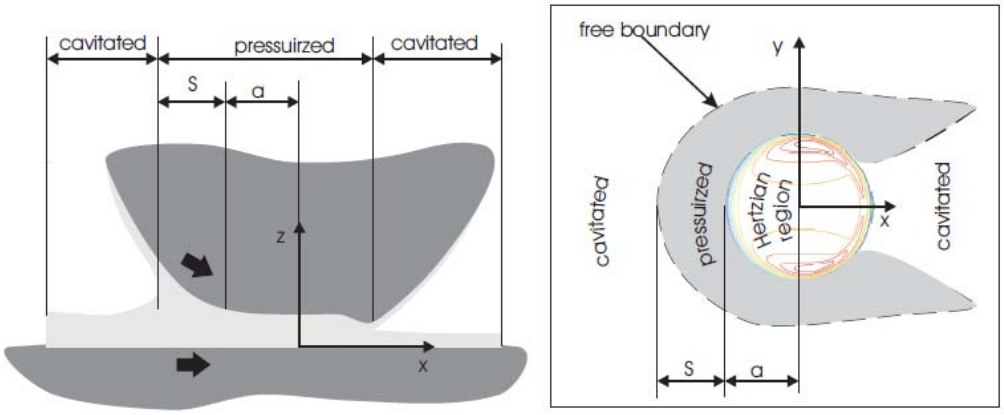

Fig-2.2: A Fully Flooded EHL Contact (37)

Starvation occurs mainly due to short lubricant supply at startup. We know it is only with the engine startup that mechanical oil pump starts sending engine oil to all critical parts including piston and rings. Due to initial non availability of oil, piston skirt operates under starved lubrication conditions. Also at very high engine speeds lubricant supply rate from oil pump is not adequate to fill the lubricated conjunction. Starvation essentially affects the film thickness and

load carrying capacity of lubricated conjunction. As mentioned earlier piston skirt operates under starvation conditions at startup and to some extent at different points in its operating strokes, starvation is major source of frictional losses and piston wear. Complete understanding and control of starvation phenomenon, is therefore quiet essential for improving performance and life of an automobile engine. Reynolds' Equation has inherent assumption that lubricant is available abundantly at the inlet of contact region. Therefore it is applicable for fully flooded conditions only. For starvation conditions effect of lubricant supply rate must be incorporated in Reynolds' Equation.

2.2 **Degree of Starvation:**

Level of starvation in a lubricated conjunction is defined in terms of Degree of Starvation. The degree of starvation is defined as the fractional loss in the mass flow rate.

$$DOS = 1 - \frac{q_s}{q_{ff}}$$

Where, q_s is lubricant mass flow rate under starvation conditions and q_{ff} is mass flow rate under full flooding condition.

CHAPTER 3

MATHEMATICAL MODELING

MATHEMATICAL MODELING OF PISTON SKIRT LUBRICATION

3.1 As discussed earlier, elastohydrodynamic lubrication is combination of three phenomenons:

1. Hydrodynamics.
2. Elastic deformation of lubricated surfaces under huge loads.
3. Change in lubricant viscosity due to piezoviscous effects

Piston Skirt Lubrication model will essentially be based on hydrodynamic model, accounting for surface deformations and piezoviscous effects. Hydrodynamic model for piston skirt cannot be developed without considering piston dynamics, as it is the position and velocity of piston skirt at any instance, which governs hydrodynamic pressures and film thickness being developed. Therefore a complete piston dynamics model was also developed in conjunction with Reynolds equation based hydrodynamic model. For starvation conditions, a modified form of Reynolds equation, incorporating lubricant supply rate at the inlet, has been used. Lubricant supply rate is calculated from flow rate at full flooding condition. By multiplying full flooding flow rate with a factor, based on degree of starvation, lubricant supply rate under starvation conditions can be calculated. Therefore separate hydrodynamic models for full flooding and starved conditions were developed. Hydrodynamic pressure and film thickness are then modified to account for surface deformations and piezoviscous effects. An over view of these sub-models is given below:

3.2 Piston Dynamics Model

Piston dynamic model consists of governing equations for its motion in cylinder liner under the action of combustion forces. The approach adopted for developing piston dynamics model is that of Dong Zhu et al (9). According to Zhu the motion of piston can be categorized in two types. Reciprocating motion along the axis of cylinder liner, which is referred to as primary piston dynamics and transverse motion, normally known as secondary piston dynamics.

A schematic diagram showing all the forces and moments acting on piston is given below:

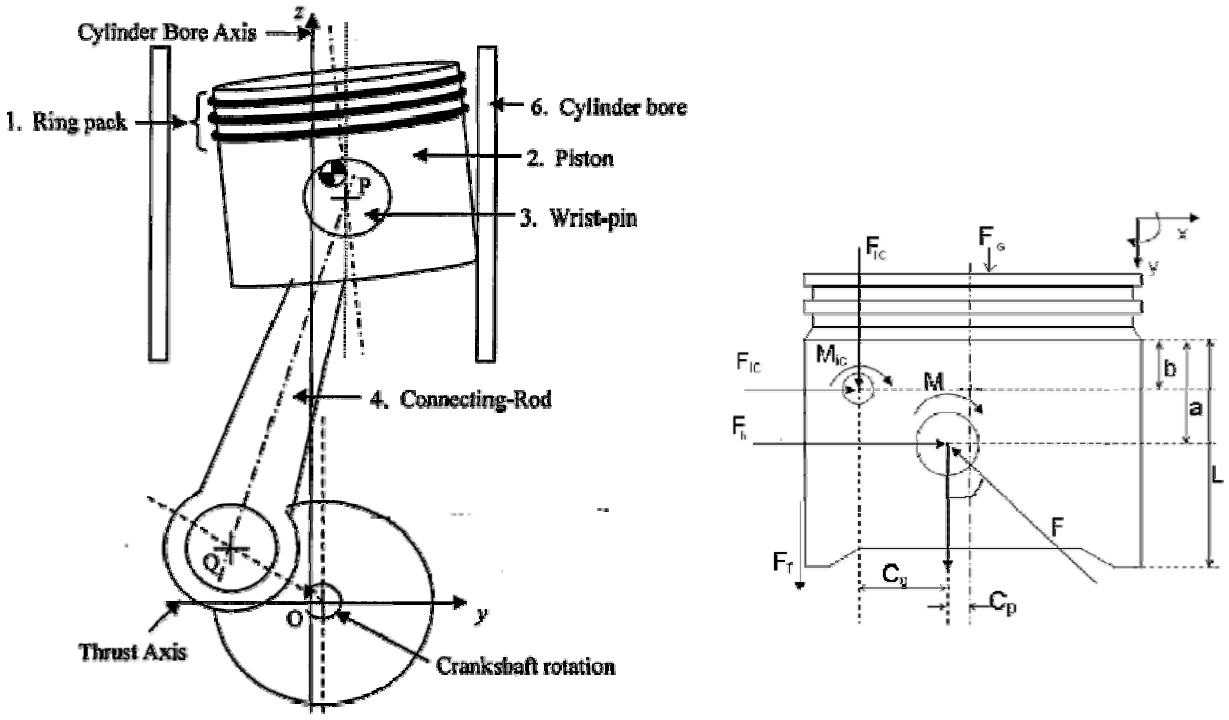

Fig-3.1: Schematic of Piston Cylinder System (2)

Position, velocity and acceleration of the piston related to primary dynamics are given by the relations:

$$Y = \left((l+r)^2 - C_P^2\right)^{0.5} - \left(l^2 - B^2\right)^{0.5} - r\cos\psi \tag{3.1}$$

$$V = \dot{Y} = r\omega\sin\psi + r\omega B\cos\psi\left(l^2 - B^2\right)^{-0.5} \tag{3.2}$$

$$\ddot{Y} = r\omega^2\cos\psi + \left(r\omega B\cos\psi\right)^2\left(l^2 - B^2\right)^{-1.5} + \left(\left(r\omega\cos\psi\right)^2 - r\omega^2 B\sin\psi\right)\left(l^2 - B^2\right)^{-0.5} \tag{3.3}$$

In equation 3.1, is the connecting rod length, crank radius, is the crank angle and is given by:

(3.4)

$'C_P'$ being the distance of the piston-pin from the axis of piston and 'ϕ' the connecting rod angle. Reciprocating motion of piston in cylinder liner is due to inertial forces. The inertial forces due to masses of piston pin and the piston $\overline{F}_{IP}$ and $\overline{F}_{IC}$ are given by:

$$F_{IP} = -m_{Pin}\ddot{Y} \tag{3.5}$$

$$F_{IC} = -m_{Pis}\ddot{Y} \tag{3.6}$$

In equation 3.5, $'m_{Pin}'$ is mass of piston pin and $'m_{Pis}'$ in equation 3.6 is the mass of piston. Secondary piston dynamics is characterized by piston's top and bottom eccentric positions $'e_t', 'e_b'$ eccentric velocities e_t^o, e_b^o and eccentric accelerations, $\ddot{e}_t$ and $\ddot{e}_b$

Applying equilibrium of all the forces and moments shown in Fig-3.1

$$F_G + F_f + \overline{F}_{IP} + \overline{F}_{IC} + \overline{F}\cos\phi = 0 \tag{3.7}$$

$$F + F_{IP} + F_{IC} - \overline{F}\sin\phi = 0 \tag{3.8}$$

$$M + M_{IC} + F_{IC}(a-b) - \overline{F}_{IC}C_g + F_G C_P + M_f = 0 \tag{3.9}$$

In equation 3.7 'F_G' is combustion gas force which acts on the top of piston 'F_f' is frictional force, 'M_f' frictional moment about piston pin. M_{fh} hydrodynamic friction moment about piston pin. C_g is horizontal distance between piston pin and piston centre of mass and C_p is the distance between piston pin and axis of piston. 'a' is the vertical distance from top of piston skirt to piston pin, 'b' is the vertical distance from top of piston skirts to piston center of gravity. From equations 3.7 and 3.8, eliminating the connecting rod force $\overline{F}$, we get:

$$-F_{IP} - F_{IC} = F_S + F_h + F_{fh}\tan\phi \tag{3.10}$$

The moment equation 3.9 can be rearranged to give:

$$-M_{IC} - F_{IC}(a-b) = M_s + M_h + M_{fh} \tag{3.11}$$

F_s and M_s in equation 3.10 and 3.11 can be given as:

$$F_S = Tan\,\phi\left(F_G + \overline{F}_{IP} + \overline{F}_{IC}\right) \tag{3.12}$$

$$M_S = F_G C_P - \overline{F}_{IC} C_g \tag{3.13}$$

The connecting rod angle is calculated by:

$$\emptyset = \tan^{-1}[B(l^2 - B^2)^{-0.5}] \tag{3.14}$$

Secondary piston dynamics equation is given by:

$$M_{IC} = {-I_{pis}\left(\ddot{e}_t - \ddot{e}_b\right)}\Big/{L} \tag{3.15}$$

In equation 3.15, I_{pis} is the rotary inertial of the piston about its center of mass and L is the length of skirt. Equation 3.5 and 3.6 are governing equations for primary piston dynamics and equation 3.15 for secondary dynamics. Putting equation 3.5, 3.6 and 3.15 into equations 3.10 and 3.11 we get final equations of piston dynamics which can be simplified to matrix form as given below:

$$\begin{bmatrix} m_{pin}\left(1-\frac{a}{L}\right)+m_{pis}\left(1-\frac{b}{L}\right) & m_{pin}\frac{a}{L}+m_{pis}\frac{b}{L} \\ \frac{I_{pis}}{L}+m_{pis}(a-b)\left(1-\frac{b}{L}\right) & m_{pis}(a-b)\frac{b}{L}-\frac{I_{pis}}{L} \end{bmatrix}\begin{bmatrix} \ddot{e}_t \\ \ddot{e}_b \end{bmatrix} = \begin{bmatrix} F + F_S + F_f \tan\phi \\ M + M_S + M_f \end{bmatrix} \tag{3.16}$$

In equation 3.16, 'F' and 'M' are the total normal force and moments acting on piston skirts. Total normal force is obtained by sum of hydrodynamic force. 'F_h' and hydrodynamic frictional force 'F_{fh}'. Likewise total normal moment 'M' is the sum of hydrodynamic force moment 'M_h' and frictional hydrodynamic moment 'M_{fh}'. These are given by:

$$F_h = R\iint_A p(\theta, y)\cos\theta\, d\theta dy \tag{3.17}$$

$$M_h = R\iint_A p\,(\theta, y)(a-y)\cos\theta\, d\theta dy \tag{3.18}$$

$$F_{fh} = R\iint_A \left(\eta\frac{U}{h} + \frac{h}{2}\frac{dp}{dy}\right) d\theta dy \tag{3.19}$$

$$M_{fh} = R \iint_A \left(\eta \frac{U}{h} + \frac{h}{2}\frac{dp}{dy}\right)(R\cos\theta - C_p)d\theta dy \quad (3.20)$$

In above relations $p(\theta, y)$ is the hydrodynamic pressure, generation of which is governed by Reynolds' Equation.

STEADY STATE HYDRODYNAMIC LUBRICATION MODEL:

Steady state hydrodynamic lubrication model consists of Steady Reynolds' Equation and film thickness equation.

3.3 Reynolds' Equation:

Hydrodynamic pressures are obtained by solving the Steady State Reynolds equation, given by:

$$\frac{\partial}{\partial x}\left(\frac{h^3}{12\eta}\frac{\partial p}{\partial x}\right)+\frac{\partial}{\partial y}\left(\frac{h^3}{12\eta}\frac{\partial p}{\partial y}\right)=\frac{1}{2}U\frac{\partial h}{\partial x} \quad (3.21)$$

Pressure obtained from the solution of (3.25) will be used in equations (3.19 & 3.20) to determine 'F_h and 'M_h'.

3.4 Film Thickness Equation:

In Reynolds' Equation, '*h'* is the hydrodynamic film thickness which is given by the gap height between the lubricated surfaces. Gap height equation is given by:

$$h = C + e_t\cos(x_1) - (e_t - e_b)y_1\cos(x_1) \quad (3.22)$$

In above equation e_t and e_b are piston top and bottom eccentricities which are given by piston dynamics model and 'C' is the piston to bore radial clearance.

UNSTEADY HYDRODYNAMIC LUBRICATION MODEL:

Unsteady hydrodynamic lubrication model consists of unsteady Reynolds' equation and film thickness equation.

3.5 Transient Reynolds Equation:

Transient Reynolds equation includes an additional time dependent squeeze term and is given by:

$$\frac{\partial}{\partial x}\left(h^3\frac{\partial p_u}{\partial x}\right)+\frac{\partial}{\partial y}\left(h^3\frac{\partial p_u}{\partial y}\right)=6\eta U\frac{\partial h}{\partial x}+12\eta\frac{\partial h}{\partial t} \tag{3.23}$$

3.6 Transient Hydrodynamic Film Thickness Equation:

In the hydrodynamic lubrication regime, film thickness is given by the contact geometry profile which is mathematically defined as:

$$h=C+e_t\cos(x_1)-(e_t-e_b)y_1\cos(x_1) \tag{3.24}$$

Under the unsteady conditions, the film thickness becomes time dependent. The time dependent term is called squeeze velocity and is given by: $\frac{\partial h}{\partial t}=\cos\theta\left[e_t^o\left(1-\frac{y}{L}\right)+e_b^o\left(\frac{y}{L}\right)\right]$

(3.25

Steady State Hydrodynamic Lubrication Model for Starvation Conditions:

3.7 Starved Film Thickness Equation:

For starvation conditions, full flooding hydrodynamic film thickness is reduced by a factor, β (42). This factor β is given by:

$$\beta=\left[1+3.02\sqrt{H_f}\left\{\left(\frac{2-H_{in}}{H_{in}}\right)^{1/2}e^{(H_{in}-1)}-1\right\}\right]^{-2} \tag{3.26}$$

Where, H_{in} is Fluid level at inlet of lubricated conjunction and H_f is dimensionless hydrodynamic film thickness under flooding conditions. For minor starvation levels hydrodynamic pressure distribution along axial direction is affected only. Equation for one dimensional pressure distribution is derived from 1-D Reynolds Equation using the same procedure as adopted by Yeau-Ren Jeng (43). The equation is

$$p(x,t) = 12\eta \int_{x_i}^{x} \frac{1}{h^3}\left[\frac{U}{2}h + \frac{\partial h}{\partial t}(x - x_i) - q_{sx}\right]dx \tag{3.27}$$

This equation has one additional parameter, q_{sx} lubricant supply rate in axial direction. It is given by

$$q_{sx} = \frac{u}{2}h + \frac{\partial h}{\partial t}(L - x_i) \tag{3.28}$$

Where, x_i is incipient pressure rise position. Due to starvation the start point of film thickness is shifted away as compared to that at fully flooded conditions. This distance x_i is given by the relation (3.30) for lubricant supply rate.

UNSTEADY HYDRODYNAMIC LUBRICATION MODEL FOR STARVATION CONDITIONS:

For more severe starvation, hydrodynamic pressure distribution in both the axial and circumferential directions is affected. The variation of hydrodynamic pressure in circumferential direction, in this case is due to time dependent squeeze velocity term, $\frac{\partial h_t}{\partial t}$. This term was ignored in full flooding conditions model. Since this term affects the hydrodynamic pressure distribution in circumferential direction only, it will be obtained by applying Reynolds equation in circumferential direction. There is no relative velocity in this direction therefore Reynolds equation is reduced to:

$$\frac{\partial}{\partial y}\left(\frac{h^3}{12\eta}\frac{\partial p}{\partial y}\right) = \frac{\partial h_t}{\partial t} \tag{3.32}$$

Final relation for two dimensional pressure distributions for a given lubricant supply rate under starvation conditions is given by:

$$p(x,y,t) = 12\eta \int_{x_i}^{x} \int_{y_i}^{y} \frac{1}{h^3} \left[\frac{U}{2} h + \frac{\partial h}{\partial t}(x - x_i) - q_{sx} + \frac{\partial h}{\partial t}(y - y_i) - q_{sy} + \frac{\partial \mathrm{h_t}}{\partial \mathrm{t}} \right] dydx \tag{3.33}$$

Where, q_{sy} is lubricant supply rate in transverse direction. y_i is starting point of pressure rise and can be calculated for a given lubricant supply rate, by the relation

$$q_{sy} = \frac{\partial h}{\partial t}(y - y_i) \tag{3.34}$$

CHAPTER 4

COMPUTATION METHODOLGY

NUMERICAL SOLUTION OF STEADY STATE REYNOLDS' EQUATION

4.1 Non-dimensionalization of Reynolds Equation

As shown earlier Reynolds' Equation is given by:

$$\frac{\partial}{\partial x}\left(\frac{h^3}{12\eta}\frac{\partial p}{\partial x}\right)+\frac{\partial}{\partial y}\left(\frac{h^3}{12\eta}\frac{\partial p}{\partial y}\right)=\frac{1}{2}U\frac{\partial h}{\partial x} \tag{4.1}$$

In above relation, 'p' is the hydrodynamic pressure generated due to relative velocity 'U' of lubricated surfaces. 'h' is thickness of the lubricant film at lubricated conjunction and 'η' is dynamic viscosity of the lubricant.

Reynolds' Equation is non-dimensionalized in order to extend the generality of solution. Non-dimensionlization is the substitution of all real variables in an equation by dimensionless fractions of two or more real parameters. The procedure used by Stachowiak and Batchelor [4] has been adopted for non-dimensionlization of Reynolds' Equation. Major benefit of non-dimensionlization is that the number of controlling parameters in an equation is reduced. Non-dimensional forms of real variables in Reynolds equation are:

$$H=\frac{h}{C}$$

$$X=\frac{x}{R}$$

$$Y=\frac{y}{L}$$

$$P=\frac{pC^2}{6U\eta R}$$

Using above non dimensional real variables, non-dimensional form of Reynolds equation is given by:

$$\frac{\partial}{\partial X}\left(H^3\frac{\partial P}{\partial X}\right)+\left(\frac{R}{L}\right)^2\frac{\partial}{\partial Y}\left(H^3\frac{\partial P}{\partial Y}\right)=\frac{\partial H}{\partial X} \tag{4.2}$$

4.2 Vogelpohl Form of Reynolds Equation

For numerical solution of Reynolds' Equation its Vogelpohl form is used. One of the advantages of using the Vogelpohl form is improvement in accuracy of the solution. The Vogelpohl parameter $'M_V'$ is defined as follows:

$$M_V = PH^{1.5}$$

Substitution of this parameter into non-dimensionalized form of Reynolds' Equation yields the Vogelpohl equation.

$$\frac{\partial^2 M_V}{\partial X^2}+\left(\frac{R}{L}\right)^2\frac{\partial^2 M_V}{\partial Y^2}=FM_V+G \tag{4.3}$$

Where

$$F=\frac{0.75\left[\left(\frac{\partial H}{\partial X}\right)^2+\left(\frac{R}{L}\right)^2\frac{\partial^2 H}{\partial Y^2}\right]}{H^2}+\frac{1.5\left[\left(\frac{\partial H}{\partial X}\right)^2+\left(\frac{R}{L}\right)^2\frac{\partial^2 H}{\partial Y^2}\right]}{H}$$

And

$$G=\frac{\partial H/\partial X}{H^{1.5}}$$

4.3 Film Thickness Equation

Film thickness 'h' of lubricant film is given by geometry of gap between the lubricated surfaces. That is why film thickness equation is also called, gap height equation.

NUMERICAL SOLUTION OF UNSTEADY REYNOLDS' EQUATION

Transient Reynolds Equation is given by:

$$\frac{\partial}{\partial x}\left(h^3\frac{\partial p_u}{\partial x}\right)+\frac{\partial}{\partial y}\left(h^3\frac{\partial p_u}{\partial y}\right)=6\eta U\frac{\partial h}{\partial x}+12\eta\frac{\partial h}{\partial t} \tag{4.4}$$

4.4 Non-Dimensionalization of Unsteady Reynolds Equation

The non dimensional form of unsteady Reynolds Equation is:

$$\frac{\partial}{\partial X}\left(H^3\frac{\partial P}{\partial X}\right)+\left(\frac{R}{L}\right)^2\frac{\partial}{\partial Y}\left(H^3\frac{\partial P}{\partial X}\right)^2+\frac{\partial H}{\partial Y}+2\frac{\partial H}{\partial T} \tag{4.5}$$

4.5 Vogelpohl Form of Reynolds Equation

Vogelpohl Form of Reynolds Equation is obtained by the substitution

$$PH^{1.5}=M_{un}$$

Substitution of this parameter, 'M_{un}' into non-dimensional form of Unsteady Reynolds Equation yields the Vogelpohl equation.

$$\frac{\partial}{\partial X^2}(M_{un})+\left(\frac{R}{L}\right)^2\frac{\partial}{\partial Y^2}\left(H^3\frac{\partial PM_{un}}{\partial X}\right)^2=MN+G \tag{4.6}$$

Where

$$F=\frac{0.75\left[\left(\frac{\partial H}{\partial X}\right)^2+\left(\frac{R}{L}\right)^2\frac{\partial^2 H}{\partial Y^2}\right]}{H^2}+\frac{1.5\left[\left(\frac{\partial H}{\partial X}\right)^2+\left(\frac{R}{L}\right)^2\frac{\partial^2 H}{\partial Y^2}\right]}{H}$$

And

$$G_{un}=\left(\frac{\frac{\partial H}{\partial Y}+\frac{\partial H}{\partial T}}{H^{1.5}}\right)$$

FINITE DIFFERENCE SCHEME

4.6 The Piston lubrication problem is solved by using the finite difference method. This method is based on approximating a differential quantity by the difference between function values at two or more adjacent nodes. For example, finite difference approximation for $\frac{\partial M_V}{\partial X}$ is given by:

$$\frac{\partial M_V}{\partial X} \approx \frac{M_{V,i+1} - M_{V,i-1}}{2\delta X} \tag{4.7}$$

The subscripts $'i+1'$ and $'i-1'$ represent the positions immediately behind and in front of the central position, $'i'$. And $'\delta X'$ is the step length between nodes in X-direction. This is known as central difference approximation. Similarly, approximation for second differentials can be obtained according to the principal, illustrated in Figure-4.1.

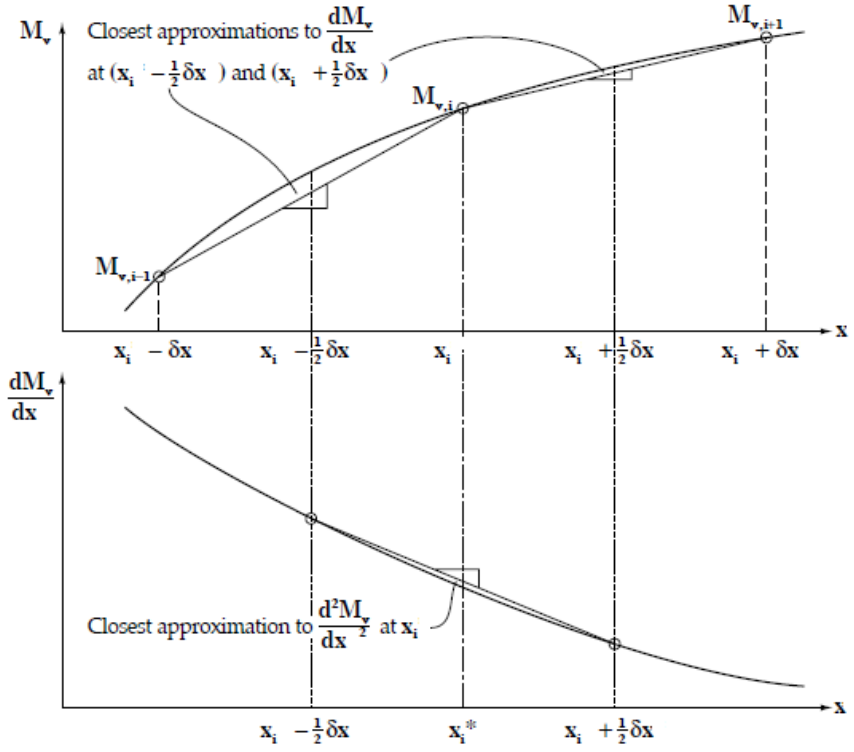

Fig-4.1: Illustration of the principal for the derivation of finite difference approximation of second derivative of a function. (4)

According to above principal, the central difference approximation for $\frac{\partial^2 M_V}{\partial X^2}$ is given by:

$$\frac{\partial^2 M_V}{\partial X^2} \approx \frac{M_{V,i+1} + M_{V,i-1} - 2M_{V,i}}{(\delta X)^2} \tag{4.8}$$

And approximations for partial derivatives with respect to 'Y' are found by considering nodal variation in direction of Y-axis. For this a second nodal position variable ' j ' is introduced along the Y-axis. Central difference approximations for $\frac{\partial M_V}{\partial Y}$ $\frac{\partial^2 M_V}{\partial Y^2}$ are given by:

$$\frac{\partial M_V}{\partial Y} \approx \frac{M_{V,j+1} - M_{V,j-1}}{2\delta Y} \tag{4.9}$$

$$\frac{\partial^2 M_V}{\partial Y^2} \approx \frac{M_{V,j+1} + M_{V,j-1} - 2M_{V,j}}{(\delta Y)^2} \tag{4.10}$$

Where, 'δY' is step length between nodes in Y-direction. The coefficients of 'M_V' at i-th node and adjacent nodes, required by the Reynolds' Equation form a 'finite difference operator' and are conveniently illustrated as a computing molecule as shown in figure below.

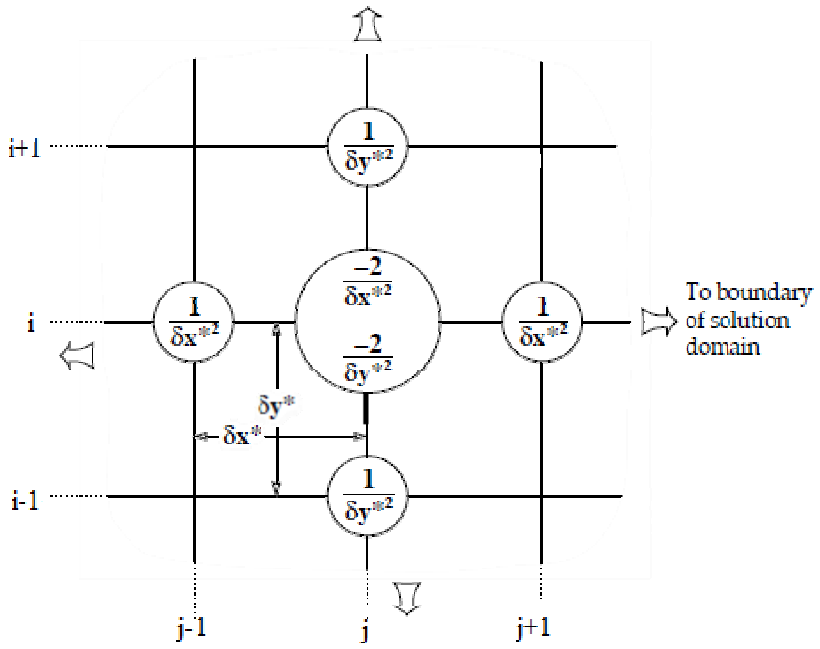

Fig-4.2: Finite Difference Operator and Nodal Scheme for Numerical Analysis of Reynolds' Equation. (4)

This finite difference operator computes for the Vogelpohl parameter throughout the computational domain and does not create any complexity while dealing with boundary conditions. The Only thing which is needed at the boundaries of solution domain is to add an additional set of imaginary nodes outside the boundary. The terms 'F' and 'G' are included with the finite difference operator to form a complete equivalent of Reynolds' Equation.

Final expression for is given by:

(4.11)

Where,

And

$$C_2 = \frac{1}{(\delta Y)^2}$$

PRESSURE CALCULATION UNDER STARVATION CONDITIONS

4.7 1-D Starvation Model

For 1-D Model, hydrodynamic pressure under starvation conditions, at any point, 'x' along the axial direction of Piston Skirt can be found by the relation:

$$p(x,t) = 12\eta \int_{x_i}^{x} \frac{1}{h^3}\left[\frac{U}{2}h + \frac{\partial h}{\partial t}(x - x_i) - q_{sx}\right]dx \tag{4.12}$$

In above equation, q_{sx} is lubricant supply rate in axial direction and x_i is position at which hydrodynamic pressures start rising. For a given supply rate, x_i can be calculated from the relation:

$$q_{sx} = \frac{u}{2}h + \frac{\partial h}{\partial t}(L - x_i) \tag{4.13}$$

The above relations give pressure distribution in axial direction for a given lubricant supply in axial direction. The lubricant supply rate is given by the output of mechanical oil pump, supplying the oil to piston skirt-liner interface. Due to non availability of experimental data, lubricant supply rate under starved conditions is computed from hydrodynamic model under full flooding conditions. A Non-dimensionalized expression for flow rate in axial direction for a given pressure gradient at a nodal point is given by:

$$Q_X = H^3 \frac{\partial P}{\partial X} - \left(\frac{L}{R}\right)H \tag{4.14}$$

Where, $\frac{\partial P}{\partial X}$ is non-dimensional pressure gradient obtained from hydrodynamic model under full flooding conditions and 'H' is non-dimensional film thickness. Actual axial flow rate for fully flooded conditions can be obtained by integration as given below:

$$q_x = -\frac{CUR}{2}\int_0^{R\alpha} Q_X dX \tag{4.15}$$

Where, $'\alpha'$ is skirt angle and $'R'$ is piston radius. This means that lubricant is to be supplied at this rate $'q_x'$ given by relation 4.15, in order to avoid starvation. Let us call it supply rate under flooding conditions $'q_{xf}'$ i.e.

$$q_{xf} = q_x$$

Now for a given degree of starvation the lubricant supply rate is found by reducing the flooding condition supply rate $'q_{xf}'$ by some factor as given below.

$$q_{sx} = (1 - DOS)q_{xf} \tag{4.16}$$

In above relation 'DOS' is the degree of starvation. Using various degrees of starvations, the lubricant supply rates and starvation pressures for different levels of starvations can be calculated.

4.8 2-D Starvation Model

The 2-D Starvation model involves numerical solution for time dependent squeeze velocity term and pressure distribution in circumferential direction. As discussed earlier, the partial differential equation, governing pressure distribution with squeeze velocity is given below:

$$\frac{\partial}{\partial y}\left(\frac{h^3}{12\eta}\frac{\partial p}{\partial y}\right) = \frac{\partial h_t}{\partial t} \tag{4.17}$$

4.9 Finite Differencing Scheme for Solution of Squeeze Velocity Equation

For numerical solution of time dependent squeeze film term we need to discritized equation 4.17 using finite difference approximations. For this purpose an explicit FTCS (Forward Time Central Space) scheme has been used. First order Forward Difference approximation for time dependent squeeze velocity term is given by:

$$\frac{\partial h}{\partial t} = \frac{h_{i,j}^{n+1} - h_{i,j}^{n}}{\delta t}$$

Second order central difference approximation for pressure distribution in circumferential direction is given by:

$$\frac{\partial^2 p}{\partial y^2} = \frac{p^n_{i,j+1} - 2p^n_{I,J} + p^n_{i,j-1}}{(\delta y)^2}$$

Finite difference form of equation 3.14 is given by:

$$\frac{h^{n+1}_{i,j} - h^n_{i,j}}{\delta t} = \frac{h^3}{12\eta}\left(\frac{p^n_{i,j+1} - 2p^n_{I,J} + p^n_{i,j-1}}{(\delta y)^2}\right) \tag{4.18}$$

Since 'h' and η are constants, let $C_1 = \frac{h^3}{12\eta}$

$$h^{n+1}_{i,j} - h^n_{i,j} = \frac{C_1 \delta t}{(\delta y)^2}\left(\frac{p^n_{i,j+1} - 2p^n_{I,J} + p^n_{i,j-1}}{(\delta y)^2}\right)$$

$$h^{n+1}_{i,j} = h^n_{i,j} + \frac{C_1 \delta t}{(\delta y)^2}\left(\frac{p^n_{i,j+1} - 2p^n_{I,J} + p^n_{i,j-1}}{(\delta y)^2}\right) \tag{4.19}$$

Once the solution is converged, squeeze velocity can be obtained as under

$$\frac{\partial h}{\partial t_t} = \frac{h^{n+1}_{i,j} - h^n_{i,j}}{\delta t}$$

Pressure distribution in axial and circumferential direction can be added to calculate net pressure distribution. The final relation for 2-D Pressure variation under starvation conditions is given by:

$$p(x,y,t) = 12\eta \int_{x_i}^{x}\int_{y_i}^{y} \frac{1}{h^3}\left[\frac{U}{2}h + \frac{\partial h}{\partial t}(x - x_i) - q_{sx} + \frac{\partial h}{\partial t}(y - y_i) - q_{sy} + \frac{\partial \mathrm{h_t}}{\partial \mathrm{t}}\right] dy dx \tag{4.20}$$

Where, q_{sy} is lubricant supply rate in transverse direction. y_i is starting point of pressure rise and can be calculated for a given lubricant supply rate, by the relation

$$q_{sy} = \frac{\partial h}{\partial t}(y - y_i) \tag{4.21}$$

Again lubricant supply rates in axial and circumferential direction is calculated from full flooding hydrodynamic pressure distribution. Axial and circumferential flow rates are given by:

$$q_x = -\frac{CUR}{2}\int_0^{R\alpha} Q_X dX \tag{4.22}$$

$$q_y = \frac{-CUR}{2}\int_0^{L} Q_Y dY \tag{4.23}$$

Where Q_X and Q_Y are non dimensional axial and circumferential flow rate and are given by:

$$Q_X = H^3 \frac{\partial P}{\partial X} - \left(\frac{L}{R}\right) H \tag{4.24}$$

$$Q_Y = H^3 \frac{\partial P}{\partial Y} \tag{4.25}$$

Flow rates q_x and q_y are equal to lubricant supply rate in axial and circumferential directions q_{fx} and q_{fy} under full flooding conditions. Lubricant supply rates for given starvation conditions are given by:

$q_{sx} = (1 - DOS) q_{fx}$ and

$q_{sy} = (1 - DOS) q_{fy}$

From above relations lubricant supply rates in axial and circumferential direction can be found for a given degree of starvations. From these supply rates start points are found by using the relations. Consequently the pressure distribution for starvation conditions can be obtained.

SOLUTION DOMAIN AND BOUNDARY CONDITIONS

4.10 Solution domain for piston skirt lubrication mode consists of the piston skirt dimensions over which hydrodynamic pressures are generated. Boundary conditions can be defined as the computational variable 'M_V' and hence the hydrodynamic pressure has zero values at the edges of piston skirt surface. Also there is no negative pressure inside the domain as cavitation phenomenon is allowed. Range of circumferential dimension 'Y' is between $(0 - R\alpha)$ where α is skirt angle and is taken 75^o for combined length of both skirts of piston. The range of axial dimension 'X' is from 0 to 1. The whole piston skirt area is shown below:

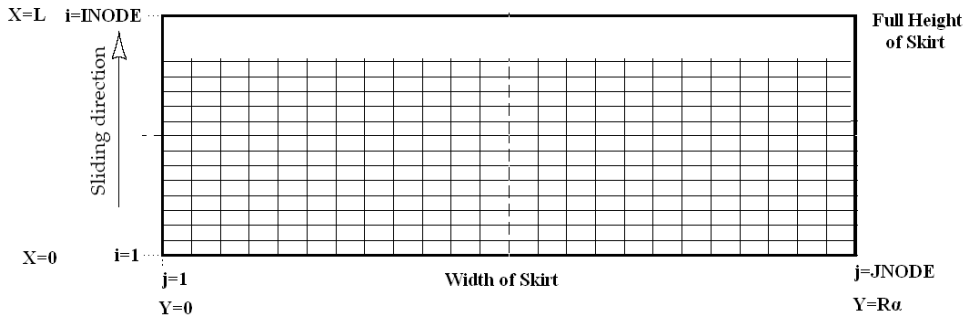

Fig-4.3: Nodal Pressure or Vogelpohl Parameter domain for Finite Difference Analysis of Piston Skirt.

According to boundary conditions, all the nodes at edges of the surface have zero values for the computed variable and others require solution / computation by difference approximation method. Point to be noted is that more accurate operators than "Vogelpohl" are available but they are difficult to apply as these require extra nodes outsides the solution domain.

NUMERICAL SOLUTION FOR PISTON SKIRT EHL

4.11 For EHD regime, hydrodynamic film thickness equation is modified in order to account for bulk elastic deformation of lubricated surfaces [19]. Final form of EHD film thickness equation is given by:

$$h_{ehl} = h + f(\theta, y) + \nu \tag{4.26}$$

Where, 'h' hydrodynamic film thickness and is calculated by gap height equation. $f(\theta, y)$ defines the skirt surface profile due to manufacturing imperfections and 'ν' is surface deformation. The term $f(\theta, y)$ is usually neglected and surface deformation 'ν' is calculated from equation, given below

$$d\nu = \frac{1}{\pi \acute{E}} \frac{p(x,y)dxdy}{\acute{r}} \tag{4.27}$$

$$\text{Where } \acute{r} = \sqrt{(x - x_o)^2 - (y - y_o)^2} \tag{4.28}$$

$$\text{And} \quad \frac{1}{\acute{E}} = \frac{1}{2}\left[\frac{1-\nu_1^2}{E_1} + \frac{1-\nu_2^2}{E_2}\right] \tag{4.29}$$

Elastic deformation at a particular point (x_o, y_o) can be calculated from the relation:

$$v(x_o\ , y_o) = \frac{1}{\pi \acute{E}} \iint_A \frac{p(x,y)dxdy}{\acute{r}} \tag{4.30}$$

In EHD regime, the pressures rise tremendously. This high pressure drastically affects the viscosity of lubricant. Exponential rise in lubricant viscosity, under high pressure is given by Barus Equation [19].

$$\eta = \eta_o e^{\alpha P} \tag{4.31}$$

Where, $\eta_o$is ambient viscosity, α is pressure-viscosity cofficient and η is pressure dependent viscosityfor Computational Scheme

4.12 Matlab Code was developed for simulation of Piston Skirt Lubrication at initial engine startup, under starvation conditions. The mathematical model for Piston Skirt Lubrication consists of:

- Piston Dynamics Model
- Hydrodynamic Lubrication Model
- Elastohydrodynamic Lubrication Model
- Starved Lubrication Model

These sub-models are solved iteratively in the form of nested loops. Output of one sub-model loop may be used by another as an input. Integration of these sub-models form the complete lubrication model.

4.13 Piston Dynamics Model formulates a set of differential equations, defining the piston dynamics. Piston dynamics equations are in terms of piston top and bottom eccentricities 'e_t' and 'e_b' respectively and their time derivatives e_t^o, e_b^o , e_{2b} and e_{2t}. Eccentricity parameters 'e_t', 'e_b' give the position of the piston at a particular instant and their first and 2nd order derivatives give velocity and acceleration. The differential equations defining the piston dynamics are solved by Matlab routine, ODE 45. This routine is based on integration of the system of differential equations from time T_0 to T_{FINAL} with initial conditions, Y_0 . Output of the routine is a column

vector of eccentricities and eccentric velocities. These eccentricities are used by hydrodynamic model to define gap height geometry between the lubricated surfaces.

4.14 Hydrodynamic pressure built up in Piston Cylinder conjunction has been calculated by numerical solution of by Reynold's Equation. Finite difference approximation of Vogelpohl form of Reynold's Equation is obtained by 2^{nd} order Central Differencing scheme. The solution of Finite Difference approximation was obtained using Iterative Relaxation method. The solution contains Vogelpohl parameter 'M' which can be used to give pressure distribution for given film thickness under flooding conditions.

4.15 Starvation lubrication model requires lubricant supply rate for given starvation conditions. Lubricant supply rate under flooding conditions is calculated from hydrodynamic pressures and that supply rate is multiplied by some factor to calculate supply rate under given starvation conditions. The flow chart of calculation procedures for piston skirt's EHL is given in Fig-4.4:

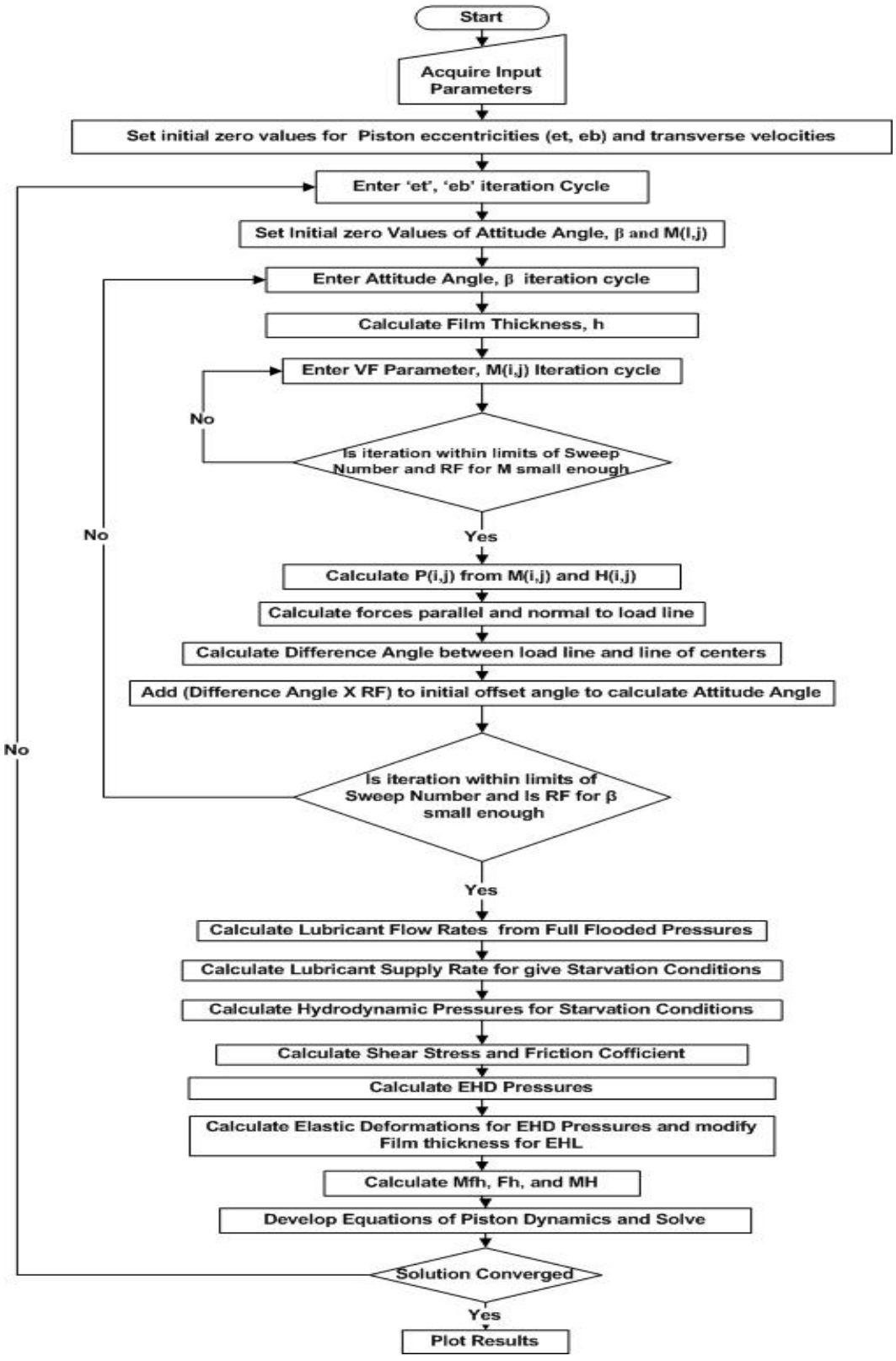

Fig-4.4: Piston Skirt Lubrication Algorithm

CHAPTER 5

SIMULATION AND ANALYSIS

5.1 Mathematical Models of Piston Skirts Lubrication under steady state and transient conditions have been developed, as a mandate of current research. The Effects of starvation are studied under two categories. For mild starvation under steady state conditions, pressure distribution is effected only in axial direction of the piston. Since the piston does not possess velocity in circumferential direction and effects of normal squeeze velocity are ignored for mild starvation conditions, 1-D starvation model suffices for simulation of Piston Skirts lubrication under such conditions. So initially, 1-D Starvation Model is solved under low engine startup speed conditions and results are compared with those under full flooding conditions.

STEADY STATE LUBRICATION OF PISTON SKIRT UNDER LOW SPEED STARTUP CONDITIONS

5.2 Simulation for steady state lubrication is carried out under low speed start up (N=600 rpm) and mild starvation (Degree of Starvation 0.1) conditions. A small radial clearance (C=10 microns), the lubricant viscosity equal to 0.03187 Pa. Sec., steady state isothermal conditions are assumed and surface roughness effects are neglected. Skirt angle is taken 75^{o} for both the skirts. The cycle of crank rotation starts at zero degree crank angle when piston is at top dead centre. The piston moves downwards in induction stroke and reaches bottom dead centre when crank angle is 180^{o}. The compression stroke is from 181 to 360 degree crank angle and the piston travels from bottom dead centre to top dead centre. The expansion and exhaust strokes are from 361 to 540 and 541 to 720 degree crank angle respectively. Four stroke cycle of piston is completed at 720^{o}. Hydrodynamic pressures are developed over the surface of the skirt during 4-stroke cycle. Variation of Hydrodynamic pressures over the skirts surface is shown by 3-D plots (Fig-5.3, 5.4, 5.5, 5.6). The simulation results are shown by plotting the Film thickness, Piston Eccentricities and secondary velocity profiles against 720^{o} crank rotation cycle (Fig-5.1, 5.2, 5.8, 5.9, 5.10 5.11). Sharp increase in EHD pressures against film thickness and skirt angle is also shown by 3-D plots (Fig-5.7). Brief description of results is given below:

5.3 Film Thickness Profiles

5.3.1 *Hydrodynamic Film*

Comparisons of starved and full flooding hydrodynamic film thickness clearly indicate a significant reduction in hydrodynamic film thickness under starvation conditions. Over all trends in film thickness profiles however, are similar. During first half of induction stroke hydrodynamic film thickness does not rise significantly. This is due to the fact that piston is completely aligned with the cylinder axis in this phase and wedging action is not present. After first half of induction stroke (90^{O} crank angle) the hydrodynamic film thickness starts rising sharply and it continues rising until the end of compression stroke. At the end of compression stroke, when the piston is starting downward motion, combustion of air-fuel mixture takes place. Due to high combustion loads, film thickness drops rapidly and comes close to zero when it starts reforming in the exhaust stroke.

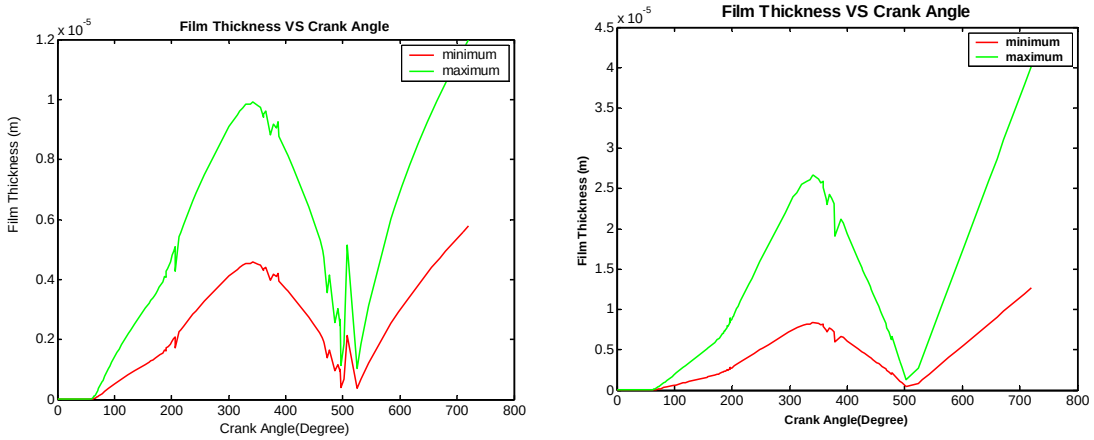

(a) (b)

Fig-5.1: Hydrodynamic Film Thickness (a) 10% Starvation (b) Flooding Condition

5.3.2 *EHD Film*

In EHD Regime, the lubricant film becomes very thin due to large EHD Pressures. However, thin EHD film layer remains present throughout the operating cycle which prevents the physical contact between the interacting surfaces. There is a sharp increase in EHD film at the end of combustion stroke, when the combustion loads are maximum and surface deformations have started taking place. In Fig-5.2, profile of very thin film prior to deformation, under application

of large pressures is shown by ‘hbar’. The EHD film is slightly thicker than ‘hbar’ due to additional space created by surface deformations of interacting surfaces.

EHD Film also shows the similar trends under mild starvation (Degree of Starvation 0.1) and flooding conditions. No significant reduction in EHD Film at mild starvation is observed.

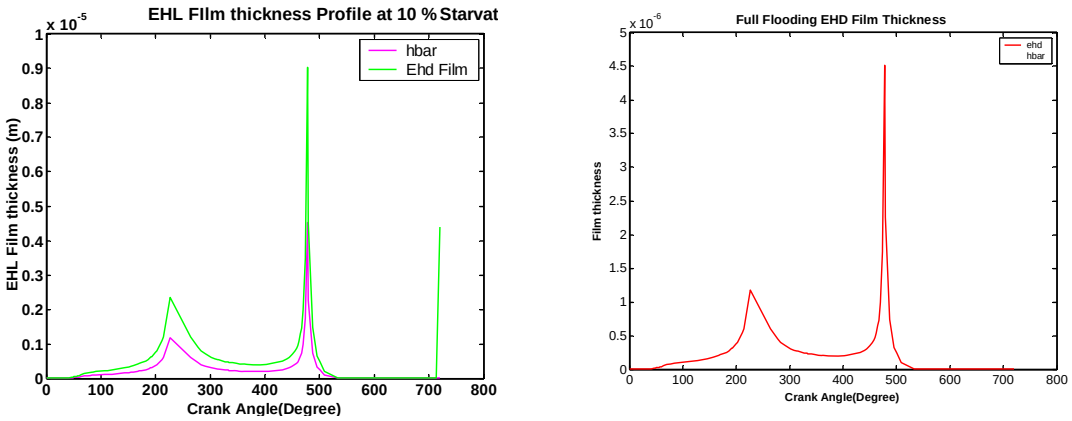

(a) (b)

Fig-5.2: EHD Film Thickness (a) 10% Starvation (b) Flooding Condition

5.4 **Pressure Profiles**

5.4.1 ***Hydrodynamic Pressures***

Figure 5.3, 5.4, 5.5 and 5.6 show the comparison of Hydrodynamic Pressures under flooding and 10% starvation conditions. These pressures are taken as % age of maximum pressures and show the trends of pressure rise in piston skirt domain.

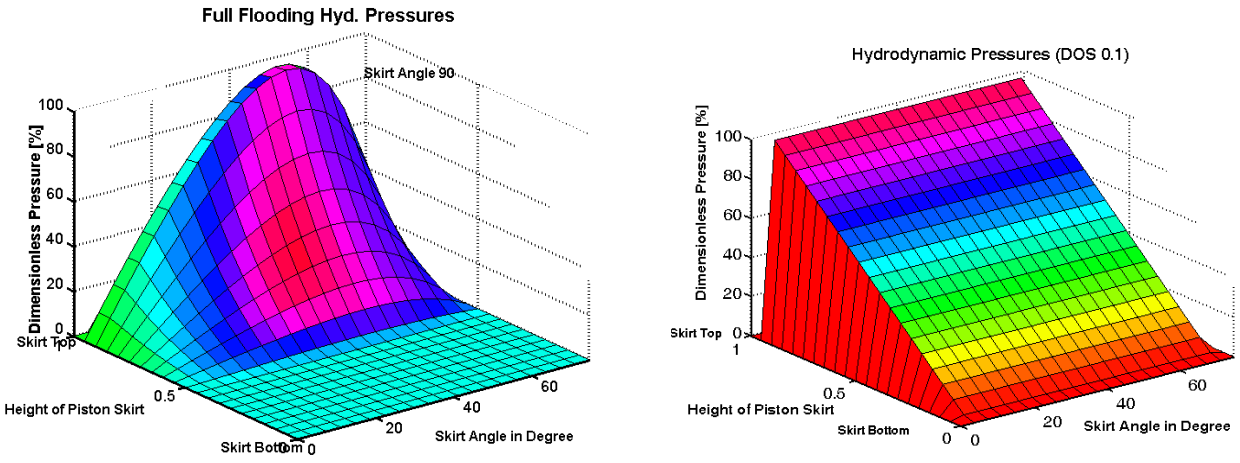

(a) (b)

Fig-5.3: Hydrodynamic Pressures at 90^{o} Crank Angle (a) Flooding Conditions (b) 10% Starvation

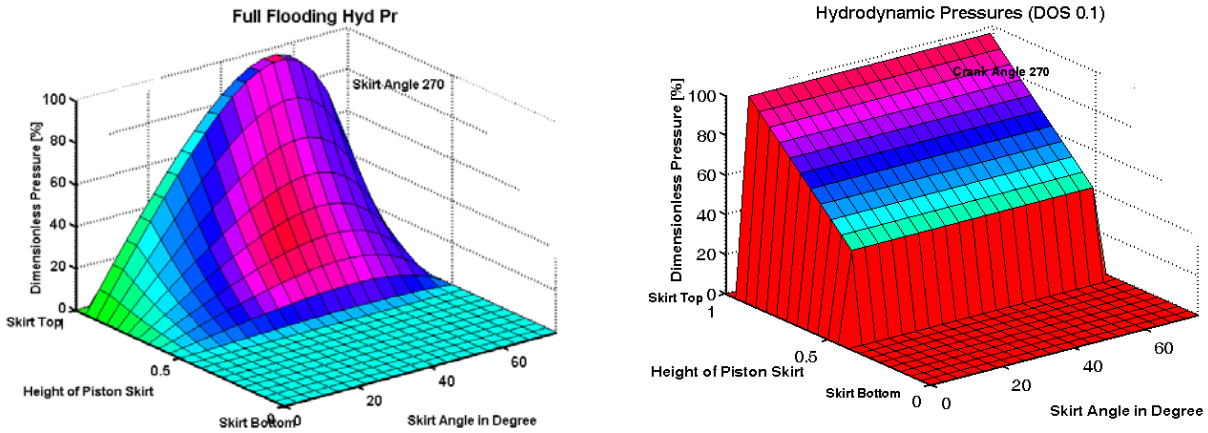

(a) (b)

Fig-5.4: Hyd. Pressures at 270 ^{o} Crank Angle (a) Flooding Condition (b) 10% Starvation

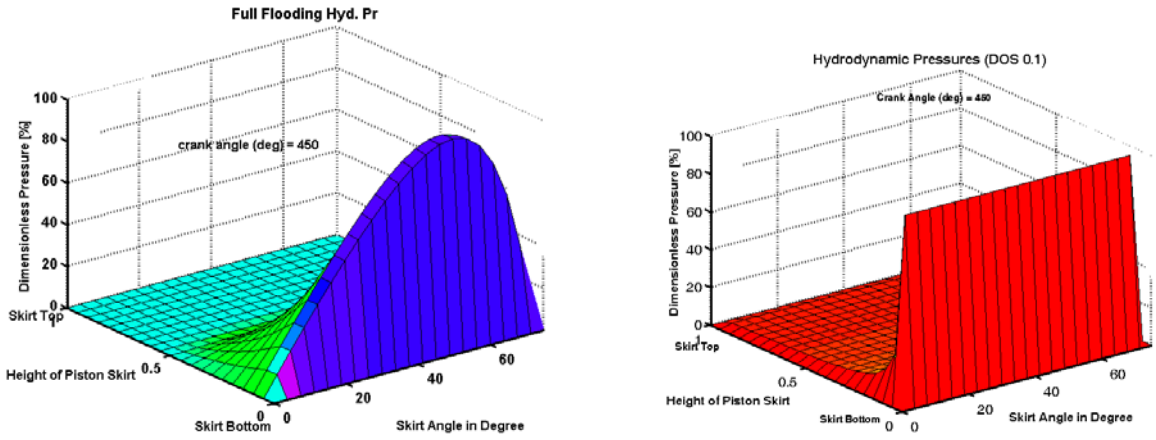

(a) (b)

Fig-5.5: Hyd. Pressures at 450 ^{o} Crank Angle (a) Flooding Condition (b) 10% Starvation

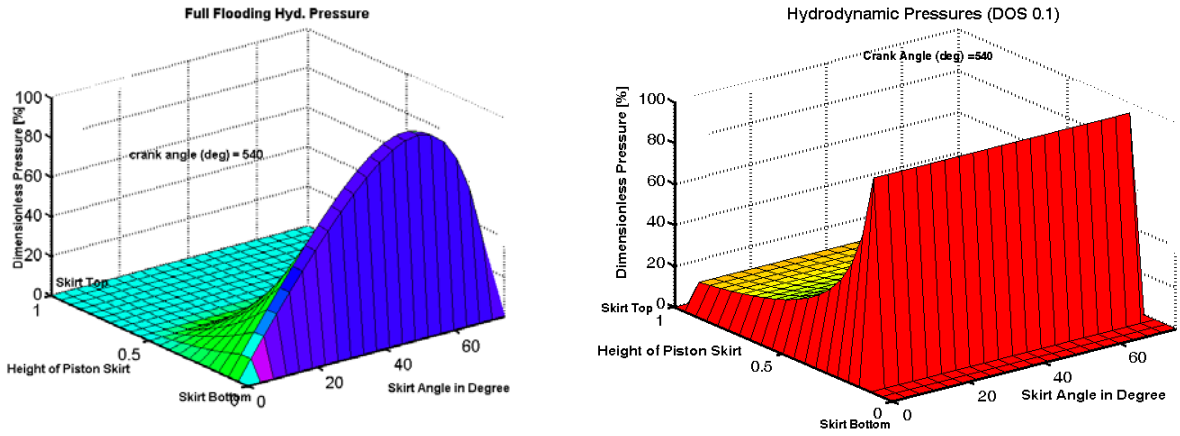

(a) (b)

Fig-5.6: Hyd. Pressures at 540 ^{o} Crank Angle (a) Flooding Condition (b) 10% Starvation

Hydrodynamic pressures, both in flooding and mild starvation conditions, show the similar trends in axial direction. However, 1-D starvation model does not show hydrodynamic pressure variation in circumferential direction. Whereas, flooding condition model shows the complete variation in both the directions. During induction and compression strokes, maximum hydrodynamic pressures are generated at the top of Piston Skirt surface (Fig-5.3 and Fig-5.4). Huge combustion loads, generated at the end of compression stroke, combined with primary and

secondary piston dynamics, cause maximum hydrodynamic pressures to shift at the bottom of Piston Skirt (Fig-5.5 and Fig-5.6).

5.4.2 ***EHD Pressures***

Elasto-hydrodynamic Pressure rise, plotted over the piston skirt surface and film thickness are shown in Fig-5.7. Large EHD Pressures generated during piston skirt EHL deform the skirt surface elastically, thereby allowing entry of additional lubricant as per deformed geometry of piston skirt, causing EHD film thickness to rise sharply at regions of deformation.

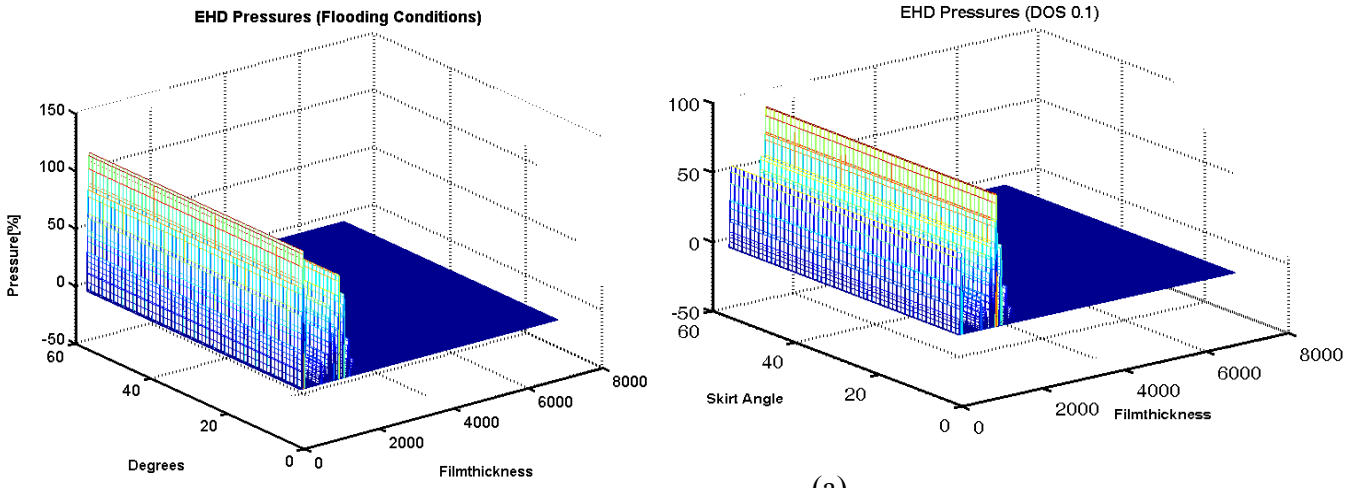

(a)

(b)

Fig-5.7: EHD Pressures (a) Flooding Conditions (b) 10 % Starvation Conditions

5.5 **Eccentricities and Secondary Velocities**

Profiles of dimensionless eccentricities are shown in Fig-5.8. Zero value of eccentricities at the centre means that piston is concentric with the liner axis. The maximum values -1 and +1 correspond to major thrust and minor thrust side of liner wall, respectively. If an eccentricity curve, E_t or E_b touches the major or minor thrust side of liner at -1 or +1, than it means that physical contact between the piston and liner has taken place which will cause adhesive wear.

5.5.1 ***Hydrodynamic Eccentricities***

In hydrodynamic lubrication regime, top surface of piston skirt becomes close to the thrust side of liner in expansion stroke and chances of physical contact between the two surfaces are high till the completion of the cycle at the end of exhaust stroke. In case of starvation conditions, chances of physical contact between piston and liner surfaces during the expansion stroke increase slightly as compared to flooding conditions (Fig-5.8). E_b curve shows minor amplitude changes and remain well away from thrust and non-thrust sides of liner during the entire four stroke cycles of crank rotation. Variation in E_t curve amplitude, however, is more prominent during the four cycles. In the beginning of induction stroke, piston remains concentric with the liner axis. Towards the end of induction stroke E_t curve shift towards non-thrust side. The amplitude of E_t curve further increases and moves towards upper horizontal line in compression stroke. During the firing and expansion stroke, there is significant change in E_t curve as it moves towards lower horizontal line.

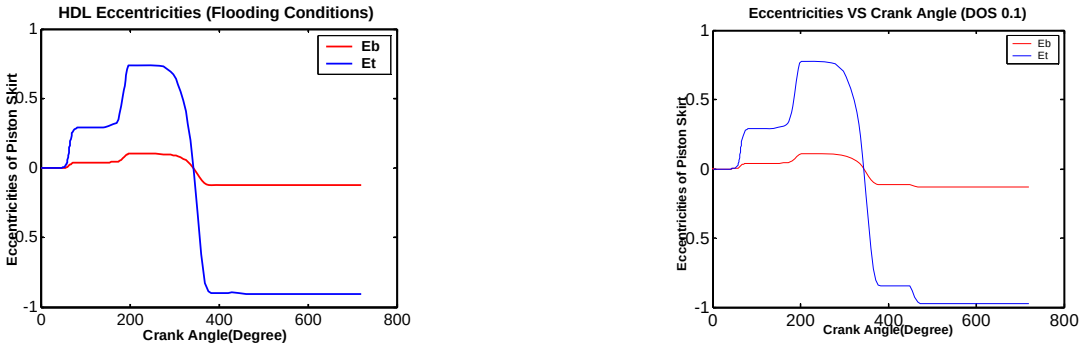

(a) (b)

Fig-5.8: Hydrodynamic Eccentricities (a) Flooding Conditions (b) 10 % Starvation Conditions

5.5.2 ***EHD Eccentricities***

In Elasto-hydrodynamic Lubrication Regime, the hydrodynamic pressures rise very steeply. These extremely high pressures cause the film become thin prior to elastic deformation of the surfaces. Both E_t and E_b profiles are improved, such that E_t remains well apart from touching the lower horizontal line (Major thrust side of liner) during expansion and exhaust stroke. Thus, chances of contact between skirt and liner surfaces are reduced. For both the cases of starvation and flooding conditions, there is no significant change in chances of contact between the interacting surfaces.

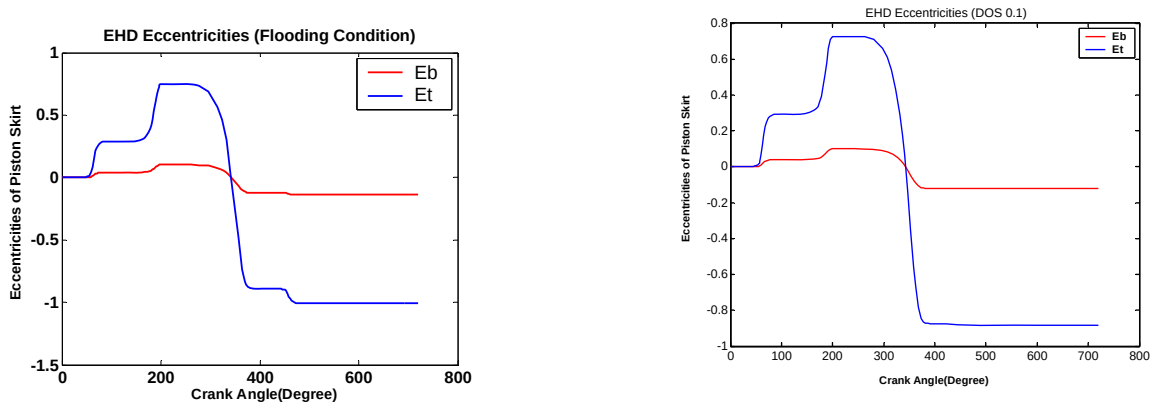

(a) (b)

Fig-5.9: EHD Eccentricities (a) Flooding Conditions (b) 10 % Starvation

5.5.3 ***Hydrodynamic Eccentric Velocities***

In hydrodynamic regime, transverse secondary velocities are larger as compared to those at EHD regime. In hydrodynamic regime, lubricant viscosity is reduced due to shear heating and combustion heat. That's why hydrodynamic transverse velocities are higher as compared to EHD transverse velocities. As shown by Fig-5.11, mild starvation does not affect hydrodynamic eccentricities significantly.

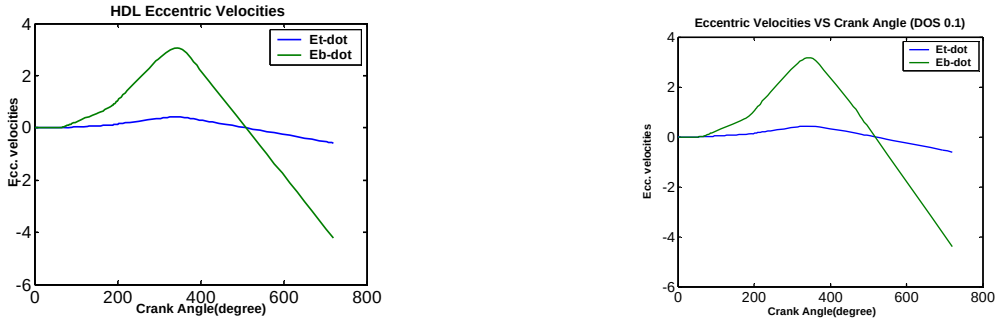

(a) (b)

Fig-5.10: Hydrodynamic Eccentric Velocities (a) Flooding Conditions (b) 10 % Starvation

5.5.4 ***EHD Eccentric Velocities***

In EHD regime, viscosity of lubricant is higher due to its dependence on pressure. Therefore eccentric velocities are decreased slightly in EHD Regime. Again, mild starvation has no significant effect on eccentric velocity profiles (Fig-5.11).

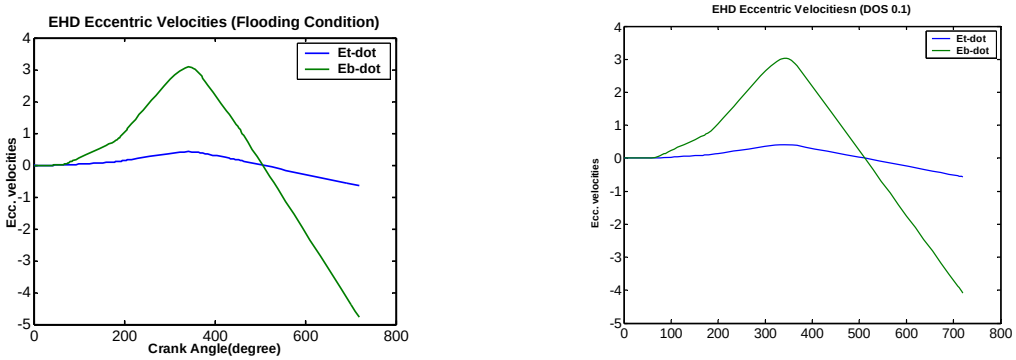

(a) (b)

Fig-5.11: EHD Eccentric Velocities (a) Flooding Conditions (b) 10 % Starvation

5.6 **Conclusion of Study**

Following conclusions can be drawn from the results of steady state lubrication model simulation:

- Mild starvation conditions (DOS 0.1) cause hydrodynamic film thickness to reduce slightly.
- Mild starvation does not have significant effect on EHD film.
- Hydrodynamic pressures and hence the load carrying capacity is slightly reduced under mild starvation conditions.
- Starvation conditions increase the chances of metal to metal contact in expansion and exhaust stroke.

TRANSIENT LUBRICATION OF PISTON SKIRT UNDER LOW ENGINE SPEED STARTUP CONDITIONS

5.7 Although the simulation of Piston Skirts starved lubrication under steady state conditions leads to some useful conclusions, in reality initial engine startup is a transient phase of an IC Engine. The engine attains the steady state conditions in a few seconds or even minutes after initial startup. Therefore a transient lubrication model is needed for simulation of piston skirt lubrication at startup. A transient lubrication model for piston skirt at initial startup was, therefore developed and detailed studies were carried out in order to observe the effects of starvation. Some of the cases considered are given below:

- Transient lubrication of Piston Skirt at startup under flooding conditions.
- Transient lubrication of Piston Skirt at startup under mild starvation conditions (Degree of Starvation 0.1-0.2)
- Transient Lubrication of Piston Skirt at startup under moderate starvation conditions (Degree of Starvation 0.2-0.3)
- Transient Lubrication of Piston Skirt at startup under severe starvation conditions (Degree of Starvation 0.5-0.7)

A brief discussion of the results is given below:

5.8 Film Thickness Profiles

5.8.1 *Hydrodynamic Film Thickness*

Hydrodynamic film thickness profile, under flooding conditions is shown in Fig-5.12 (a). Fig-5.12 (b), (c), (d), (e) and (f) show the film thickness profiles under 10 %, 20 %, 30 %, and 50 % starvation conditions respectively.

Hydrodynamic film thickness reduces significantly with increasing degree of starvation. Also trend followed by hydrodynamic film thickness profile is changed. Under flooding conditions, film thickness changes linearly whereas in starvation conditions, film thickness shows a second order variation. Comparison of film thicknesses at various degrees of starvation reveals that degree of starvation equal to 0.3 results in film thickness of the order of 100^{th} of a micron. This film thickness is not sufficient to separate the interacting surfaces. Therefore the lubrication

regime changes to mixed lubrication at severe starvation conditions. In mixed lubrication regime physical contact between interacting surfaces cannot be avoided and hence the friction losses and wear cannot be controlled.

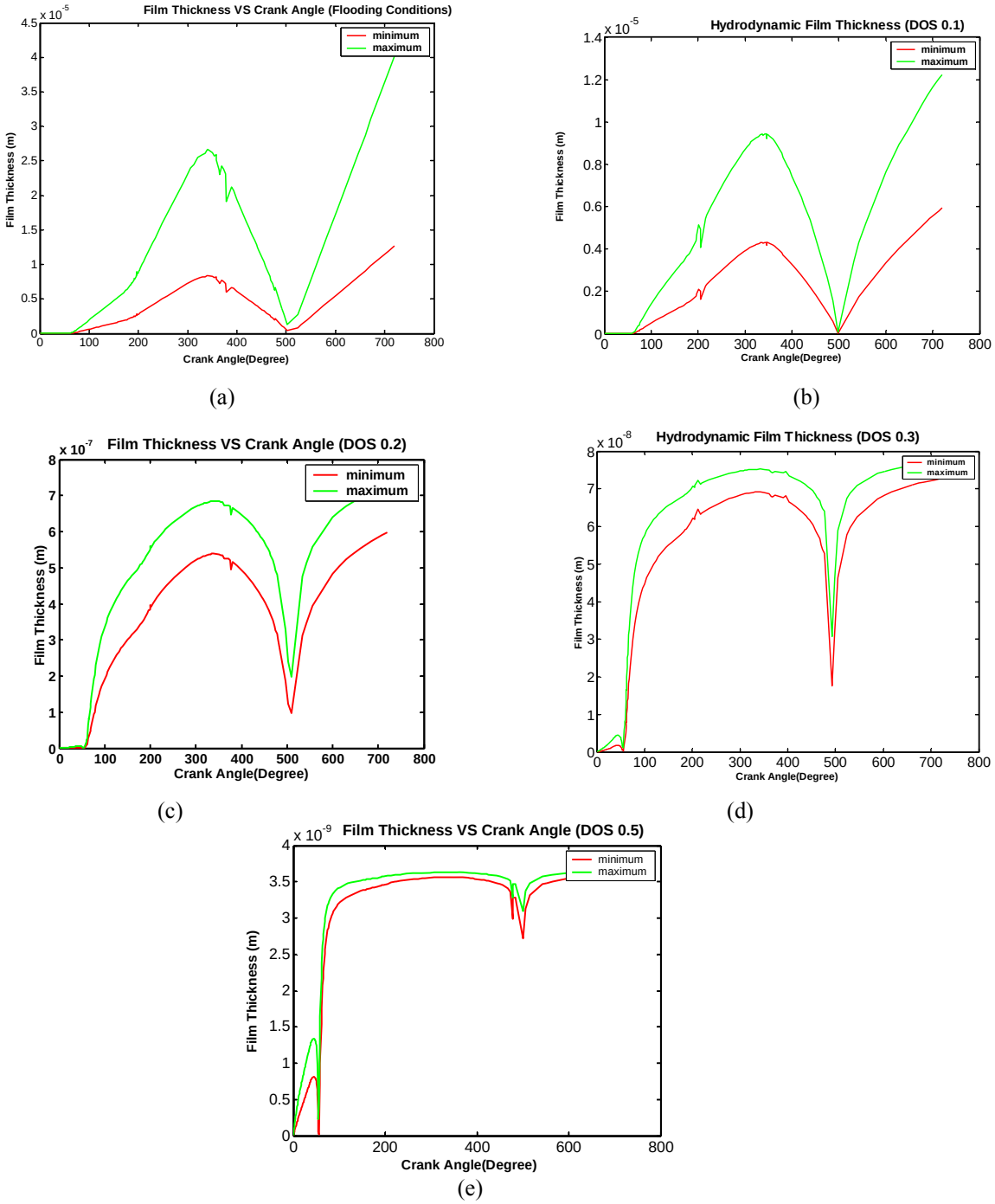

Fig-5.12: Hydrodynamic Film Thickness (a) Flooding Conditions (b) 10 % Starvation (c) 20 % Starvation (d) 30 % Starvation (e) 50 % Starvation

5.8.2 ***EHD Film Thickness***

EHD film thickness profile, under flooding conditions is shown in Fig-5.13 (a). Fig-5.13 (b), (c), (d), (e) and (f) show the film thickness profiles under 10 %, 20 %, 30 %, 50 % and 50 % starvation conditions respectively.

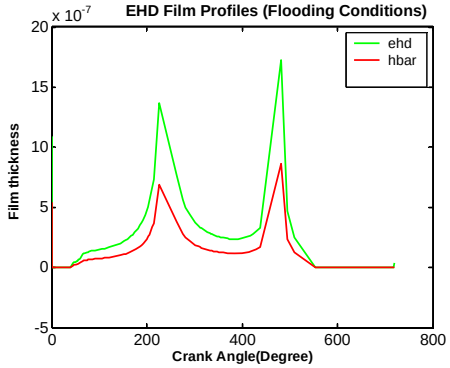

(a)

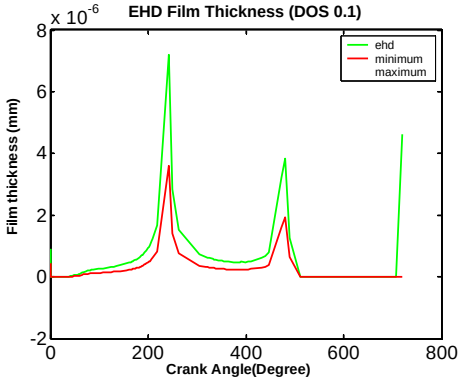

(b)

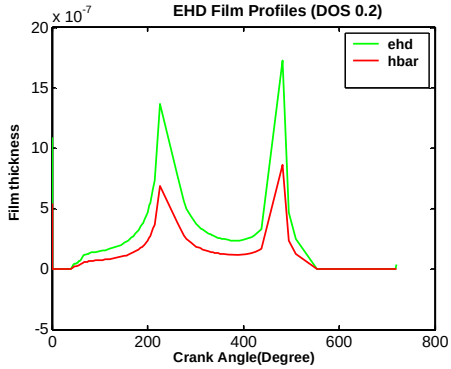

(c)

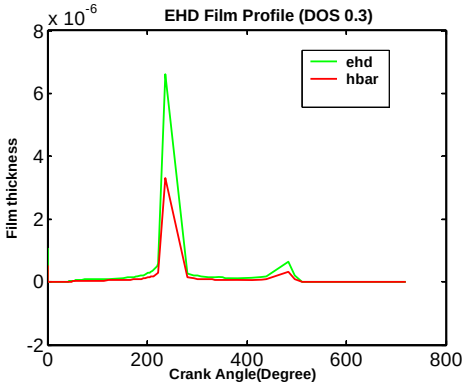

(d)

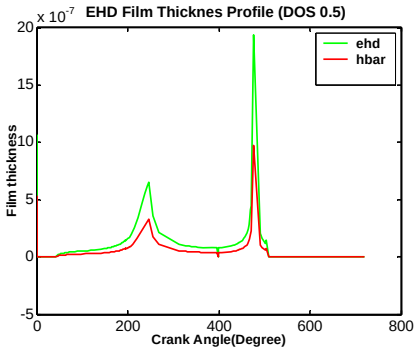

(e)

Fig-5.13: EHD Film Thickness (a) Flooding Conditions (b) 10 % Starvation (c) 20 % Starvation

(d) 30 % Starvation (e) 50 % Starvation

Maximum EHD Film thickness achieved under starvation conditions is reduced with increasing degrees of starvation. This means that beyond a certain level of starvation, EHD film generated is not sufficient to separate the interacting surfaces.

5.9 Pressure Profiles

5.9.1 *Hydrodynamic Pressure*

Full flooding hydrodynamic pressures at 90^{o}, 270^{o}, 450^{o} and 540^{o} crank angle are shown in Fig-5.14 a, b, c, d respectively.

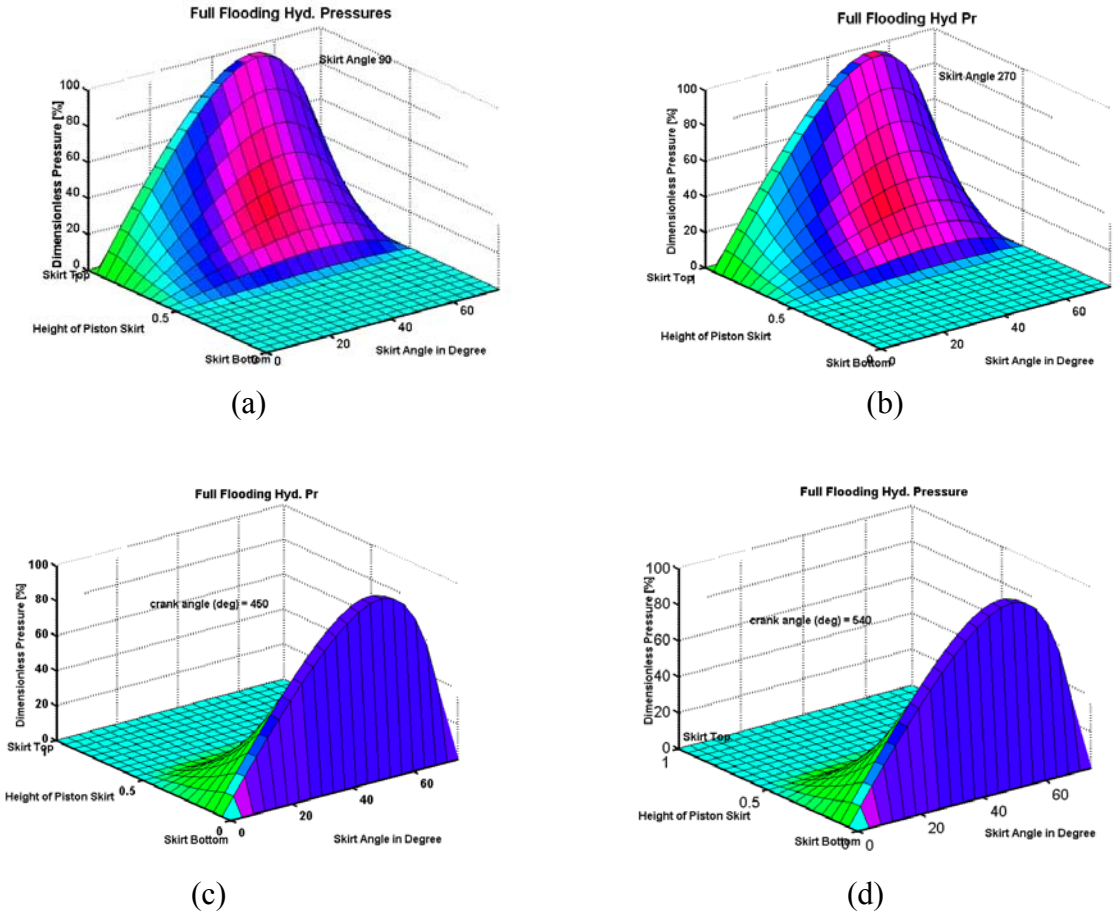

Fig 5.14: Full flooding Hydrodynamic Pressures at (a) 90^{o} (b) 270^{O} (c) 450^{o} and (d) 540o Crank Angle.

Non-dimensional hydrodynamic pressures plotted in Fig-5.14 are taken as percentage of maximum pressure in order to show variation of pressures over the skirt surface. At the beginning of 4-stroke cycle, maximum hydrodynamic pressure is developed at the top and mid position of the skirt surface (Fig-5.14a). This pressure distribution is maintained until the end of compression stroke (5.14b). After combustion of air-fuel mixture, maximum hydrodynamic pressures are shifted to bottom-mid position (Fig 5.14c and 5.14d).

Fig-5.15 a, b, c, d show variation of hydrodynamic pressures under mild starvation conditions (degree of starvation 0.1) over the piston skirt surface at 90^o, 270^o, 450^o and 540^o crank angles respectively.

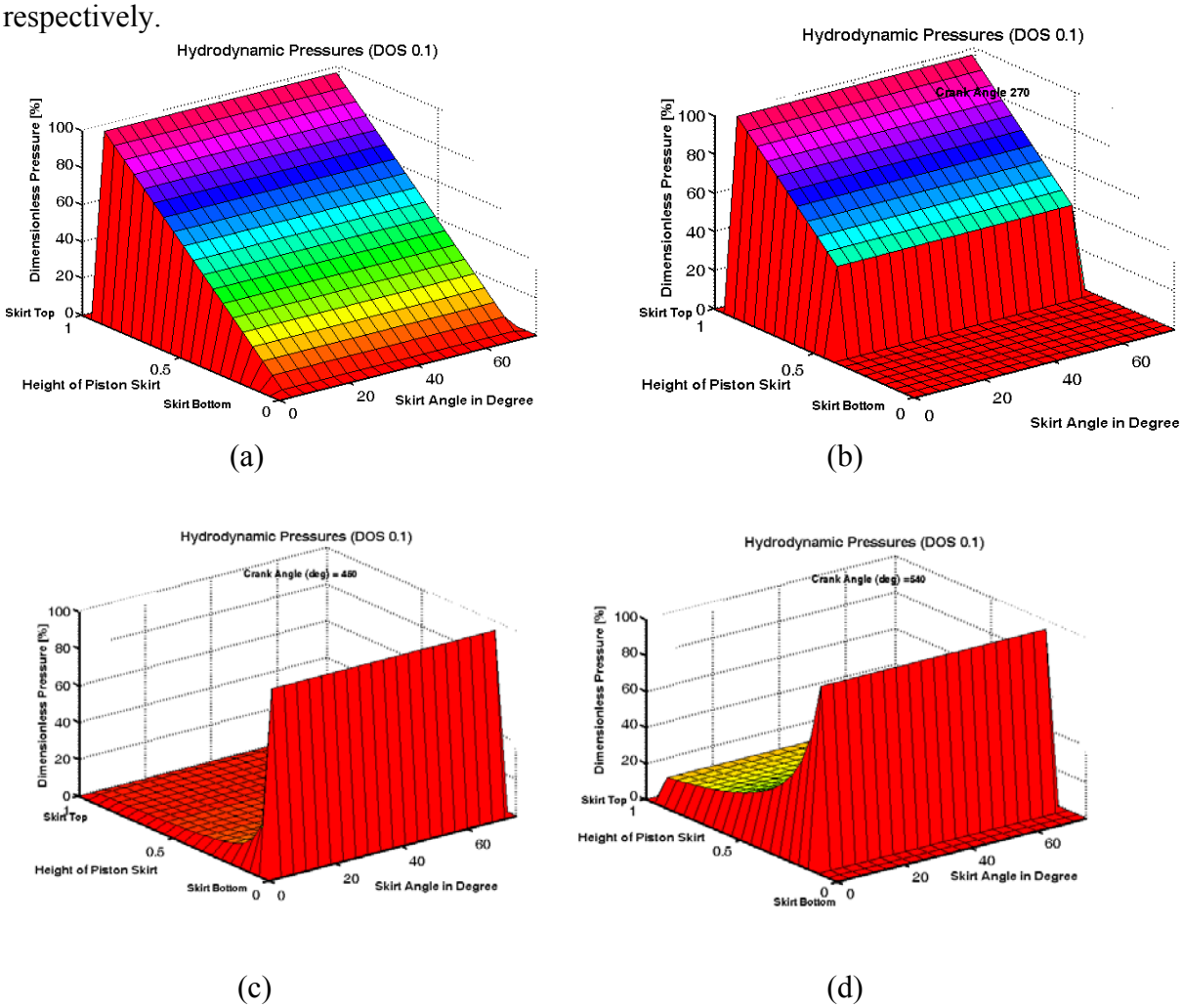

Fig 5.15: Hydrodynamic Pressures under Starvation Conditions (DOS 0.1)

at (a) 90^o (b) 270^o (c) 450^o and (d) 540^o Crank Angle.

Fig-5.15 show variation of hydrodynamic pressures in axial direction (i.e. along skirt length) only. Variation along the skirt angle is ignored for minor starvation levels. Quantity of hydrodynamic pressures and load carrying capacity is significantly reduced under starvation conditions.

Variation of hydrodynamic pressures under various starvation conditions (DOS 0.2, 0.3, 0.4 and 0.5) are shown in Fig-5.16, 5.17, 5.18 and 5.19).

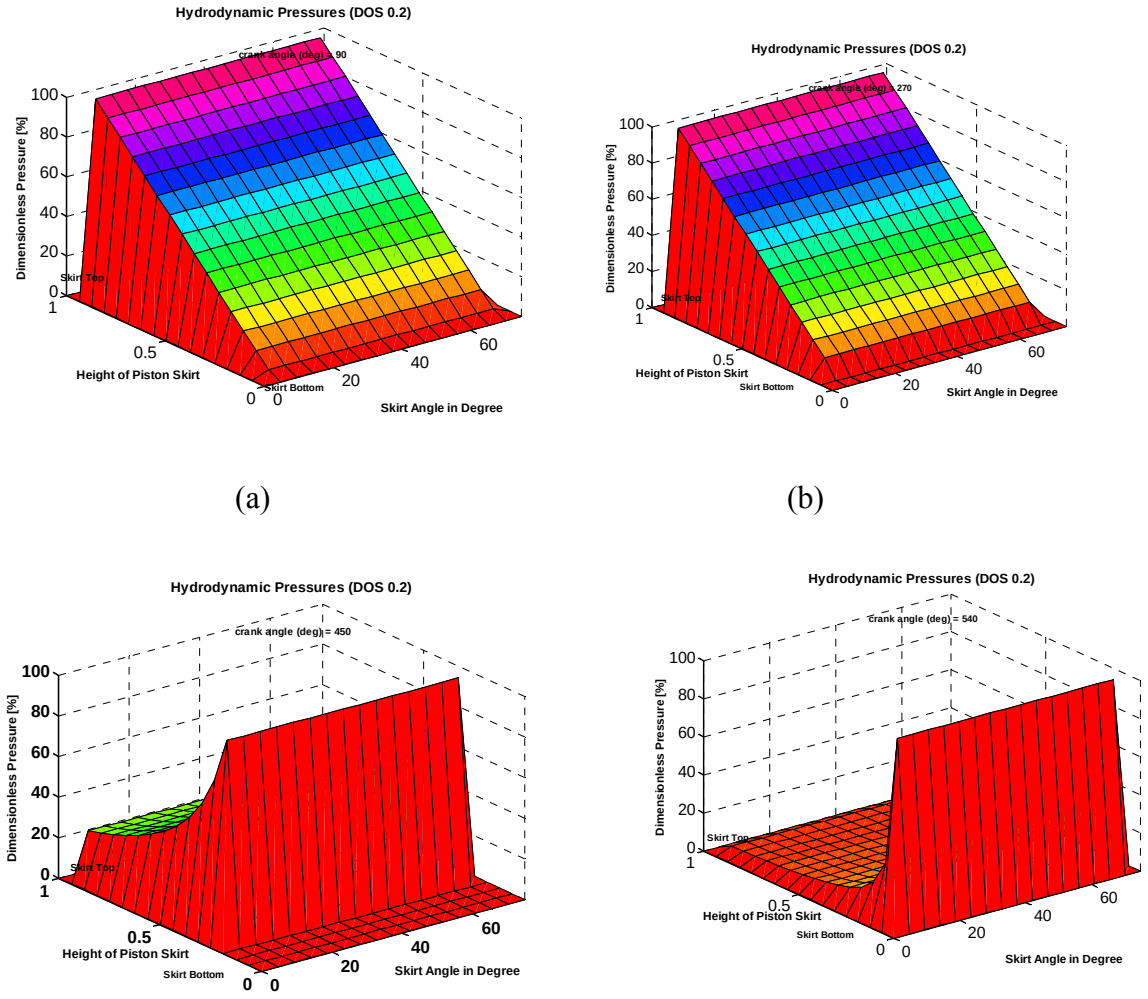

Fig 5.16: Hydrodynamic Pressures under Starvation Conditions (DOS 0.2) at (a) 90^{o} (b) 270^{O} (c) 450 and (d) 540 Crank Angle.

EHD Pressure

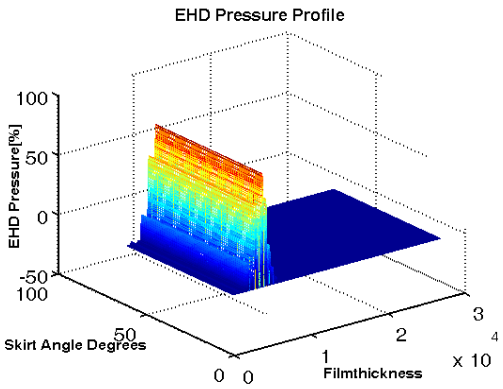

(a)

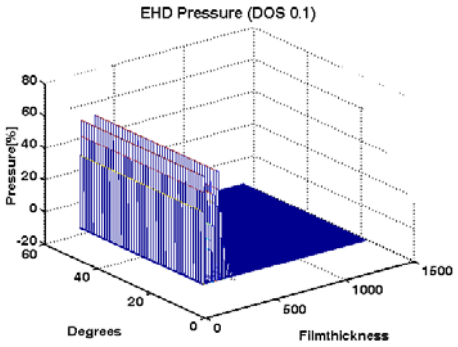

(b)

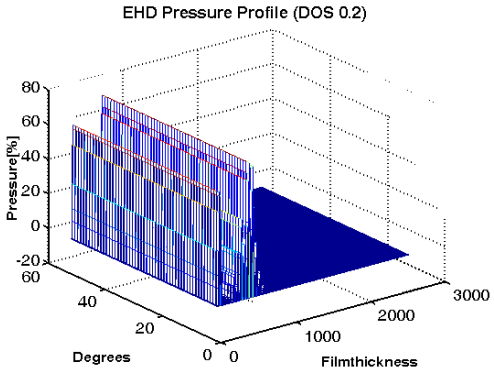

(c)

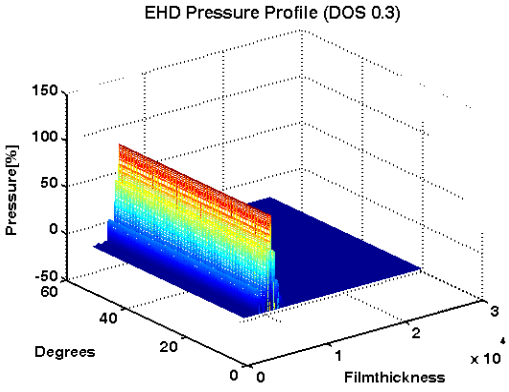

(d)

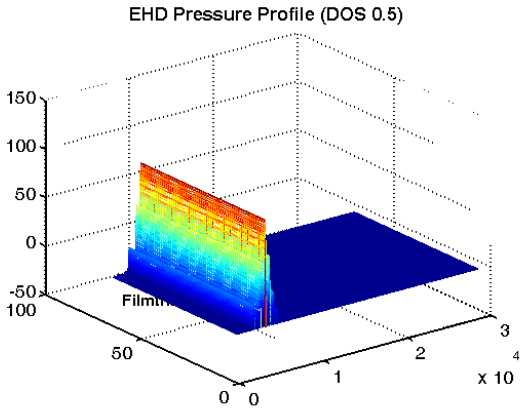

(e)

Fig-5.17: EHD Pressure Profiles (a) Flooding Conditions (b) 10 % Starvation (c) 20 % Starvation

(d) 30 % Starvation (e) 50 % Starvation

Fig-5.17 (a), (b), (c), (d), (e) show EHD pressure profiles under flooding conditions and 10%, 20%, 30%, 50% starvation levels respectively. EHD pressures are not affected significantly by starvation conditions (Fig-5.17).

5.10 **Eccentricities and Secondary Velocities**

5.10.1 ***Hydrodynamic Eccentricities***

Hydrodynamic eccentricities profile, under flooding conditions is shown in Fig-5.15 (a). Fig-5.15 (b), (c), (d) and (e) show the film thickness profiles under 10 %, 20 %, 30 %, and 50 % starvation conditions respectively.

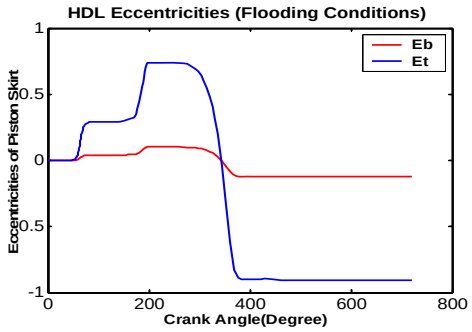

(a)

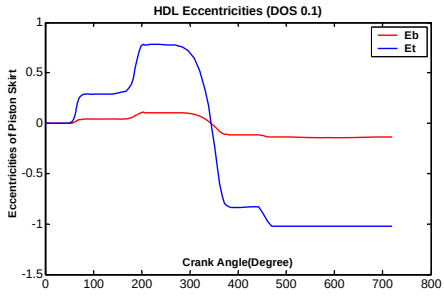

(b)

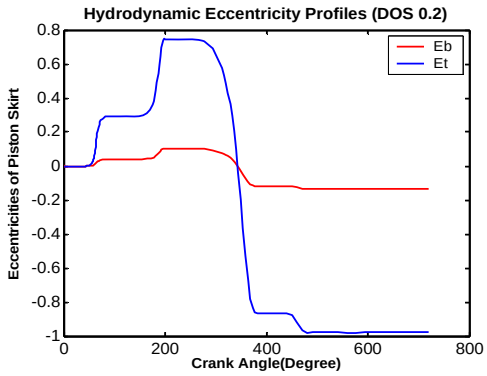

(b)

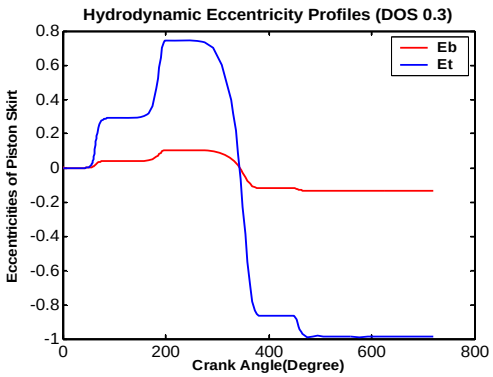

(d)

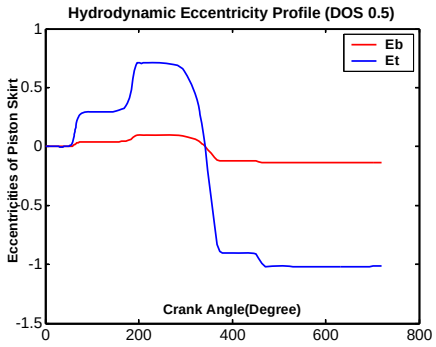

(e)

Fig-5.15: Hydrodynamic Eccentricity Profiles (a) Flooding Conditions (b) 10 % Starvation (c) 20 % Starvation (d) 30 % Starvation (e) 50 % Starvation

It is clear from Fig-5.15 that under full flooding conditions, E_t and E_b curves do not touch thrust or non thrust side of liner. Therefore physical contact between piston and liner surfaces is completed prevented in hydrodynamic regime, under flooding conditions. Under starvation conditions however, the probability of contact increases as the level of starvation increases.

5.10.2 ***EHD Eccentricities:***

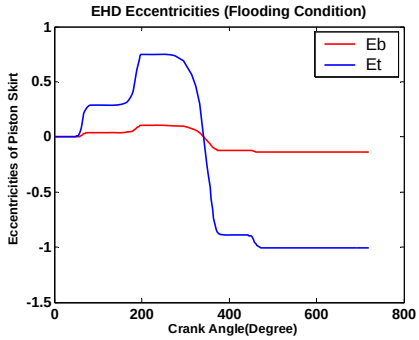

(a)

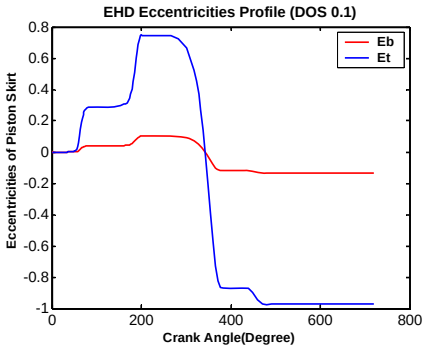

(b)

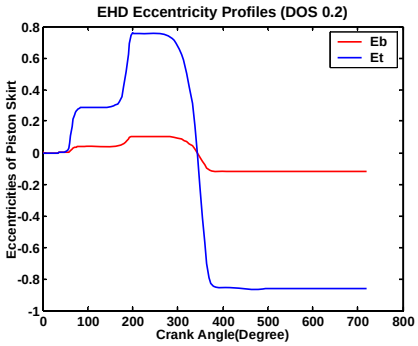

(c)

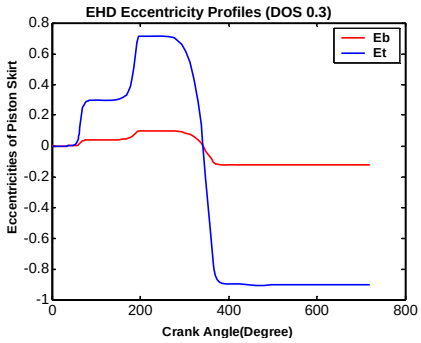

(d)

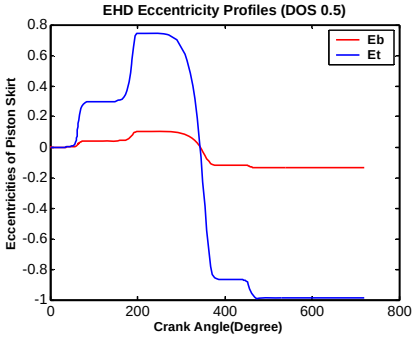

(e)

Fig-5.16: EHD Eccentricity Profiles (a) Flooding Conditions (b) 10 % Starvation (c) 20 % Starvation (d) 30 % Starvation (e) 50 % Starvation

EHD eccentricities profile under flooding conditions, 10 %, 20 %, 30 %, and 50 % starvation conditions are shown in Fig-5.17 (a), (b), (c), (d) and (e) respectively. It is obvious from the figure that starvation conditions do not have significant effect on EHD Eccentricity profiles.

5.10.3 ***Hydrodynamic Eccentric Velocities***

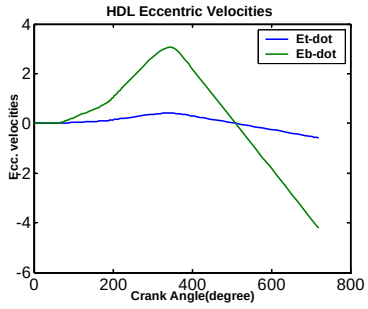

(a)

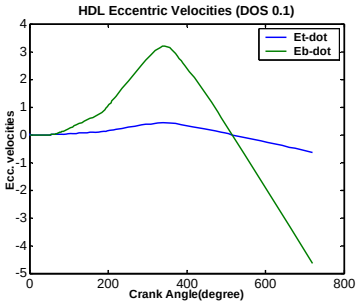

(b)

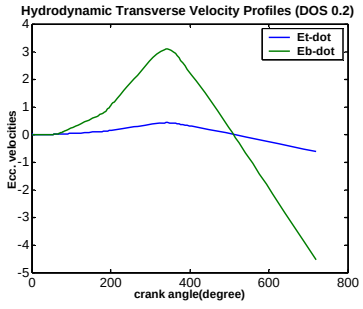

(c)

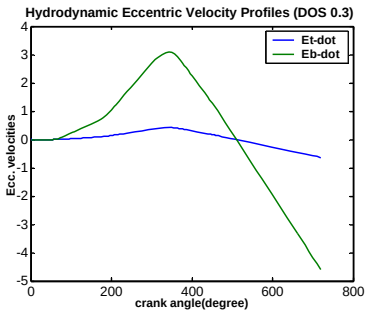

(d)

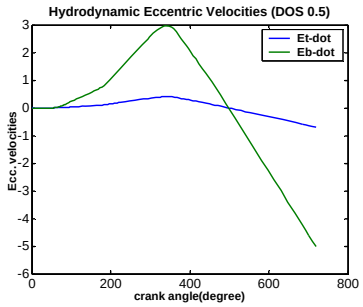

(e)

Fig-5.17: Hydrodynamic Ecc. Velocity Profiles (a) Flooding Conditions (b) 10 % Starvation (c) 20 % Starvation (d) 30 % Starvation (e) 50 % Starvation

Hydrodynamic eccentric velocity profiles under flooding conditions, 10%, 20%, 30% and 50% starvation levels are shown in Fig-5.17 (a), (b), (c), (d) and (e) respectively. Comparison of velocity profiles at various degrees of starvation indicate that transverse velocities of piston skirt increase with degree of starvation.

5.10.4 ***EHD Eccentric Velocities:***

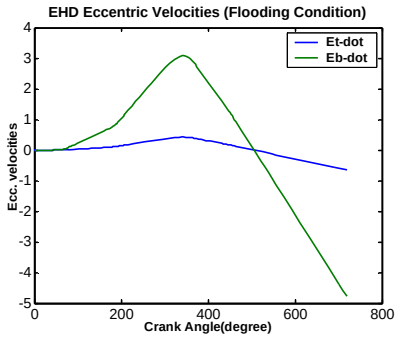

(a)

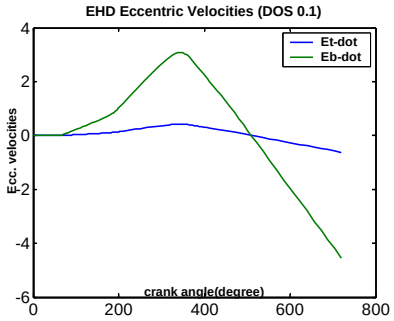

(b)

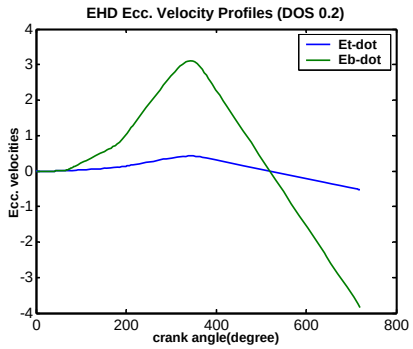

(c)

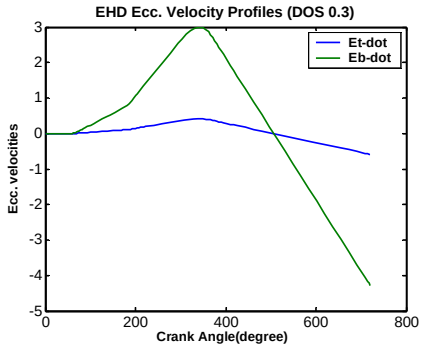

(d)

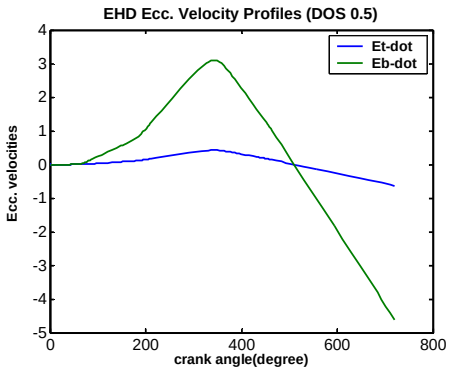

(e)

Fig-5.18: EHD Ecc. Velocity Profiles (a) Flooding Conditions (b) 10 % Starvation (c) 20 % Starvation (d) 30 % Starvation (e) 50 % Starvation

EHD eccentric velocity profiles under flooding conditions, 10%, 20%, 30% and 50% starvation levels are shown in Fig-5.18 (a), (b), (c), (d) and (e) respectively. Comparison of velocity profiles at various degrees of starvation indicate that transverse velocities of piston skirt increase with degree of starvation.

5.11 **Conclusions Of Study:**

Following conclusions can be drawn from the comparison of the results of transient lubrication model at low speed engine startup, under starvation and flooding conditions:

- Although Hydrodynamic film thickness is significantly reduced under mild starvation (10% starvation), EHD Film is not much affected. EHD film thickness is still sufficient to prevent physical contact between the interacting surfaces of piston skirt and liner.
- Under starvation conditions, hydrodynamic pressure variation, in axial direction is calculated only. Quantity of net hydrodynamic pressure and hence the load carrying capacity is significantly reduced.
- Finally we can conclude that minor starvation of does not significantly affect the EHD Film and physical contact between the surfaces can still be avoided at low radial clearance between the piston and cylinder bore and low startup speeds.
- Piston Eccentricities and Ecc. Velocities increase with increasing starvation level.
- As the starvation conditions become more severe, chances of physical contact between the interacting surfaces of piston and liner are increased thereby, causing increase in friction losses and wear. Hence starvation conditions must be avoided and controlled within a certain level (Degree of Starvation less than 0.2) in order to optimize the performance of an IC engine and increase its life.

VALIDATION AND VERIFICATION OF RESULTS:

Results of steady state and transient lubrication models of piston skirt under low speed startup conditions, developed as a mandate of current research can be validated by comparison with the past research in the relevant field. Dr. S. A. Qasim (5) has developed elasto-hydrodynamic lubrication model of piston skirt under ideal conditions in his PhD thesis research (5). The results of steady state, elasto-hydrodynamic model under low initial engine startup speed of 600 rpm from his thesis report are shown here for the comparison:

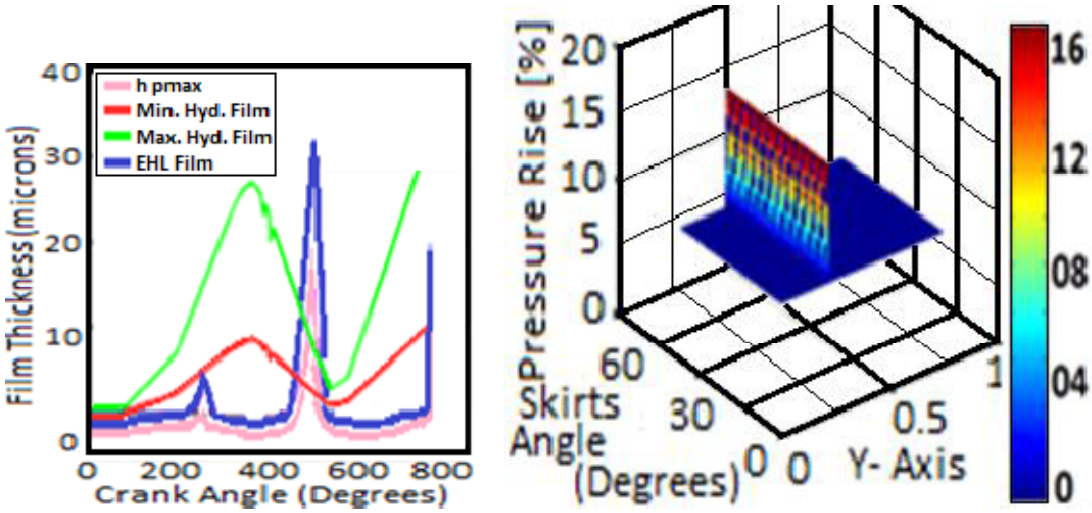

(a) **(b)**

Fig-5.19: (a) Film thickness profiles (b) EHL Pressure Field (5)

Fig-5.19 (a) shows the profiles of maximum and minimum hydrodynamic and elastohydrodynamic film thicknesses. EHL pressure profile is shown in Fig-5.19 (b). The results of steady state lubrication model under flooding conditions (zero degree of starvation) from current work were shown in the beginning of this chapter. These results are copied again for comparison with those given above.

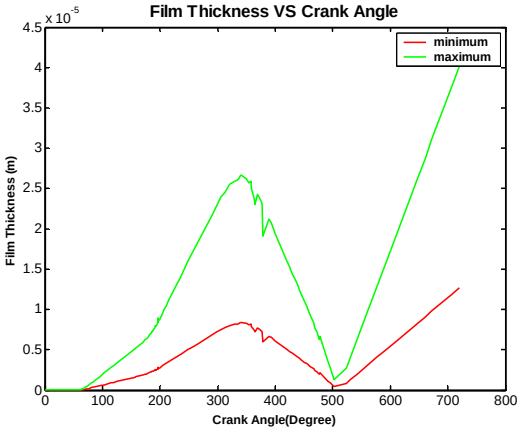

(a)

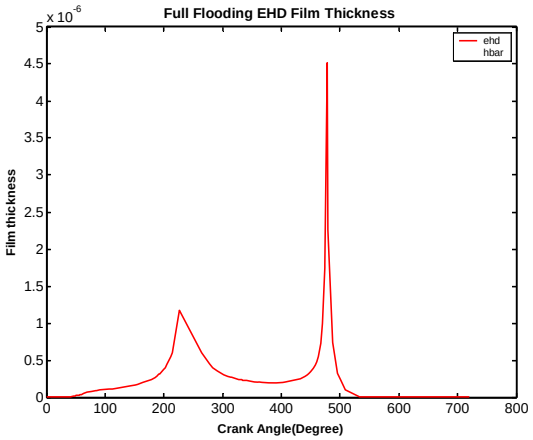

(b)

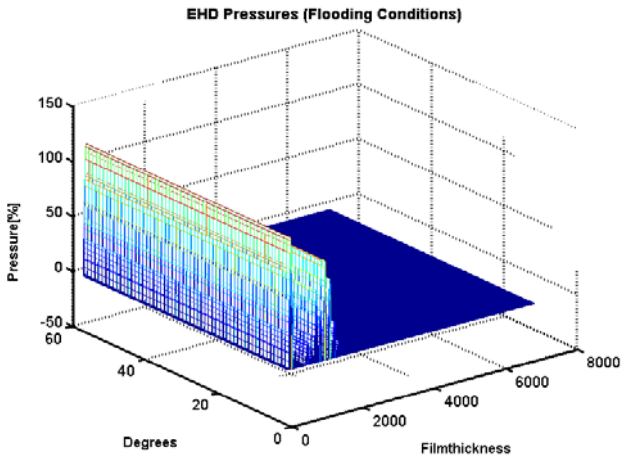

(c)

Fig-5.20: (a) Hydrodynamic Film profiles (b) EHL Film profile (c)EHD Pressure Field

Comparison of Fig-5.19 and 5.20 shows that hydrodynamic and EHD film thickness show the similar patterns under flooding conditions. Also EHD Pressure variation is similar in both the cases. Note that in case of referenced work, EHL Pressure variation along the skirt surface is

given in Fig-5.19 (b) whereas in current research, EHL pressure variation along the skirt angle and film thickness are shown in Fig-5.20 (c). So the results of current research under flooding conditions are in agreement with those of referenced research in the relevant field. Under starvation conditions, results from thesis report of Hooshang Heshmat's are selected for comparison (36).

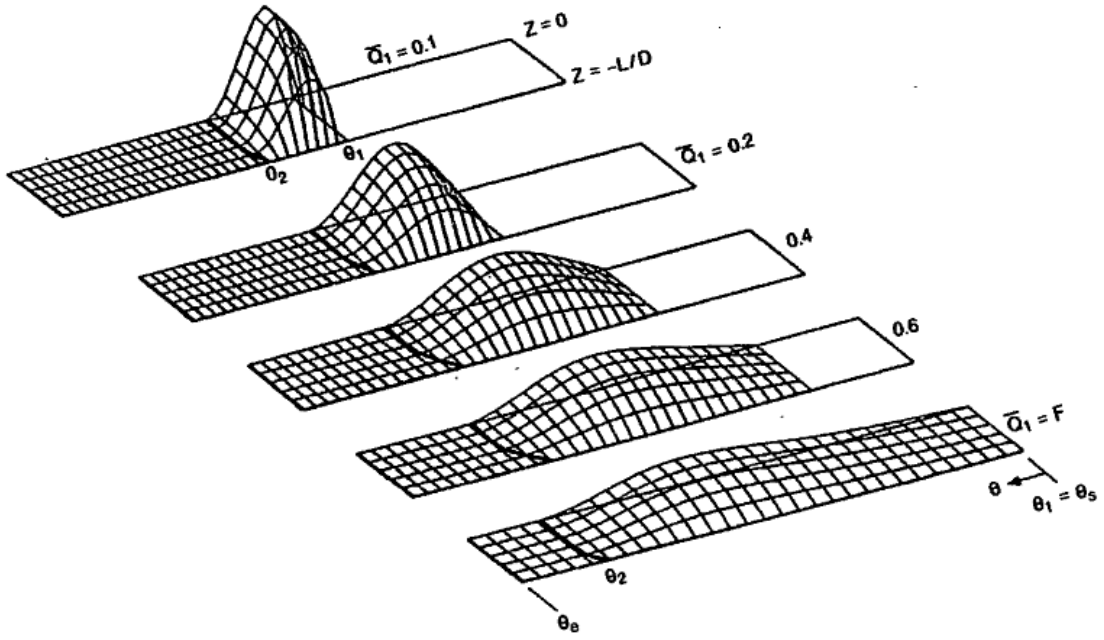

Fig-5.21: Pressure Distribution for Various Degrees of Starvation (36)

Figure 5.21 show hydrodynamic pressure profiles for a journal bearing at different degrees of starvation. L/D ratio for this case is 0.5. Flooded conditions are shown at the bottom of figure, followed by increasing degrees of starvations (Q1= 0.6, 0.4, 0.2 and 0.1). We see that as the starvation increases, the active part of the fluid film shrinks. Hydrodynamic pressure profiles for various degrees of starvations for the current research have been shown in Fig-5.16, 5.17, 5.18 and 5.19. In case of referenced research, starvation problem has been treated as free boundary problem and boundaries of starved film are found as a part of the solution. Also in case of journal bearings there are not very huge pressure variations due to combustion like phenomenon. In current research, the effects of starvation have been studied by a film thickness reduction factor corresponding to fluid level at the inlet. Therefore hydrodynamic pressure profiles do not match. However there is a commonality in both the cases that hydrodynamic pressures and hence

the load carrying capacity is significantly reduced as the starvation increases. From simulation results of transient lubrication model under various degrees of starvations, a very serious consequence of starvation observed in the current research is significant reduction and rupture of hydrodynamic film. This fact can be verified by a number of sources from past research. Research work of Rajesh Kumar and his co-workers (32) brings forward the same conclusion. Variation of film thickness with degree of starvation is given by the plots shown in Fig-5.22.

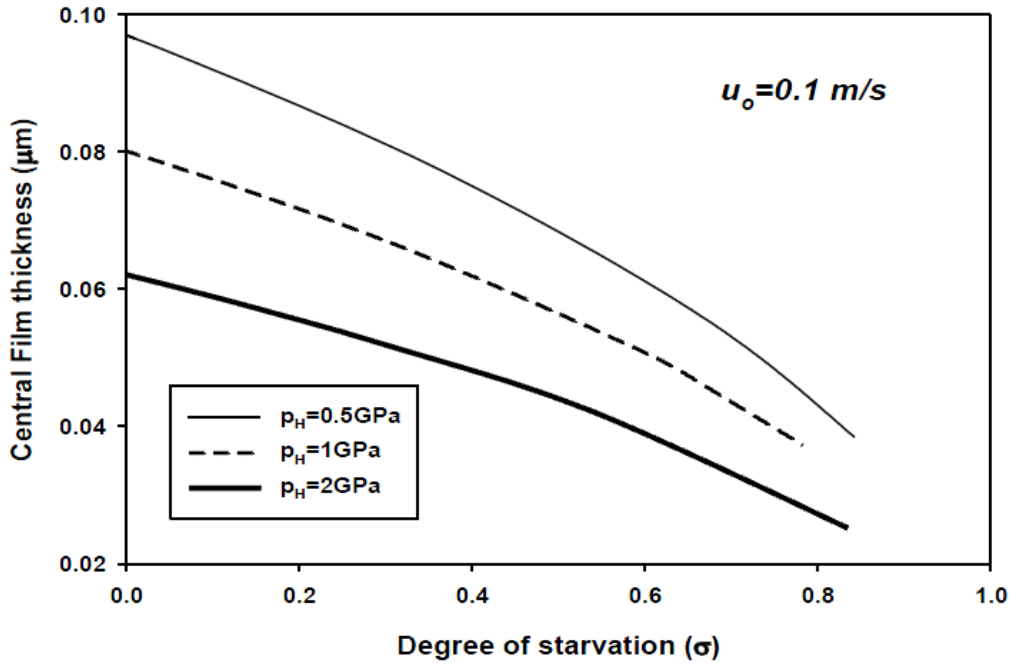

Fig-5.22: (a) Variation of Central Film Thickness with degrees of starvation for different Herzian pressures at rolling speed 0.1 m/s (32)

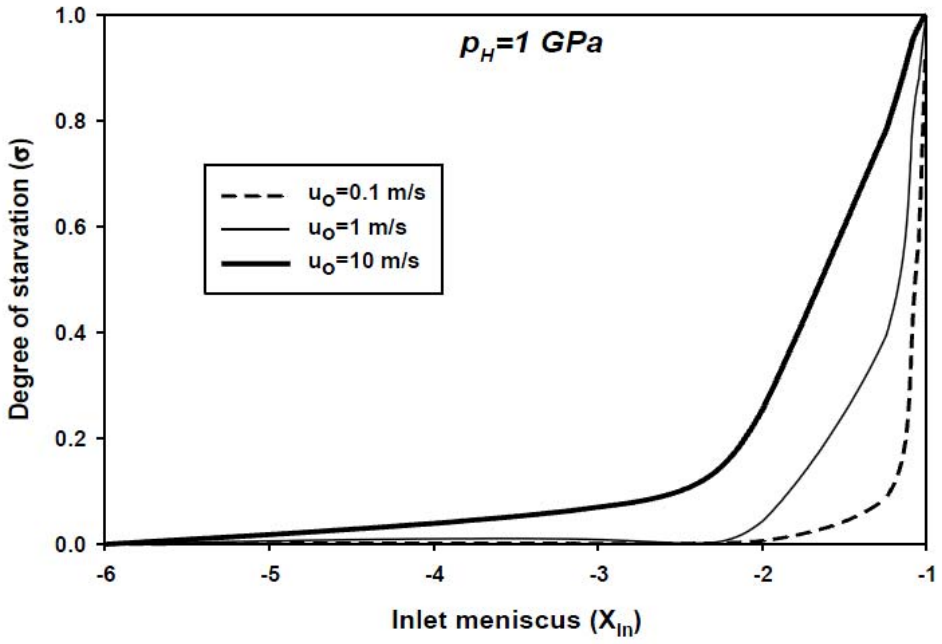

Fig-5.22: (b) Variation of Central Film Thickness with degrees of starvation for different Rolling Speeds Hertizian Pressure of 1 GPa (32)

CHAPTER 6

PARAMETRIC STUDIES

6.1 A wide range of parametric studies have been carried out in order to find out, the optimum operating conditions for minimizing friction losses and wear at initial engine startup. Results and discussions of only a few of them are presented here. The important parameters, affecting the startup conditions are:

- Engine Startup Speed.
- Piston to Cylinder Bore Radial Clearance.
- Lubricant Viscosity.

A medium starvation level (Degree of Starvation 0.3) has been selected for optimization studies.

TRANSIENT LUBRICATION OF PISTON SKIRT AT VARIOUS ENGINE STARTUP SPEEDS

This study includes optimization of engine startup speed at low radial clearance (C=10 micron) for a low viscosity grade lubricant oil (η=0.03187 Pa. Sec). The study includes simulation of transient lubrication model of piston skirt under starvation conditions at low (600 rpm), medium (800 rpm) and high engine speeds (1100 rpm). Results of simulations at various startup speeds are discussed below:

6.2 Film Thickness Profiles

6.2.1 *Hydrodynamic Film Thickness*

Fig-6.1 (a), (b) and (c) represent the Hydrodynamic Film thickness profiles at startup speeds of 600 rpm, 800 rpm and 1100 rpm respectively. Hydrodynamic film thickness increases with startup speed. So high startup speeds are favorable for sufficient hydrodynamic film development.

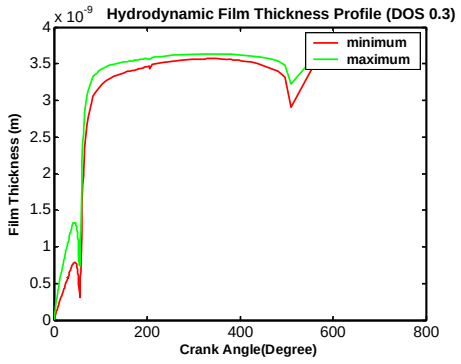

(a)

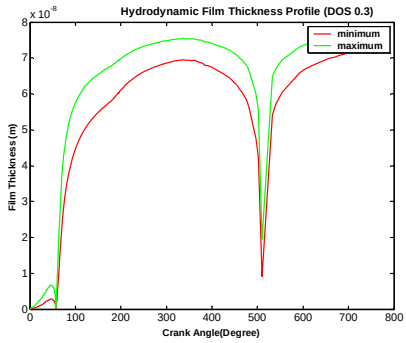

(b)

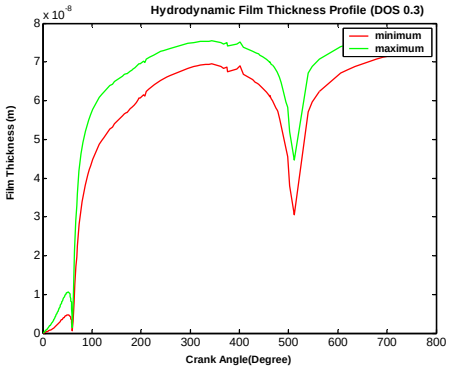

(c)

Fig-6.1: Hydrodynamic Film thickness Profiles at (a) Startup Speed 600 rpm (b) 800 rpm (c) 1100 rpm

6.2.2 ***EHD Film Thickness***

Fig-6.1 (a), (b) and (c) represent the EHD Film thickness profiles at startup speeds of 600 rpm, 800 rpm and 1100 rpm respectively. EHD film thickness also increases with startup speed.

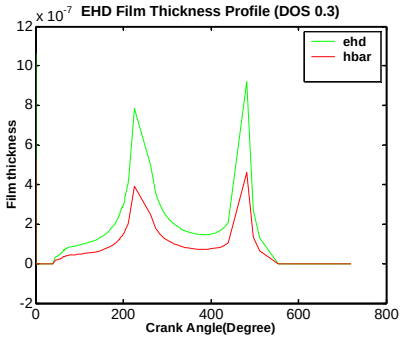

(a)

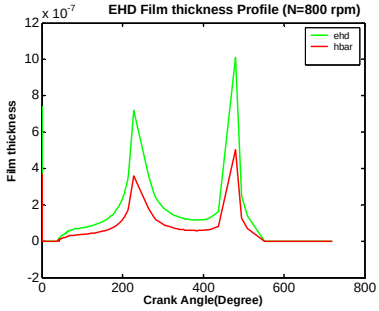

(b)

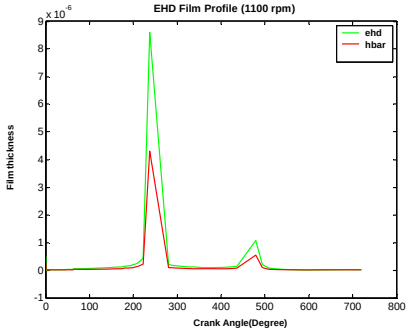

(c)

Fig-6.2: EHD Film thickness Profiles at (a) Startup Speed 600 rpm (b) 800 rpm (c) 1100 rpm

6.3 Piston Eccentricities and Transverse Velocities

6.3.1 *Hydrodynamic Eccentricities*

Hydrodynamic Eccentricity profiles at 600 rpm, 800 rpm and 1100 rpm are shown in Fig-6.3 (a), (b) and (c) respectively. Physical contact of piston skirt with thrust side of liner cannot be avoided at 600 and 1100 rpm in expansion and exhaust strokes. However at 800 rpm startup speed contact is avoided. Therefore 800 rpm is optimum startup speed for avoiding friction losses and wear.

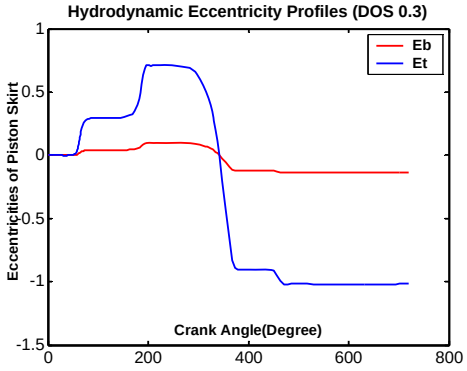

(a)

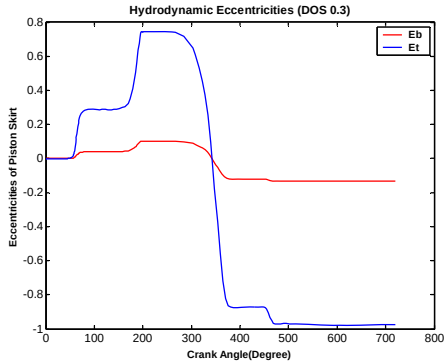

(b)

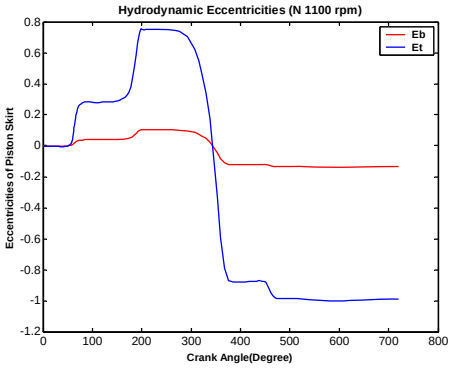

(c)

Fig-6.3: Hydrodynamic Eccentricity Profiles at (a) Startup Speed 600 rpm (b) 800 rpm (c) 1100 rpm

6.3.2 ***EHD Eccentricity Profiles***

As shown in Fig-6.4, Physical contact between piston skirt and liner surfaces is avoided at 600 and 800 rpm startup speeds. Only at 1100 rpm, the contact between piston and thrust side of liner takes place. So 1100 rpm startup speed should be avoided in order to control friction losses and surface wear.

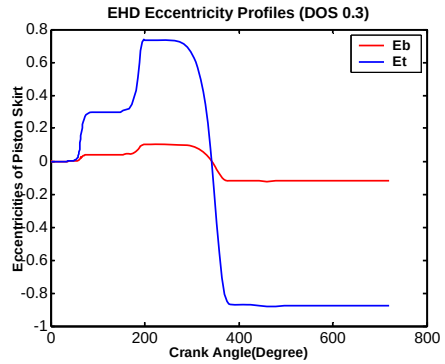

(a)

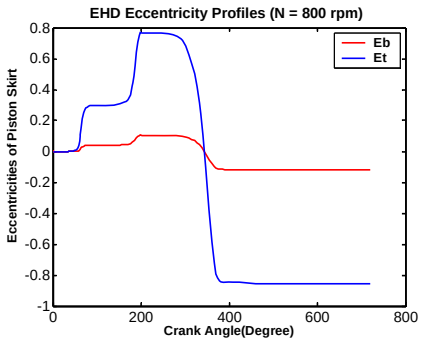

(b)

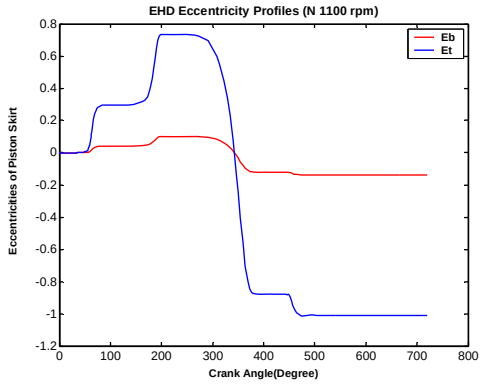

(c)

Fig-6.4: EHD Eccentricity Profiles at (a) Startup Speed 600 rpm (b) 800 rpm (c) 1100 rpm

6.3.3 ***Hydrodynamic Eccentric Velocity Profiles***

Hydrodynamic eccentric velocity profiles for startup speeds 600 rpm, 800 rpm and 1100 rpm are shown in Fig-6.5 (a), (b) and (c) respectively. At low startup speeds eccentric velocities are lower and they increase with increasing startup speed. Therefore high startup speeds are not suitable for optimum operation of an IC engine because increase in eccentric velocities results in increase of metal to metal contact probability.

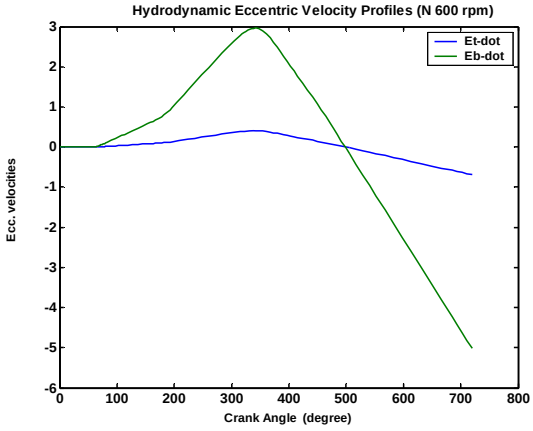

(a)

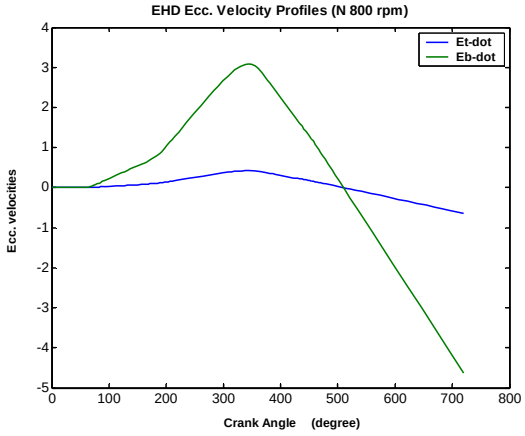

(b)

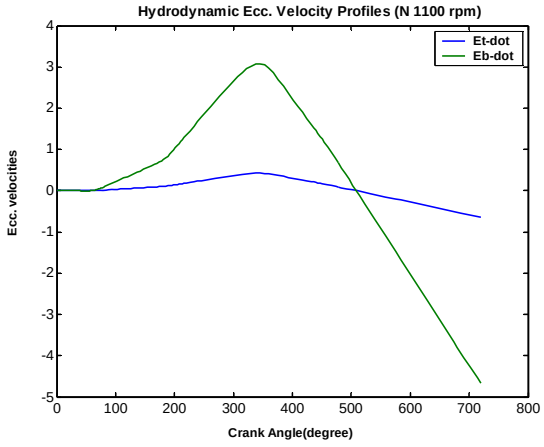

(c)

Fig-6.5: EHD Eccentricity Profiles at (a) Startup Speed 600 rpm (b) 800 rpm (c) 1100 rpm

6.3.4 ***EHD Eccentric Velocity Profiles***

EHD eccentric velocity profiles for startup speeds 600 rpm, 800 rpm and 1100 rpm are shown in Fig-6.6 (a), (b) and (c) respectively

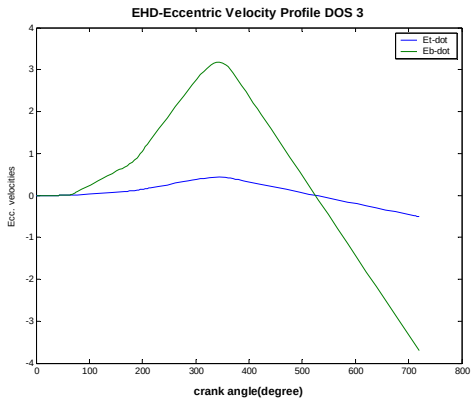

(a)

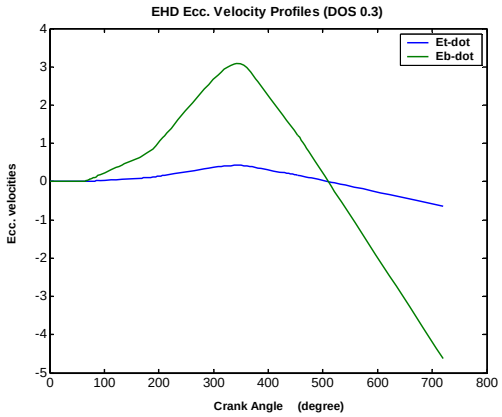

(b)

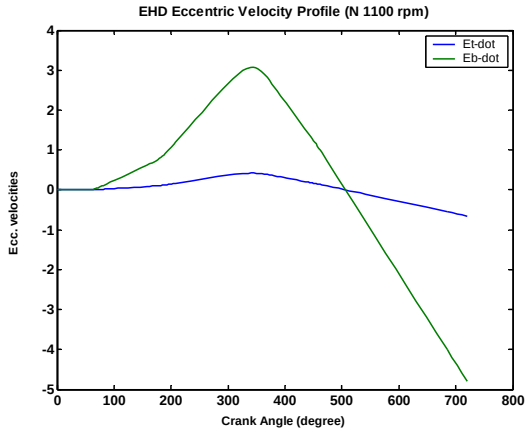

(c)

Fig-6.6: EHD Eccentricity Profiles at (a) Startup Speed 600 rpm (b) 800 rpm (c) 1100 rpm

EHD eccentric velocities also increase with increasing startup speeds. Therefore high startup speeds should be avoided.

6.4 **Conclusions of Study**

Following conclusions can be drawn from parametric studies for optimum startup speed.

- High film thicknesses in hydrodynamic and elastohydrodynamic regime are favored at high startup speeds. Low startup speed of 600 rpm is not recommended under starvation conditions in order to reduce friction losses and prevent wear of interacting surfaces.
- Startup speed of 1100 rpm results in contact between interacting surfaces of Piston and liner in EHD Regime, therefore startup speed of 1100 rpm is also not recommended, in order to reduce friction losses and wear.
- 800 rpm is found to be optimum startup speed for minimizing friction losses and wear of components.

TRANSIENT LUBRICATION OF PISTON SKIRT UNDER VARIOUS RADIAL CLEARANCES

6.5 This study includes optimization of radial clearance at low speed engine startup conditions (N=600 rpm) for a high velocity lubricant (η=0.1891 Pa. Sec.). The study is based on simulation of transient lubrication model of piston skirt under starvation conditions (DOS 0.3) with low (C=10 micron), medium (C=50 micron) and high (C=100 micron) radial clearances at the startup phase of an IC Engine. Results of simulations at various clearances are given below:

6.6 Film Thickness Profiles

6.6.1 *Hydrodynamic Film Thickness*

Fig-6.7 (a), (b) and (c) represent the Hydrodynamic Film thickness profiles at Piston to Cylinder radial clearances of 10, 50 and 100 microns respectively. Hydrodynamic film is increased at large radial clearances, therefore large clearance is favorable for minimized friction and wear.

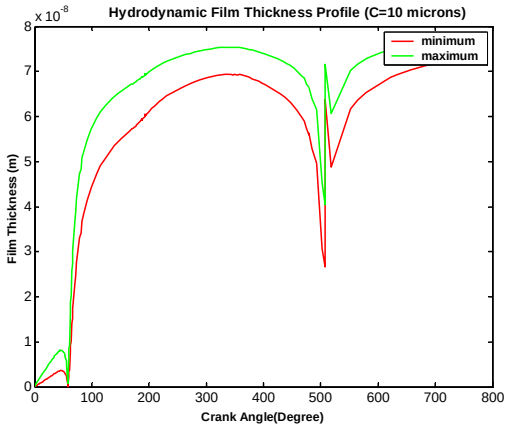

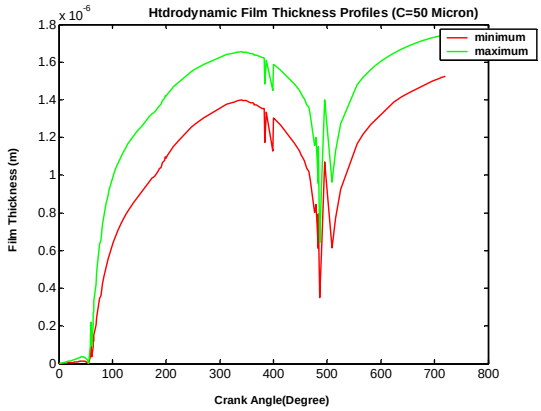

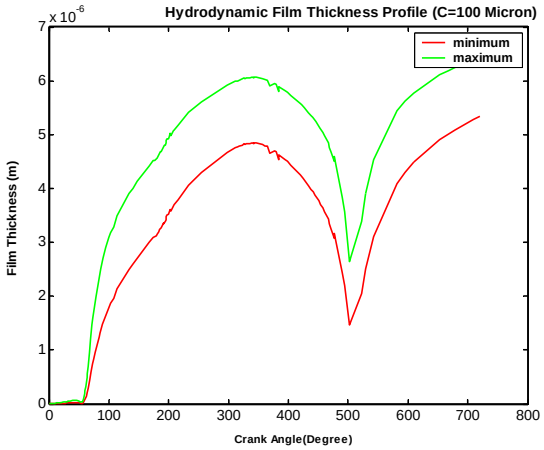

(c)

Fig-6.7: Hydrodynamic Film Thickness Profile (a) Radial Clearance 10 Mic. (b) 50 Mic. (c) 100 Mic.

6.7 **EHD Film Thickness**

Fig-6.8 (a), (b) and (c) represent the EHD Film thickness profiles at Piston to Cylinder radial clearances of 10, 50 and 100 microns respectively. EHD film thickness show the same trend as Hydrodynamic Film thickness. i.e. High radial clearance is favorable for minimized friction and wear.

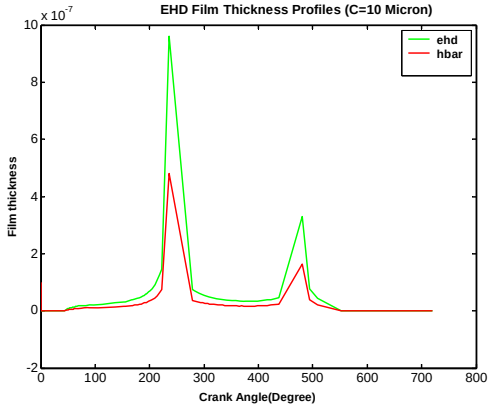

(a)

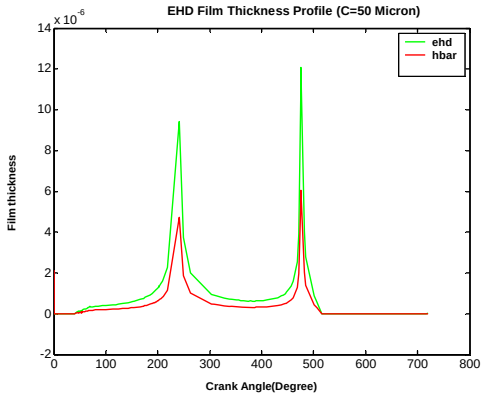

(B)

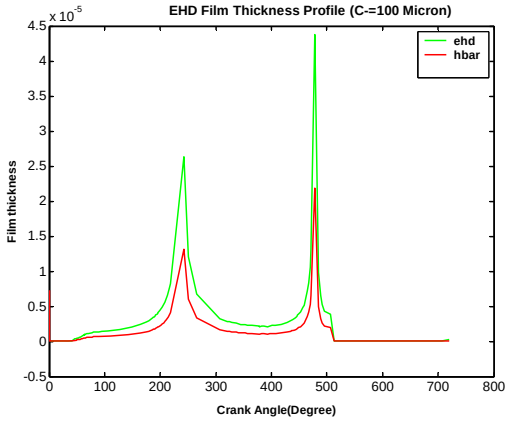

(C)

Fig-6.8: EHD Film Thickness Profile (a) Radial Clearance 10 Mic. (b) 50 Mic. (c) 100 Mic.

6.8 **Piston Eccentricities and Transverse Eccentric Velocities**

6.8.1 ***Hydrodynamic Eccentricities***

Fig-6.9 (a), (b) and (c) represent the Hydrodynamic eccentricity profiles at Piston to Cylinder radial clearances of 10, 50 and 100 microns respectively.

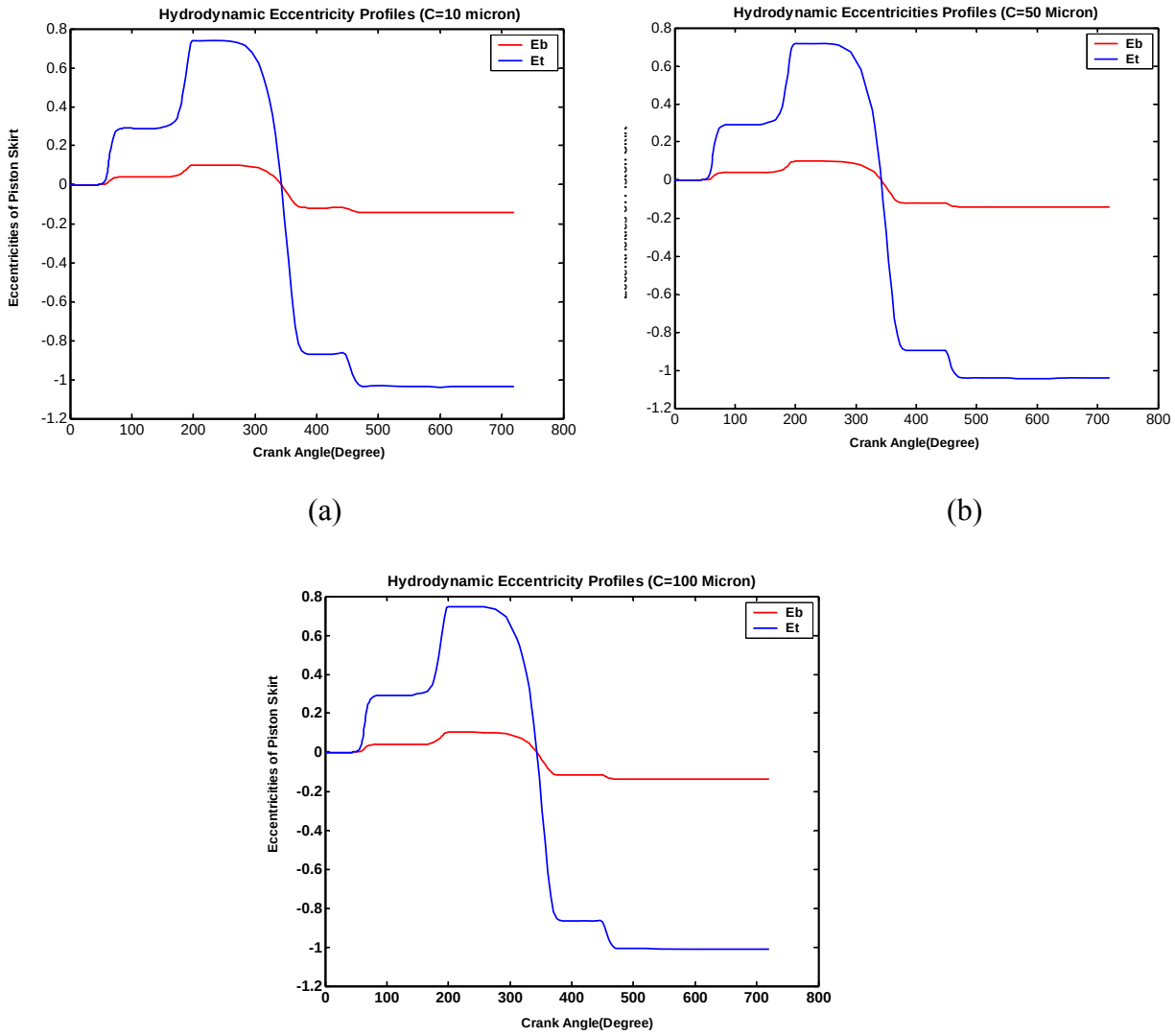

Fig-6.9: Hydrodynamic Eccentricity Profiles (a) Radial Clearance 10 Mic. (b) 50 Mic. (c) 100 Mic.

It is clear from the figure-6.9, that contact between piston and cylinder surface cannot be avoided at all the radial clearances in hydrodynamic regime. Therefore no conclusion can be drawn about optimization of radial clearance from Hydrodynamic eccentricity profiles.

6.8.2 ***EHD Eccentricities***

EHD Eccentricity profiles for radial clearances of 10, 50 and 100 Micron are shown in Fig-6.10 (a), (b) and (c) respectively. From the comparison of results it is obvious that physical contact between piston and liner surface is avoided with radial clearance of 10 Micron. So C=10 micron is the optimized radial clearance for minimum friction and wear.

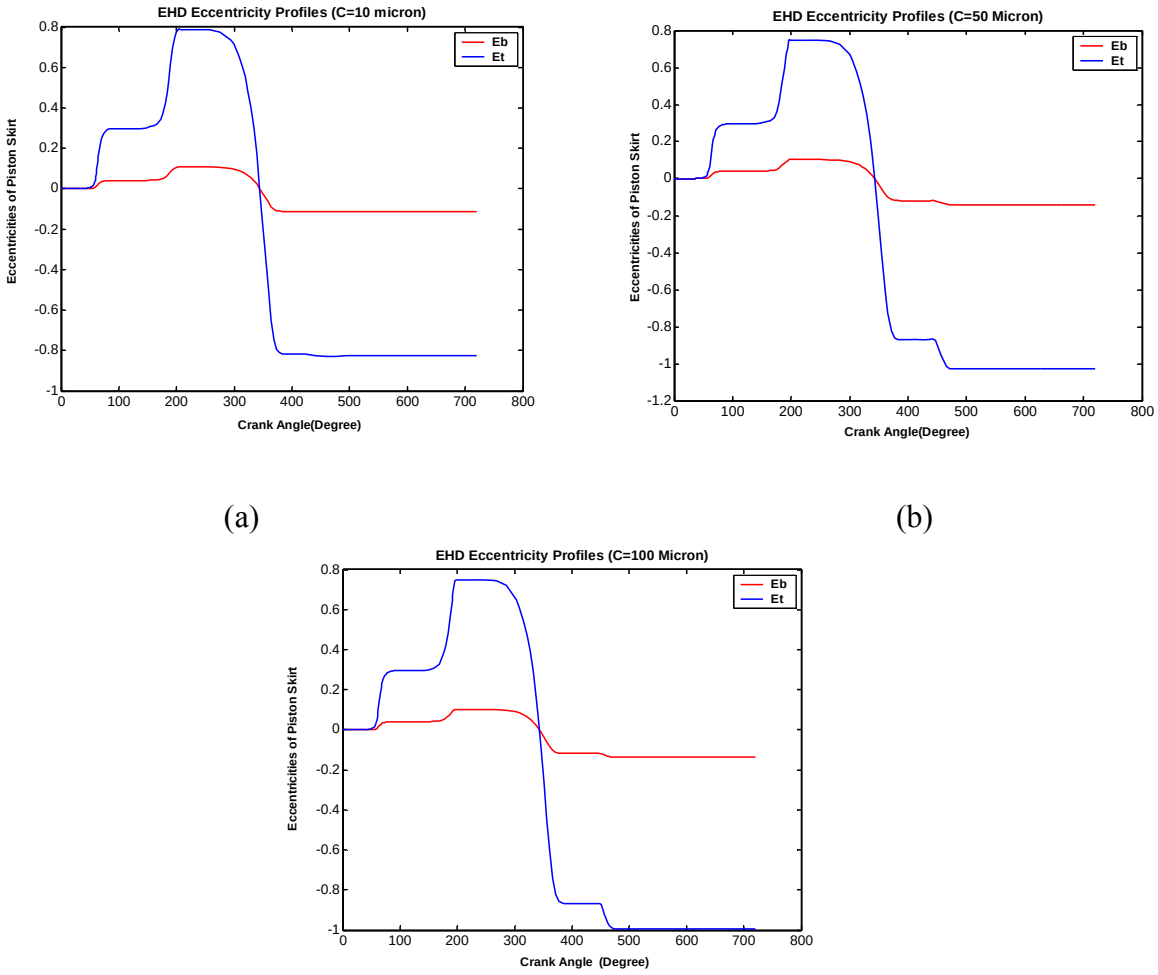

Fig-6.10: Hydrodynamic Eccentricity Profiles (a) Radial Clearance 10 Mic. (b) 50 Mic. (c) 100 Mic.

6.8.3 ***Hydrodynamic Eccentric Velocities***

Hydrodynamic eccentric velocity profiles for radial clearances of 10, 50 and 100 Micron are shown in Fig-6.11 (a), (b) and (c) respectively. From the comparison of results it is obvious that

eccentric velocities increase with larger radial clearances. Therefore small radial clearances are more preferable for reduced friction and wear.

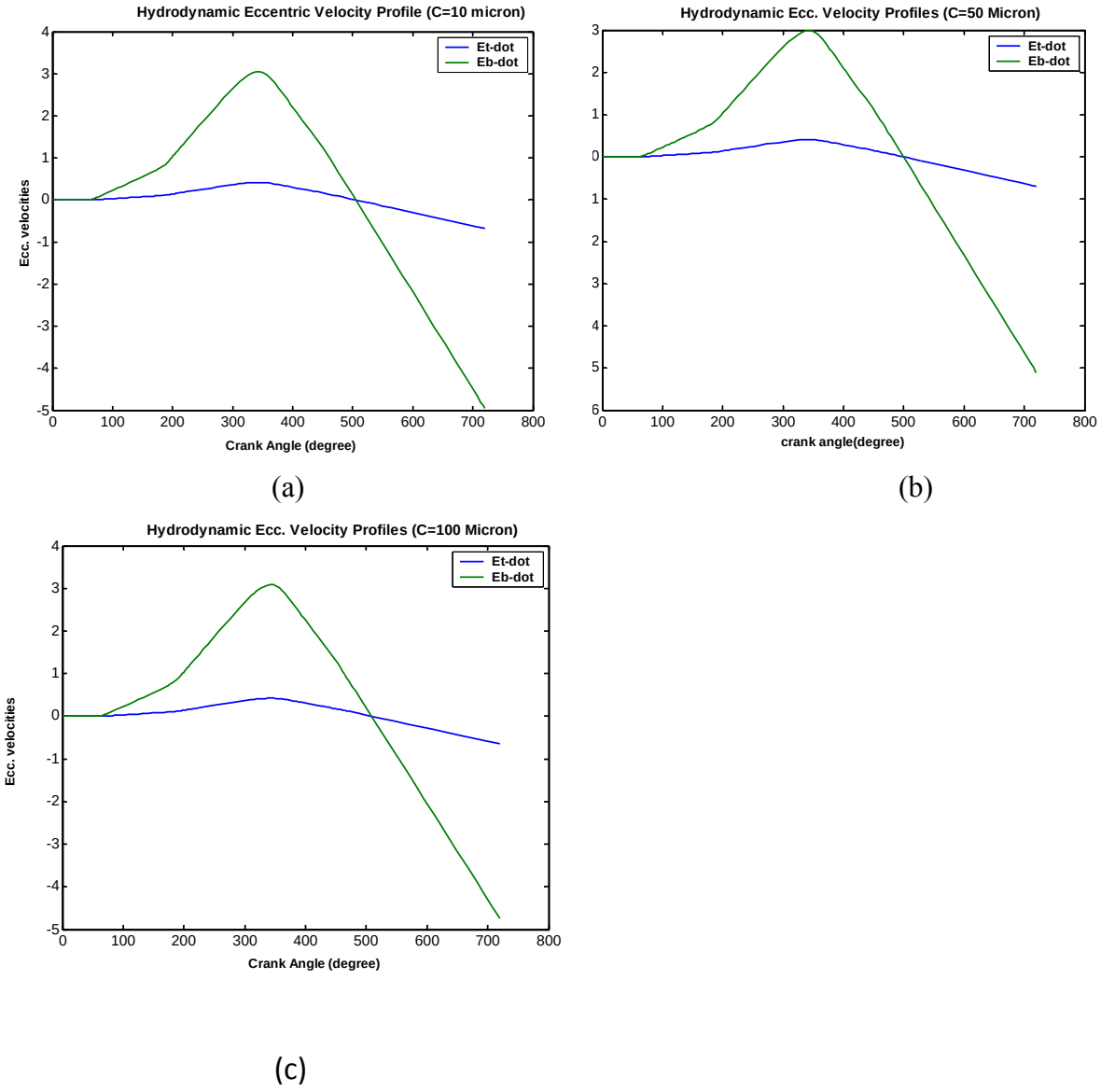

Fig-6.11: Hydrodynamic Ecc. Velocity Profiles (a) Radial Clearance 10 Mic. (b) 50 Mic. (c) 100 Mic.

6.8.4 ***EHD Eccentric Velocities***

EHD eccentric velocity profiles for radial clearances of 10, 50 and 100 Micron are shown in Fig-6.12 (a), (b) and (c) respectively. From the comparison of results it is obvious that small radial clearances are desirable for minimum eccentric velocities so that friction and wear can be minimized.

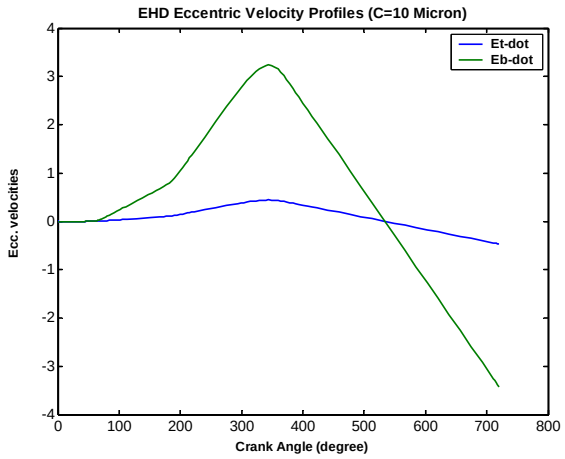

(a)

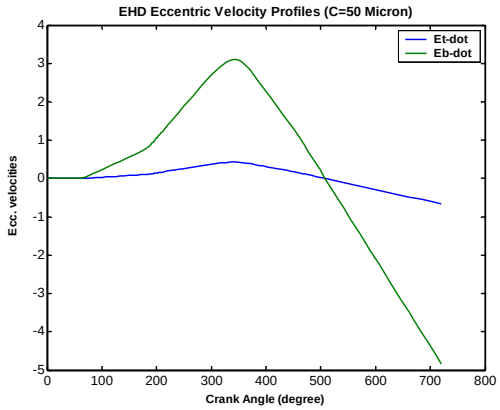

(b)

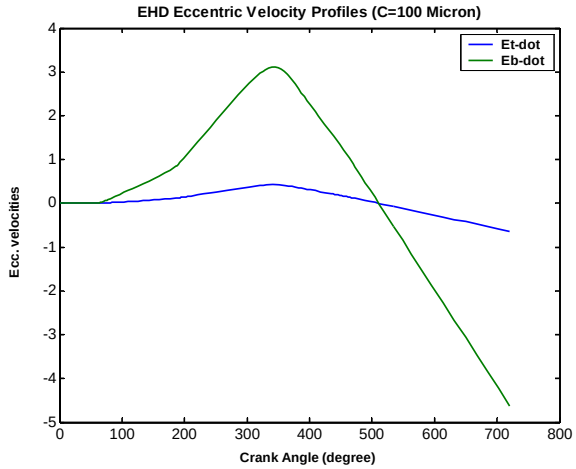

(c)

Fig-6.12: EHD Ecc. Velocity Profiles (a) Radial Clearance 10 Mic. (b) 50 Mic. (c) 100 Mic.

6.9 **Conclusions of Study**

From findings of results it is clear that friction and wear losses are minimized for small radial clearances. Therefore C=10 micron is found to be the optimum radial clearance for efficient and reliable operation of engine.

TRANSIENT LUBRICATION OF PISTON SKIRT WITH VARIOUS VISCOSITY GRADE LUBRICANTS

This study includes optimization of lubricant viscosity at low speed (N=600 rpm) engine startup conditions under large radial clearance (C=100 Micron). The study is based on simulation of transient lubrication model of piston skirt under starvation conditions (DOS 0.3) with low (η= 0.0318 Pa.S), medium (η=0.08571 Pa.S) and high (η= 0.1891 Pa.S) viscosity grade lubricants. Results of Simulation are discussed below:

6.10 Film Thickness Profiles

6.10.1 *Hydrodynamic Film Thickness*

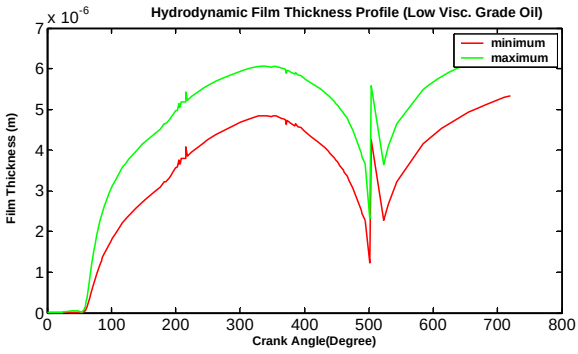

(a)

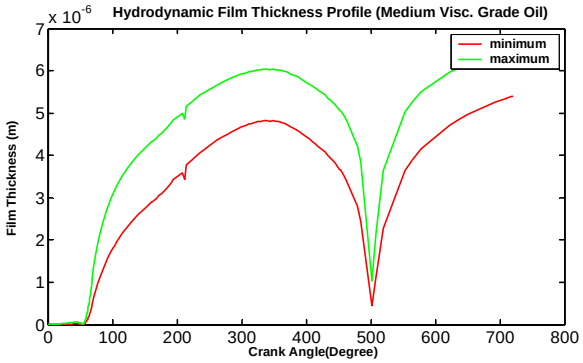

(b)

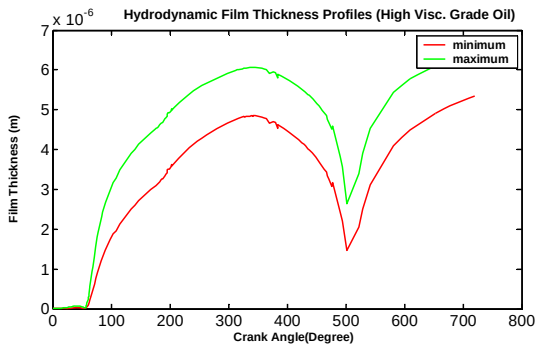

(c)

Fig-6.13: Hydrodynamic Film Thickness Profiles (a) Low Visc. Grade Oil (b) Medium Visc. Grade Oil (c) High Visc. Grade Oil

Hydrodynamic Film thickness does not so significant variation for different viscosity grade lubricants.

6.10.2 ***EHD Film Thickness***

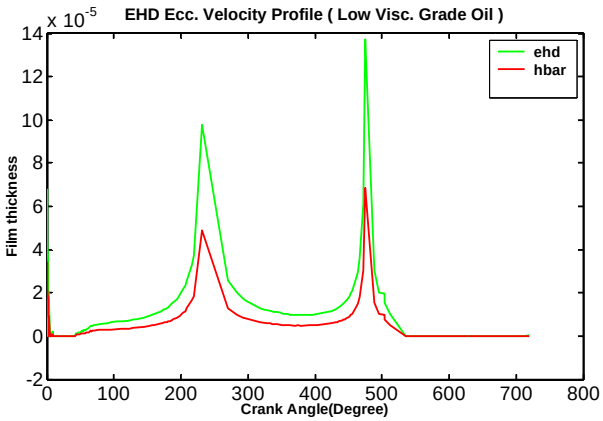

(a)

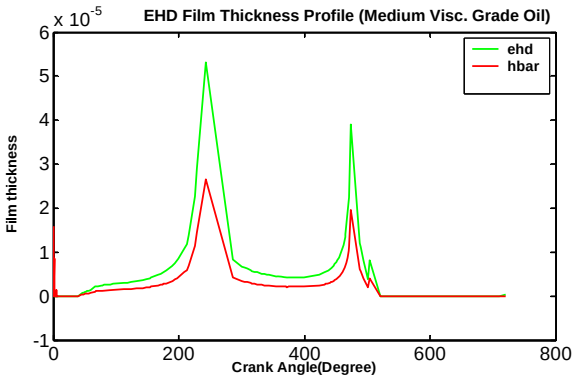

(b)

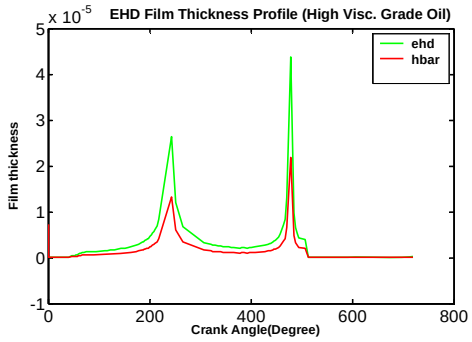

(c)

Fig-6.14: EHD Film Thickness Profiles (a) Low Visc. Grade Oil (b) Medium Visc. Grade Oil (c) High Visc. Grade Oil

EHD Film thickness also show the same trends as Hydrodynamic film thicknesses.

6.11 **Piston Eccentricities and Transverse Velocity Profiles:**

6.11.1 ***Hydrodynamic Eccentricities:***

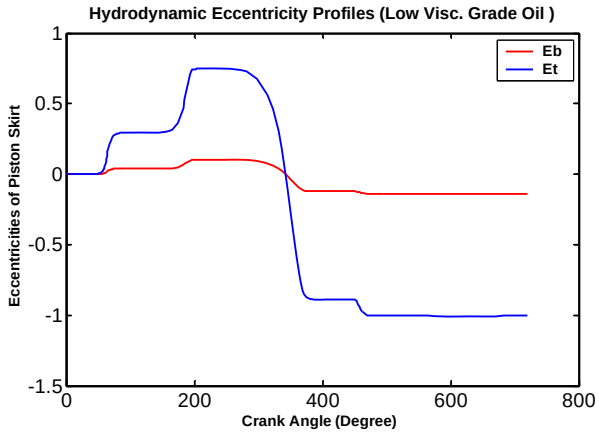

(a)

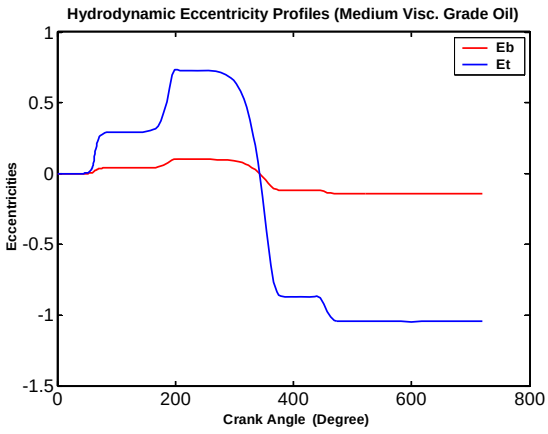

(b)

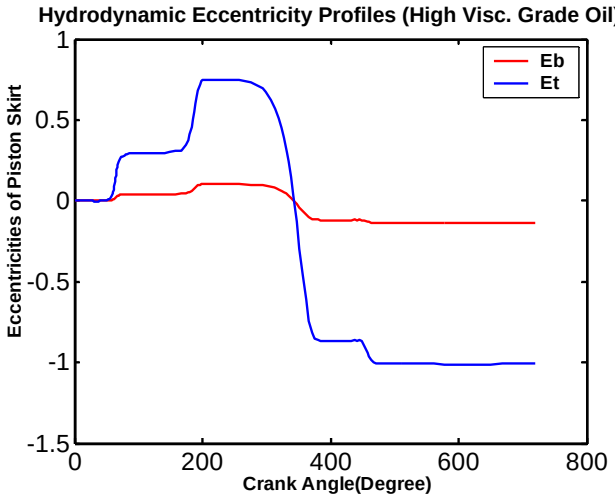

(c)

Fig-6.15: Hydrodynamic Eccentricity Profiles (a) Low Visc. Grade Oil (b) Medium Visc. Grade Oil (c) High Visc. Grade Oil

Findings of Hydrodynamic eccentricity profiles are that,in hydrodynamic regime contact between piston and liner cannot be avoided.

6.11.2 ***EHD Eccentricities:***

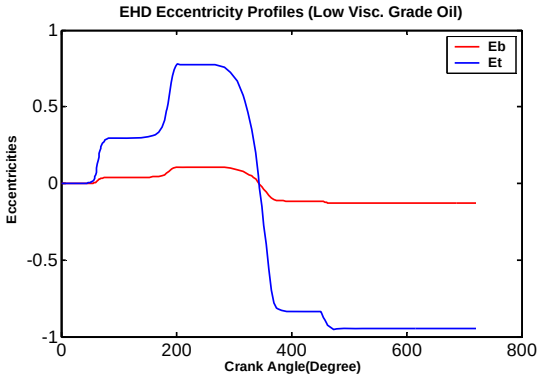

(a)

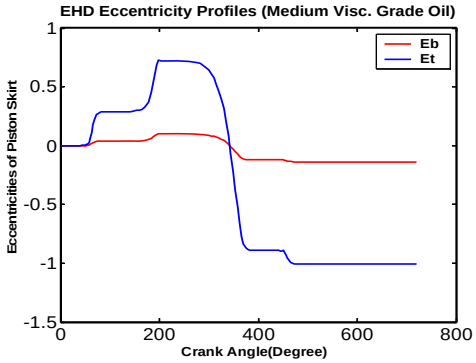

(b)

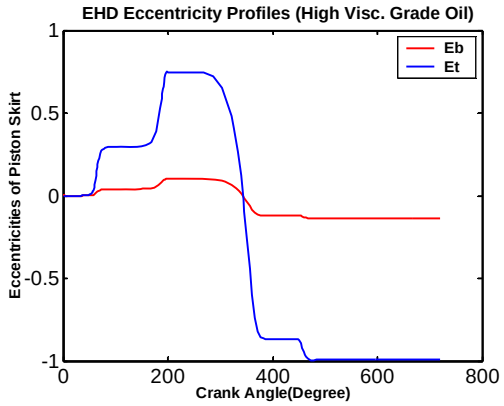

(c)

Fig-6.16: EHD Eccentricity Profiles (a) Low Visc. Grade Oil (b) Medium Visc. Grade Oil (c) High Visc. Grade Oil

In EHD regime, Contact can be avoided with low viscosity grade oil (Fig-6.16 a). Also, EHD eccentricities profile of high viscosity grade oil shows that contact is avoided. However for medium viscosity grade oil the contact cannot be avoided.

6.11.3 ***Hydrodynamic Eccentric Velocities:***

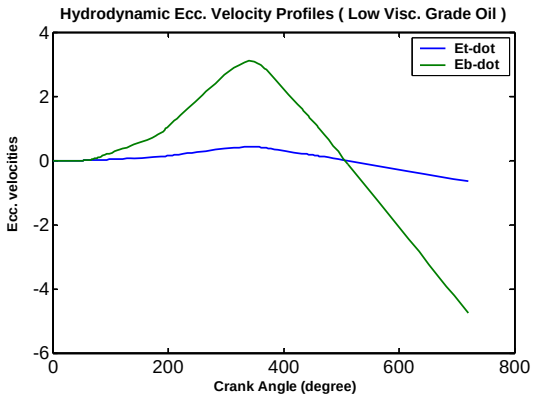

(a)

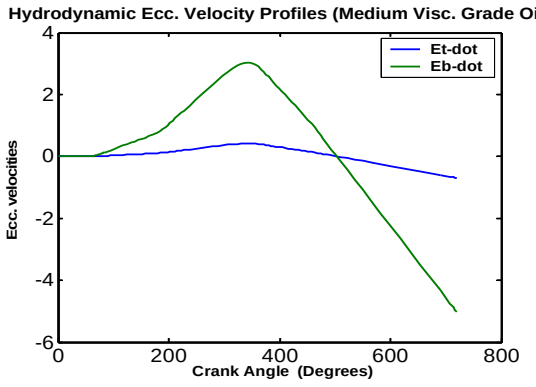

(b)

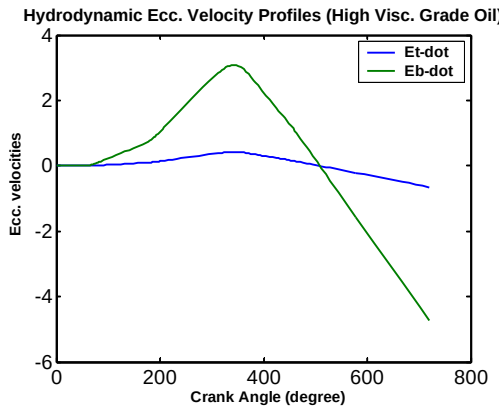

(c)

Fig-6.17: Hydrodynamic Ecc. Velocity Profiles (a) Low Visc. Grade Oil (b) Medium Visc. Grade Oil (c) High Visc. Grade Oil

Hydrodynamic eccentric velocity profiles don't show significant variations with viscosity of lubricant.

6.11.4 ***EHD Eccentric Velocities:***

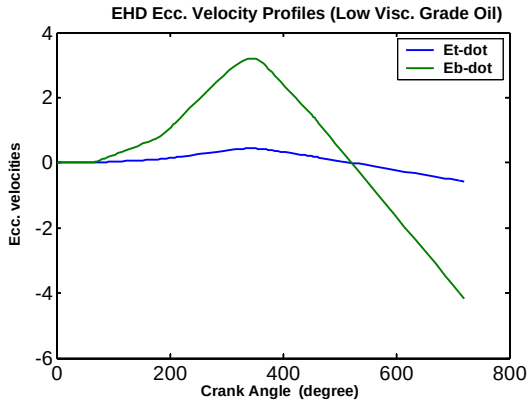

(a)

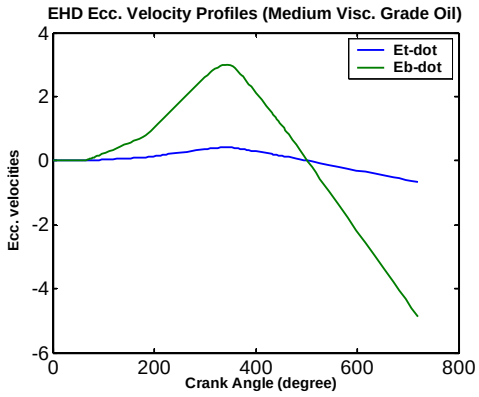

(b)

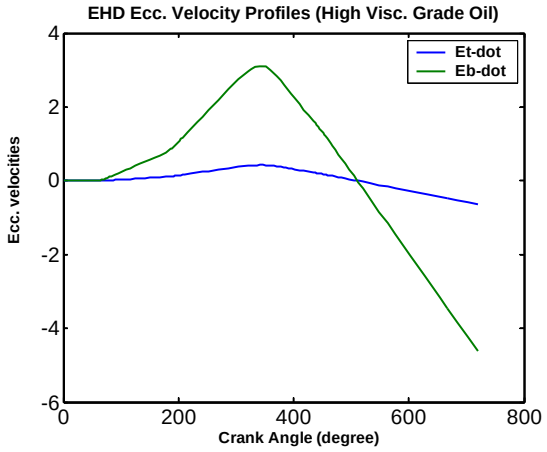

(c)

Fig-6.18: EHD Ecc. Velocity Profiles (a) Low Visc. Grade Oil (b) Medium Visc. Grade Oil (c) High Visc. Grade Oil

EHD eccentric velocity profiles don't show significant variations with viscosity of lubricant.

6.12 **Conclusion of Study:**

Low viscosity grade Oil (η=0.0318 Pa.S) is the optimum oil for minimum friction and wear losses at initial engine startup.

CHAPTER 7
CONCLUSIONS AND FUTURE WORK RECOMMENDATIONS

7.1 The life and performance of an automobile engine is greatly affected by startup wear. As discussed earlier, during few initial seconds and minutes of an engine startup, it faces starvation conditions. Due to limited lubricant supply, complete hydrodynamic and EHD lubricant films are not developed and mixed lubrication is experienced by the engine at initial startup. In mixed lubrication regime, interacting surfaces of piston and liner cannot be separated completely resulting in adhesive wear. It is quiet necessary to reduce this initial startup wear for increasing the life of an automobile engine and improving its efficiency. The current research was undertaken with a view to enhance and improve our exiting knowledge of the subject so that a solid foundation of knowledge can be established to enable the future researchers finding a permanent solution to the problem of initial engine startup wear.

7.2 Major focus of the current research is modeling of Piston Skirt lubrication under starvation conditions at initial engine startup. Initial engine startup is the most critical phase for life of an automobile engine. Most of the adhesive wear of interacting surfaces of critical parts takes place in this phase. This is due to the fact that lubricant is supplied to the engine by means of a mechanical pump which is driven by the engine itself. Also the engine speeds are low at the startup. Therefore, lubricant supply rate is very low at this stage. The engine has to run under limited lubricant supply (starvation) conditions. Due to insufficient supply of lubricant complete hydrodynamic and elastohydrodynamic films cannot be developed to prevent the contact between interacting surfaces. This results in frictional losses and adhesive wear at the startup. Lubricant supply rate is therefore, the most critical parameter for modeling of hydrodynamic and elastohydrodynamic lubrication of piston skirt at the startup phase. Lubricant supply rate at initial startup has been determined by reverse calculation from flooding conditions model. Initially lubricant flow rate is calculated from hydrodynamic pressures under flooding conditions. This flow rate is equal to lubricant supply rate under flooding conditions. By multiplying flooding conditions supply rate by a certain factor, lubricant supply rate under

starvation conditions (given degree of starvation) is calculated. Initially dry sliding and severe starvation conditions are faced by the engine after startup. As the engine operates, lubricant supply rate is improved and degree of starvation changes to medium and then mild starvation conditions. Further improvement in lubricant supply rate leads to achievement of full flooding conditions (i.e. zero degree of starvation). Therefore piston skirt lubrication has been modeled under flooding conditions, mild starvation conditions (DOS 0.1-0.2), medium starvation conditions (DOS 0.3-0.4) and severe starvation conditions (DOS 0.5 and above). Under mild starvation conditions, one dimensional steady state lubrication model is used as variation of hydrodynamic pressure only in axial direction is significant in this case. Variation of hydrodynamic pressure in circumferential direction is ignored in case of mild starvation and steady state lubrication. For medium and severe starvation conditions, 2-D transient model is developed. The transient model takes into account, time dependent squeeze velocity term (dh/dt). In addition, secondary dynamics of piston assembly are incorporated for more realistic modeling of piston skirt lubrication at startup. Initially, starved lubrication of piston skirt under steady and transient conditions have been modeled in order to have an understanding of starvation and its effects. Then some parametric studies were carried out. The parametric studies primarily focused on optimizing the initial engine startup speeds, viscosity of the lubricant oils and piston to bore radial clearances under medium starvation conditions (DOS 0.3). Conclusions of simulation results have already been narrated at the end of every simulation. However following general conclusions are narrated here:

7.2.1 Results of lubrication models accounting for secondary piston dynamics elaborate nature and duration of physical contact between piston skirt and liner.

7.2.2 Steady state model do not account for squeeze effects during the lubrication process, resulting in reduced load carrying capacity of the lubricant at startup. The unsteady conditions improve the lubrication and results in slight reduction in startup wear under certain conditions.

7.2.3 Degree of Starvation 0.2 is the critical starvation condition up to which contact of interacting surfaces can be avoided under certain conditions. At degree of starvation above this value, surface to surface contact and hence friction losses and wear cannot be prevented.

7.2.4 Low startup speed, Low piston to bore radial clearance and high lubricant velocity are found to be the optimum operating conditions at startup for minimizing frictional losses and startup wear.

RECOMMENDATIONS FOR FUTURE WORK

7.3 Following recommendations are made for the researchers of the future:

7.3.1 Future work is needed for including lubrication models of 1st, 2nd and 3rd Rings in order to develop lubrication model of Complete Ring Pack. This includes defining the secondary dynamics of 1st compression ring, Scrapper Ring and Oil Control Ring separately from the piston at initial engine startup. This will help to cater for frictional losses and wear caused by Piston Rings and Liner interface.

7.3.2 Finite Difference approach has been adopted in the current research. Future work may be done using Finite Element or Finite Volume approaches to validate the results.

BIBLIOGRAPHY

1. **Heywood, J.B.** *Internal Combustion Engine Fundamentals.* s.l. : McGraw-Hill, 1988.

2. **Fiona, McClure.** *Numerical Modeling of Piston Secondary Motion and Skirt Lubrication in Internal Combustion Engines.* MIT. 2007. PhD Thesis.

3. **Anderson, Peter.** *Piston Ring Tribology, a Literature Survey.* VTT. Tiedotteita : s.n., 2002. Research Notes.

4. **Gwidon W. Stachowiak, Andrew W. Batchelor.** *Engineering Tribology.* 2005. ISBN-10:0-7506-7836-4.

5. **Qasim, Syed Adnan.** *Modeling Realistic Piston Skirts and 1st Compression Rings EHL in the Initial Engine Startup.* NUST. Rawalpindi : s.n., 2012. PhD Thesis.

6. **Rifat Keribar, Zafar Dursunkaya.** A Comprehensive Model of Piston Skirt Lubrication. s.l. : SAE. Paper No. 920483.

7. **P.K.Goenka, P.R.Meernik.** Lubrication Analysis of Piston Skirts. s.l. : SAE, 1992. Paper No.920490.

8. **Hu, Xuijie.** *Predictive Modeling of Piston Assembly Lubrication in Reciprocating Internal Combustion Engines.* University of Texas. Austin, USA : s.n., 2005. Ph.D. Thesis.

9. **Zhu, Donng.** On the EHL Film Breakdown. *Tribology Transactions.* 1996.

10. **O. Aklin, G.M. Newaz.** Piston Ring-Cylinder Bore Friction Modeling in Mixed Lubrication regime, Part-I: Analytical Results. *Transactions, ASME Journal of Tribology.* 2001. Vol. 123, pp. 211-218.

11. An Average Reynolds Equation for Partial Film Lubrication with a Contact Factor. *ASME Transactions.* 1989. Vol. 111, pp. 188-191.

12. **D. Dowson, B. J. Hamrock.** Minimum Film Thickness in Elliptical Contacts for Different Regimes of Fluid Film Lubrication, Part-II.

13. **Y. Harigaya, J. Akaagai.** Prediction of Temperature, Viscosity and Thickness in Oil Film between Ring and Liner of an Internal Combustion Engine. *SAE* . 2000. Paper No. 2000-01-1790.

14. **Hault, P. David.** Calibration of Laser Flouroscence Measurements of Lubricant Filmthicknesses in Engines. *SAE Paper No 881587.*

15. **Taylor, C.M.** Automobile Engine Tribology-Design Considrations for Efficiency and Duarability. *Wear, 221, PP-1-8.*

16. **E. W. Schneide, DI. H. Blossfeld.** Effects of Break-In and Operating Conditions on Piston Ring and Cylinder Bore Wear in Spark Ignition Engines. *SAE Paper No. 2004-01-2917* .

17. **Y. Chung, H. J. Schock, L. J. Brombolich.** Fire Ring Wear Analysis for a Piston Engine. *SAE Paper No. 930797.*

18. **Rob Galbraith, Chris May.** A Cold Start and Pumpability Study of Fresh and High Sooted Engine Oils in 1999 Heavy-Duty Diesel Emission Engines. *SAE Paper No 2003-01-3224.* 2003.

19. **A. G. Alexander, C. J. May, C. R. Smith.** Factors Affecting Pumpability and Cold Cranking in Heavy-Duty Diesel Truck Engines at Low Ambient Temperatures, Part-II. *SAE Paper No. 920023.*

20. **Kaytlar, Matti.** Engine Lubrication in Cold Startup. *SAE Paper No. 890033.* 1989.

21. **Zhang, Y.** Numerical Investigations of the EHL Performance of Piston Ring with the Considration of 2-D Deformation of Cylinder Liner. *SAE Paper No 2001-01-1989.* 2001.

22. **M. J. A. Holmes, H. P. Evans, R. W. Snidle.** Comparison of Transient EHL Calculations with Startup Experiments. *Leeds-Lyon Tribology Symposium.* 2002.

23. **K. Perrin, J. Pandosh, A. Searle.** Radioactive Tracer Study of Startup Wear Versus Steady-State Wear in a 2.3 Liter Engine. *SAE Paper No. 952474.* 1995.

24. **Ueno, Masakai.** A Quick Warm-Up System During Engine Start-Up Period using Adaptive Control of Intake Air and Ignition Timing . *SAE paper No 2000-01-0551.* 2000.

25. **J. C. Danos, B. Tourneire, J.Frene.** Thermodynamic Lubricatio of Mechanical Face Seals During Trasient Period after Start-Up: 2-D Modelization. *Proc. 29th, Leeds-Lyon Tibol Symposium.* 2002.

26. **S. Bair, S. Qureshi.** Ordinary Shear Thinning Behavior and its Effects Upon EHL Film Thickness. . *Proc. 29th, Leeds-Lyon Tribol Symposium.* 2002.

27. **B.J. Hamrock, D. Dowson.** *Isothermal Elastohydrodynamic Lubrication of Point Contacts-Theoratical Formulation.* NASA. October 1976. Technical Notes.

28. *Lubrication of Rolling-Contact Instrument Bearings.* **F.K. Orcutt, H.S. Cheing.** [ed.] Mass. Inst. Technol. Instru. Lab. 1966. Gyro Spin Axis Hydrodynamic Bearing Symposium. Vol. 2.

29. **B.J. Hamrock, D Dowson.** Isothermal Elastohydrodynamic Lubrication of Point Contacts-Starvation Results.

30. **Floberg, L.** On Hydrodynamic Lubrication with Special Reference to sub cavity Pressures and Number of Streamers in Cavitation Regions . *Acta. Polytech. Scand.* 1965 .

31. **L. D. Wedeven, D. Evans, A. Cameron.** Optical Analysis of Ball Bearing Starvation . *Journal of Lubrication Technology.* July 1971. Vol. 93.

32. **Rajesh. Kumar, M. Gupta.** Starvation Effects in Elasto-Hydrodynamically Lubricated Line Contacts.

33. **M. K. Ghosh, B. J. Hamrock, D. E. Brew.** Starvation Effects on the Hydrodynamic Lubrication of Rigid Non Conforming Contacts in Combined Rolling and Normal Motion.

34. **D. E. Brew, B. J. Hamrock.** *Analysis of Starvation Effects on Hydrodynamic Lubrication* .

35. **Boness, R. J.** The effects of Oil Supply on Cage and Roller Motion in a Lubricated Roller Bearing. *Journal of Lubrication Technology.* Jan 1970. . Vol. 92.

36. **Heshmat, Hoshang.** *Starved Bearing Technology Theory and Experiment.* Rensselaer Polytechnic Institute. New York : s.n., December 1988. Ph.D. Thesis.

37. **Popovici, G.** *Effects of Lubricant Starvation on Performance of Elasto-hydrodynamically Lubricated Contacts.* University of Twente. 2005. Ph.D Thesis.

38. **B. Jakobsson, L. Floberg.** The Finite Journal Bearing, considering vaporization. *Trans. Chalmer's University.* Vol. 190.

39. **Elord, H. G.** A Cavitation Algorithem. *ASME Journal of Lubricant Technplogy.* 1981.

40. Film Thickness in Standard EHL Point Contacts . 1998. Vol. 120.

41. **Wijnant, Y. H.** *Contact Dynamics in the field of Elastohydrodynamic Lubrication.* University of Tewente. Enschede, Netherlands : s.n., 1998. Ph.D. Thesis.

42. **D. E. Brew, B. J. Hamrock.** *Analysis of Starvation Effects on Hydrodynamic Lubrication in Non Conforming Contacts.* Lewis Research Center, National Aeronautics and Space Administration. Cleveland, Ohio

43. **Jeng, Yeau Ren.** *Theoratical Analysis of Piston-Ring Lubrication, Part II Starved Lubrication and its Application to a complete Ring Pack.* Engine Research Department, General Motors Research Laboratories. 1992.